Experimental and numerical study on the contribution of acoustic test fixtures to hearing protector sound attenuation: Sound transmission paths in the case of a double hearing protector and influence of eardrum acoustic impedance

by

Yu LUAN

MANUSCRIPT-BASED THESIS PRESENTED TO ÉCOLE DE TECHNOLOGIE SUPÉRIEURE IN PARTIAL FULFILLMENT FOR THE DEGREE OF DOCTOR OF PHILOSOPHY
Ph.D.

MONTREAL, DECEMBER 16, 2021

ÉCOLE DE TECHNOLOGIE SUPÉRIEURE
UNIVERSITÉ DU QUÉBEC

BOARD OF EXAMINERS

THIS THESIS HAS BEEN EVALUATED

BY THE FOLLOWING BOARD OF EXAMINERS

Mr. Olivier Doutres, Thesis Supervisor
Department of Mechanical Engineering, École de Technologie Supérieure

Mr. Franck Sgard, Thesis Co-Supervisor
Scientific Division, Institut de recherche Robert-Sauvé en santé et en sécurité du travail

Mr. Hugues Nélisse, Thesis Co-Supervisor
Scientific Division, Institut de recherche Robert-Sauvé en santé et en sécurité du travail

Mr. Jean-Philippe Roberge, Chair, Board of Examiners
Department of System Engineering, École de Technologie Supérieure

Mr. Jérémie Voix, Member of the Jury
Department of Mechanical Engineering, École de Technologie Supérieure

Mr. Pascal Hamery, External Examiner
Institut franco-allemand de recherches de Saint-Louis, France

Mr. William Murphy, External Examiner
National Institute for Occupational Safety and Health, USA

THIS THESIS WAS PRESENTED AND DEFENDED

IN THE PRESENCE OF A BOARD OF EXAMINERS AND THE PUBLIC

ON DECEMBER 13, 2021

AT ÉCOLE DE TECHNOLOGIE SUPÉRIEURE

ACKNOWLEDGEMENTS

This thesis would not have been accomplished without the support of many people. Je souhaite tout d'abord remercier Franck Sgard, Olivier Doutres et Hugues Nélisse, mes directeurs de thèse, pour leur gentillesse, leur disponibilité permanente, et surtout leurs judicieux conseils tout au long de ce doctorat. Merci infiniment Franck pour ta rigueur et les nombreux encouragements que tu m'as prodigués. À toi Olivier, merci infiniment pour m'avoir fait partager tes brillantes intuitions. Un immense merci Hugues pour ton expertise et expériences enrichissantes en terme de mesures expérimentales. Merci à vous pour l'honneur que vous me faites d'être mes directeurs de thèse.

I would like to thank the Board of Examiners for kindly evaluating this doctoral thesis and giving their expert feedback: Nicola Hagemeister, Jérémie Voix, Pascal Hamery and William Murphy.

I would also like to gratefully acknowledge the financial support from the Natural Sciences and Engineering Research Council of Canada (NSERC).

Je tiens à remercier spécialement Simon Benacchio pour sa contribution directe à l'étude sur le simulateur d'oreille évoquée dans cette thèse et Thomas Padois pour son aide précieuse durant les diverses campagnes de mesures effectuées.

Je remercie aussi Kévin Carillo pour les nombreuses discussions lors de nos rencontres fortuites au labo les week-ends.

J'adresse également mes remerciements à Olivier Bouthot et Éric Marcoux. Ce travail n'aurait pu être mené à bien sans leurs soutiens technique et matériel.

Merci à tous mes collègues du labo et aux membres de CRITIAS, je pense particulièrement à Fabien, Maxime, Bastien, Simon, Hugo, Valentin, Louis, Saber, Alexis et Marc-Olivier, pour le partage des connaissances, l'ambiance amicale et les repas aux trois brasseurs les vendredis midis.

I am grateful for my beloved parents for their constant support, and for encouraging me to go abroad and jump on this wonderful journey.

Finally, I want to express my deepest gratitude to Huiyang, colleague in my research group as well as partner in my life, for her love and unconditional help as always.

Étude expérimentale et numérique sur la contribution des montages d'essai acoustique à l'atténuation sonore des protecteurs auditifs : Chemins de transmission sonore dans le cas d'une double protection auditive et influence de l'impédance acoustique du tympan

Yu LUAN

RÉSUMÉ

Les montages d'essai acoustique (acoustic test fixtures – ATFs) peuvent être utilisés pour évaluer l'atténuation sonore des protecteurs auditifs (par exemple, bouchons d'oreille et serre-têtes). Ces montages facilitent les mesures et permettent l'acquisition de données dans des conditions de bruit très élevé. Cependant, les ATFs standardisées ne sont pas suffisamment réalistes pour bien capturer l'atténuation subjective de tous les types de protecteurs et leurs ajustements sur une grande majorité de sujets humains. En tant que première étape vers une évaluation plus précise de l'atténuation des protecteurs auditifs sur les ATFs, cette thèse vise à résoudre deux principales problématiques liées à leurs caractéristiques de conception vibroacoustique : (i) prédiction de l'atténuation des doubles protections auditives (bouchon d'oreille combiné avec un serre-tête) qui implique la transmission solidienne à travers l'ATF ; (ii) impact de l'impédance acoustique du simulateur d'oreille IEC 60318-4 dans le conduit auditif de l'ATF sur l'atténuation des protecteurs auditifs.

D'une part, l'effet double protection sur un ATF commercial est étudié grâce à une campagne expérimentale impliquant des expériences spécialement conçues en modifiant les conditions de couplage du système ou en contrôlant le niveau de pression sonore sous la coquille du serre-tête. Un tel effet se réfère au phénomène où l'atténuation totale de la double protection est inférieure à la somme algébrique de l'atténuation individuelle de chaque protecteur, et est caractérisé par la diminution de la réduction du bruit du bouchon d'oreille après l'ajout du serre-tête. Les données expérimentales suggèrent que l'effet double protection est principalement associé à l'énergie solidienne transmise depuis la coquille du serre-tête, à travers l'ensemble du coussin/ATF et enfin au conduit auditif en raison du rayonnement acoustique du bouchon d'oreille et/ou des parois latérales du conduit, qui domine la « directe » transmission aérienne via la surface extérieure du bouchon. Un modèle d'éléments finis est ensuite développé et validé expérimentalement pour prédire l'effet double protection sur un ATF. La contribution cruciale de la transmission solidienne est confirmée par les bilans de puissance simulés avec des configurations choisies de l'ATF. Il est démontré que l'effet double protection provient de la puissance solidienne injectée à partir des surfaces extérieures de l'ATF et/ou du coussin de la coquille. L'influence importante de la vibration des parois du conduit auditif est mise en évidence lorsque la peau artificielle est prise en compte. Un chemin indirect de transmission solidienne correspondant au rayonnement du bouchon d'oreille excité par les parois du conduit est identifié.

D'autre part, un modèle de matrice de transfert du simulateur d'oreille est proposé basé sur une évaluation directe de ses dimensions géométriques, et validé par des approches numérique et expérimentale. Comparé au modèle à constantes localisées couramment utilisé dans la littérature, ce modèle prend en compte avec précision les effets thermo-visqueux dans le simulateur et

représente son impédance d'entrée dans une relativement large gamme de fréquences. Il permet aussi de récupérer une impédance tympanique équivalente du simulateur qui est imposée comme condition aux limites d'impédance au « niveau du tympan » dans le modèle d'éléments finis des conduits ouvert et occlus de l'ATF pour simuler la perte par insertion d'un bouchon d'oreille. Par ailleurs, un processus similaire est adopté pour étudier l'influence de la variabilité interindividuelle de l'impédance du tympan sur l'atténuation des bouchons. Ceci est réalisé grâce à une simulation Monte Carlo de 1000 impédances tympaniques équivalentes obtenues en faisant varier les dimensions du simulateur dans le modèle de matrice de transfert. Les résultats de la simulation sont considérés comme représentatifs de la variabilité de l'impédance du tympan humain. Des groupes représentatifs d'impédance tympanique équivalente sont ensuite sélectionnés parmi ces résultats et appliqués comme des conditions aux limites d'impédance dans un modèle d'éléments finis pour simuler la perte par insertion du bouchon d'oreille dans un conduit auditif de forme réaliste. On montre que la variabilité de l'impédance tympanique équivalente induit des différences non négligeables dans les résultats de perte par insertion, indiquant que la diversité de l'impédance du tympan humain doit être prise en compte par le simulateur d'oreille pour des mesures d'atténuation du bouchon.

Dans l'ensemble, cette thèse présente la méthodologie expérimentale et les modèles numériques pour étudier les caractéristiques vibroacoustiques d'intérêt de l'ATF, et à long terme, pourrait servir de base pour guider la conception et la mise en œuvre des ATFs pour une évaluation plus réaliste de l'atténuation des protecteurs auditifs.

Mots-clés: montage d'essai acoustique, double protection auditive, simulateur d'oreille, modélisation par éléments finis, atténuation sonore

Experimental and numerical study on the contribution of acoustic test fixtures to hearing protector sound attenuation: Sound transmission paths in the case of a double hearing protector and influence of eardrum acoustic impedance

Yu LUAN

ABSTRACT

Acoustic test fixtures (ATFs) can be adopted to assess the sound attenuation of hearing protectors (e.g., earplugs and earmuffs) as they can facilitate measurements, and allow data acquisition under severe noise conditions. However, standardized ATFs are not realistic enough to closely capture the subjective attenuation of all types of protectors and their fitting on a large majority of human subjects. As an initial step towards a more accurate evaluation of hearing protector attenuation on ATFs, this thesis seeks to address two primary issues related to their vibroacoustic design features: (i) sound attenuation prediction of double hearing protectors (DHPs, i.e., earplugs combined with earmuffs) which involves structure-borne sound transmission through the ATF; (ii) impact of the IEC 60318-4 ear simulator acoustic impedance in the ATF earcanal on the hearing protector attenuation.

On the one hand, the DHP effect on a commercial ATF is studied through specially designed experiments by modifying the system coupling conditions or controlling the sound pressure level under the earmuff. Such an effect refers to the phenomenon where the DHP overall attenuation falls short of the algebraic sum of each single protector's attenuation, and is particularly characterized by the decrease of the earplug noise reduction after adding the earmuff. Experimental data suggest that the DHP effect is mainly associated with the structure-borne energy transmitted from the earcup, through the earmuff cushion/ATF assembly and finally into the earcanal due to the sound radiation of the earplug and/or earcanal lateral walls, which dominates over the "direct" airborne transmission via the earplug outer surface. A finite element model is afterwards developed and experimentally validated to predict the DHP effect on an ATF. The crucial contribution of structure-borne transmission is further confirmed through the power balances simulated with selected configurations of the ATF. The DHP effect is shown to originate from the structure-borne power injected from the ATF boundaries and/or earmuff cushion. The important influence of earcanal wall vibration is highlighted when the artificial skin is accounted for. An indirect structure-borne path is identified which corresponds to the radiation of the earplug excited by the earcanal walls.

On the other hand, a transfer matrix model of an ear simulator is proposed based on a direct assessment of its geometric dimensions, and validated through numerical and experimental approaches. Compared to the lumped parameter model commonly used in the literature, this model is shown to accurately account for the thermo-viscous effects in the simulator, and represent its input impedance in a relatively wide frequency range. The transfer matrix model enables to retrieve an equivalent tympanic impedance of the simulator which is imposed as an impedance boundary condition at the "eardrum position" in the finite element model of open and occluded ATF earcanals to simulate the insertion loss of an earplug. Furthermore, a

similar process is adopted to investigate the influence of the eardrum impedance inter-individual variability on the earplug attenuation. This is achieved through a Monte Carlo simulation of 1000 equivalent tympanic impedances obtained by varying the simulator dimensions in the transfer matrix model. The simulation results are deemed representative of the variability in the human eardrum impedance. Representative sets of equivalent tympanic impedance are then selected among these results, and applied as impedance boundary conditions in a finite element model to simulate the earplug insertion loss in a realistic-shaped earcanal. The variability in the equivalent tympanic impedance is shown to induce non-negligible differences in the insertion loss results, indicating that the human eardrum impedance diversity should be accounted for by the ear simulator for earplug attenuation measurements.

Overall, this thesis presents the experimental methodology and numerical models for investigating the ATF vibroacoustic features of interest, and in the long term, could serve as a foundation to guide the design and implementation of ATFs for more realistic characterization of hearing protector attenuation.

Keywords: acoustic test fixture, double hearing protector, ear simulator, finite element modeling, sound attenuation

TABLE OF CONTENTS

Page

INTRODUCTION 1
0.1 Context 1
0.2 Common design of acoustic test fixtures 2
0.3 Research problems 3
0.3.1 Sound attenuation of double hearing protectors 5
0.3.2 Modeling of the ear simulator for the prediction of hearing protector sound attenuation 6
0.4 Research objectives 7
0.4.1 General research objective 7
0.4.2 Specific research objectives 7
0.5 Structure of the thesis 9
0.5.1 Chapter 1: Literature review 9
0.5.2 Chapter 2: Experimental study of earplug noise reduction of a double hearing protector on an acoustic test fixture (article n^{o} 1) 9
0.5.3 Chapter 3: A finite element model to predict the double hearing protector effect on an in-house acoustic test fixture (article n^{o} 2) 10
0.5.4 Chapter 4: A transfer matrix model of the IEC 60318-4 ear simulator: Application to the simulation of earplug insertion loss (article n^{o} 3) 11
0.5.5 Chapter 5: Influence of the inter-individual variability in the eardrum impedance on the earplug insertion loss 11
0.5.6 Conclusion and recommendations 12

CHAPTER 1 LITERATURE REVIEW 13
1.1 Sound attenuation of double hearing protectors 13
1.1.1 Experimental measurements 13
1.1.2 Empirical and numerical modeling 16
1.2 Modeling of the ear simulator for the prediction of hearing protector sound attenuation 18
1.2.1 Analytical and numerical modeling of the ear simulator 19
1.2.2 Simulation of earplug sound attenuation based on the ear simulator acoustic impedance 21

CHAPTER 2 EXPERIMENTAL STUDY OF EARPLUG NOISE REDUCTION OF A DOUBLE HEARING PROTECTOR ON AN ACOUSTIC TEST FIXTURE 23
2.1 Abstract 23
2.2 Introduction 24
2.3 Analytical model of the double hearing protector 28
2.3.1 Transmission paths 28

2.3.2 Prediction of the DHP effect ... 30
2.4 Experimental setup and methodology ... 33
2.4.1 Hearing protection devices of interest ... 33
2.4.2 Acoustical test bench ... 33
2.4.3 Sound attenuation indicators ... 35
2.4.4 Experimental methodology ... 36
2.4.4.1 Acoustical test ... 36
2.4.4.2 Mechanical test ... 41
2.5 Results and discussion ... 42
2.5.1 Assessment of the ATF self-insertion loss ... 42
2.5.2 Observation of the DHP effect ... 43
2.5.3 Contributions of structure-borne paths SB1, SB2 and SB3 ... 44
2.5.4 Contribution of structure-borne path SB4 ... 46
2.5.5 Relative contributions of airborne and structure-borne paths ... 47
2.5.6 Discussion on the DHP effect ... 51
2.6 Conclusion ... 52
2.7 Acknowledgement ... 53

CHAPTER 3 A FINITE ELEMENT MODEL TO PREDICT THE DOUBLE HEARING PROTECTOR EFFECT ON AN IN-HOUSE ACOUSTIC TEST FIXTURE ... 55
3.1 Abstract ... 55
3.2 Introduction ... 56
3.3 Finite element modeling of the DHP/ATF system ... 58
3.3.1 Geometry ... 58
3.3.2 Loading, coupling and boundary conditions ... 60
3.3.3 Material properties ... 62
3.3.4 Meshing and solving ... 63
3.3.5 Calculation of acoustic and vibratory indicators ... 64
3.3.5.1 Sound attenuation indicators ... 64
3.3.5.2 Exchanged powers ... 65
3.4 Experimental setup ... 66
3.5 Results and discussion ... 68
3.5.1 Sound attenuation of hearing protectors ... 68
3.5.1.1 Validation of the finite element model ... 68
3.5.1.2 Analysis of the contribution of the ATF on the DHP effect ... 71
3.5.2 Analysis of the contribution of each sound path using power balances ... 74
3.5.2.1 ATF#1: fully “rigid” ATF ... 75
3.5.2.2 ATF#2: ATF with artificial skin ... 80
3.5.2.3 Summary on power balances ... 85
3.5.3 Discussion ... 87

3.6 Conclusion 88
3.7 Acknowledgement 89

CHAPTER 4 A TRANSFER MATRIX MODEL OF THE IEC 60318-4 EAR SIMULATOR: APPLICATION TO THE SIMULATION OF EARPLUG INSERTION LOSS 91
4.1 Abstract 91
4.2 Introduction 92
4.3 Modeling of the IEC 60318-4 ear simulator 95
4.3.1 Geometry 95
4.3.2 Lumped parameter model 97
4.3.3 Transfer matrix model 99
4.3.4 Finite element model 101
4.4 Modeling of the open and occluded ATF earcanals 102
4.4.1 Insertion loss of the earplug 102
4.4.2 Equivalent tympanic impedance 103
4.5 Experimental measurements 105
4.5.1 Measurements of the IEC 60318-4 ear simulator input impedance 105
4.5.2 Measurements of the earplug insertion loss using an ATF 105
4.6 Results and discussion 106
4.6.1 Input impedance of the IEC 60318-4 ear simulator 106
4.6.2 Equivalent tympanic impedance 110
4.6.3 Insertion loss of the earplug 110
4.7 Conclusion 112
4.8 Acknowledgement 113

CHAPTER 5 INFLUENCE OF THE INTER-INDIVIDUAL VARIABILITY IN THE EARDRUM IMPEDANCE ON THE EARPLUG INSERTION LOSS 115
5.1 Calculation of representative impedance 116
5.2 Finite element modeling of the open and occluded earcanals of realistic geometry 120
5.3 Influence of the eardrum impedance variability on the earplug insertion loss 122

CONCLUSION AND RECOMMENDATIONS 125
6.1 Synthesis of research problems and objectives 125
6.2 Sound attenuation of double hearing protectors: contributions, limitations and perspectives 126
6.2.1 Chapter 2: Experimental study of earplug noise reduction of a double hearing protector on an acoustic test fixture (article n° 1) 126
6.2.2 Chapter 3: A finite element model to predict the double hearing protector effect on an in-house acoustic test fixture (article n° 2) 129
6.3 Modeling of the ear simulator for the prediction of hearing protector sound attenuation: contributions, limitations and perspectives 131

6.3.1 Chapter 4: A transfer matrix model of the IEC 60318-4 ear simulator: Application to the simulation of earplug insertion loss (article n° 3) ... 131
6.3.2 Chapter 5: Influence of the inter-individual variability in the eardrum impedance on the earplug insertion loss ... 133
6.4 General conclusion ... 134

APPENDIX I ACOUSTIC INDICATORS IN THE DOUBLE HEARING PROTECTOR ANALYTICAL MODEL ... 137

APPENDIX II BACKGROUND NOISE COMPARED TO THE SOUND PRESSURE LEVELS IN THE EARCANAL OF CONFIGURATIONS 3.1 AND 4.1 ... 139

APPENDIX III EARPLUG NOISE REDUCTION MEASUREMENT RESULTS OF CONFIGURATIONS 2.2, 2.3 AND 2.4 ... 141

APPENDIX IV COMPARISON BETWEEN THE DOUBLE HEARING PROTECTOR EFFECTS ON AN ACOUSTIC TEST FIXTURE AND A HUMAN SUBJECT ... 143

APPENDIX V SIMULATIONS USING ATF#3 AND ATF#4 ... 147

APPENDIX VI YOUNG'S MODULUS AND LOSS FACTOR OF THE SILICONE CUSHION ... 153

APPENDIX VII INPUT IMPEDANCE OF THE HELMHOLTZ RESONATORS ... 155

BIBLIOGRAPHY ... 158

LIST OF TABLES

Page

Table 2.1 Test matrix for earplug NR measurements: maximum level of the internal source is used for configurations 3.2 and 4.2; five different levels of the internal source are used for configurations 3.3 and 4.3 (referred to as 3.3a – 3.3e and 4.3a – 4.3e) 37

Table 3.1 Key geometric dimensions of the components in the FE model 61

Table 3.2 Mechanical properties of the components in the FE model 63

Table 4.1 Component geometric dimensions of the IEC 60318-4 ear simulator 97

Table 4.2 Parameters of the thermo-viscous fluid 99

LIST OF FIGURES

Page

Figure 0.1 Schematic representation of an IEC 60318-4 ear simulator included in an ATF earcanal 2

Figure 1.1 Conventional lumped TI model derived from the LPM of the IEC 60318-4 ear simulator and its application in the 2D FE model for earplug IL simulation. Adapted from (Viallet, Sgard, Laville & Boutin, 2013) 19

Figure 2.1 Possible sound transmission paths through the DHP/ATF system 29

Figure 2.2 Studied hearing protection devices: (a) silicone earplug; (b) EAR-MODEL-1000 earmuff 33

Figure 2.3 Experimental setup: (a) G.R.A.S. 45CB ATF supported by a tripod; (b) “rigid-walled” earcanal and aluminum plate with a groove 34

Figure 2.4 Schematic representation of test configurations 37

Figure 2.5 Configurations to test the effects of the earmuff headband and the sound transmission through the ATF and its tripod: (a) configuration 2.2, earmuff headband not in contact with the ATF; (b) configuration 2.3, ATF wrapped with soundproof material; (c) configuration 2.4, ATF suspended using bungee cords 38

Figure 2.6 Experimental setup to test structure-borne sound transmission through the earmuff cushion 41

Figure 2.7 Self-IL: required self-IL limit (black dots); measured self-IL of the ATF (blue) 42

Figure 2.8 (a) Earplug NR, (b) ΔNR_{DHP} with reference to the NR of the single earplug (configuration 1) and (c) SPL measured under the earmuff excited by the external source alone: configuration 2.1 (grey), original cushion without foam liner; configuration 3.1 (blue diamonds), original cushion with foam liner; configuration 4.1 (red circles), lead cushion with foam liner. Earplug NR and SPL at the earcanal entrance in the case of single earplug are presented for comparison (black dots). Results are displayed as “mean ± standard deviation” 45

Figure 2.9 Magnitude of the measured accelerance (transfer function between the acceleration on the aluminum plate and force on the earmuff headband) in the cases of the original cushion (blue diamonds) and lead cushion (red circles). Results are displayed as “mean ± standard deviation” 46

Figure 2.10 Earplug NR measured under the earmuff with the original cushion (left) and lead cushion (right): configurations 3.1 & 4.1 (grey), external source alone; configurations 3.2 & 4.2 (blue diamonds), internal source alone (level max); configurations 3.3 & 4.3 (with increasing levels a – e corresponding respectively to purple asterisks, cyan crosses, orange pentagrams, green squares and red circles), external source + internal source (five levels). NR of the single earplug (configuration 1) is presented for comparison (black dots). Results are displayed as “mean ± standard deviation” 48

Figure 2.11 ΔNR_{DHP} with reference to the NR of the single earplug (configuration 1) with the original cushion (left) and lead cushion (right): configurations 3.1 & 4.1 (grey), external source alone; configurations 3.2 & 4.2 (blue diamonds), internal source alone (level max); configurations 3.3 & 4.3 (with increasing levels a – e corresponding respectively to purple asterisks, cyan crosses, orange pentagrams, green squares and red circles), external source + internal source (five levels). Results are displayed as “mean ± standard deviation” 49

Figure 2.12 SPL measured under the earmuff with the original cushion (left) and lead cushion (right): configurations 3.1 & 4.1 (grey), external source alone; configurations 3.2 & 4.2 (blue diamonds), internal source alone (level max); configurations 3.3 & 4.3 (with increasing levels a – e corresponding respectively to purple asterisks, cyan crosses, orange pentagrams, green squares and red circles), external source + internal source (five levels). SPL at the earcanal entrance in the case of single earplug (configuration 1) is presented for comparison (black dots). Results are displayed as “mean ± standard deviation” 50

Figure 3.1 Geometry of the DHP/ATF system (symmetric view): global view (left); earmuff with a silicone cushion (upper right); earplug inserted into the earcanal (lower right) 59

Figure 3.2 Schematic representation of the DHP worn on (a) fully “rigid” ATF#1 and (b) ATF#2 with artificial skin portions (cross-section view) 61

Figure 3.3 Experimental setup adopted to validate the FE model: (a) global view; (b) earmuff with a silicone cushion; (c) earplug inserted into the earcanal 67

Figure 3.4 NRs of the single earmuff measured and simulated using ATF#1: measurement results (averaged value with 95% confidence interval, grey zone); simulation result (blue curve with dots) 69

Figure 3.5 NRs of the earplug measured and simulated using ATF#1: measurement results of the single earplug (averaged value with 95% confidence interval, black zone) and earplug in the DHP (averaged value with 95% confidence interval, grey zone); simulation results of the single earplug (blue dots) and earplug in the DHP (green diamonds) 70

Figure 3.6 Simulation results of (a) earplug NRs: results of the single earplug on ATF#1 (black dots) and ATF#2 (blue diamonds), and results of the earplug in the DHP on ATF#1 (dotted black crosses) and ATF#2 (dotted blue pentagrams); (b) ΔNR_{DHP}: results on ATF#1 (black dots) and ATF#2 (blue diamonds) 73

Figure 3.7 Power balances in the earcanal cavity of ATF#1 for (a) single earplug configuration and (b) DHP configuration: power spectra levels exchanged at the earplug/earcanal cavity interface (red); exchanged at the earcanal lateral walls (blue); exchanged at the earcanal terminal surface (black); dissipated in the earcanal cavity (green). Numbers 1 – 4 correspond to the associated geometric zones where the powers are calculated. Solid line: power flowing into the earcanal cavity; dashed line: power flowing out of (or dissipated in) the earcanal cavity 75

Figure 3.8 Power balances in the earplug in ATF#1 for (a) single earplug configuration and (b) DHP configuration: power spectra levels exchanged at the earplug outer surface (red); exchanged at the earplug/earcanal walls interface (blue); exchanged at the earplug/earcanal cavity interface (black); dissipated in the earplug (green). Numbers 1 – 4 correspond to the associated geometric zones where the powers are calculated. Solid line: power flowing into the earplug; dashed line: power flowing out of (or dissipated in) the earplug 77

Figure 3.9 Power balance in ATF#1 for the DHP configuration: power spectra levels exchanged at the silicone cushion/ATF interface (red); exchanged at the ATF exterior boundaries outside the earmuff (blue); exchanged at the microphone holder/ATF interface (orange); exchanged at the earcanal lateral walls (purple); exchanged at the earplug/earcanal walls interface (cyan); exchanged at the ATF boundaries under the earmuff (black); dissipated in the ATF (green). Numbers 1 – 7 correspond to the associated geometric zones where the powers are calculated. Solid line: power flowing into the ATF; dashed line: power flowing out of (or dissipated in) the ATF 79

Figure 3.10 Power balances in the earcanal cavity of ATF#2 for (a) single earplug configuration and (b) DHP configuration: power spectra levels exchanged at the earplug/earcanal cavity interface (red); exchanged at the earcanal lateral walls (blue); exchanged at the earcanal terminal surface (black); dissipated in the earcanal cavity (green). Numbers 1 – 4 correspond to the associated geometric zones where the powers are calculated. Solid line: power flowing into the earcanal cavity; dashed line: power flowing out of (or dissipated in) the earcanal cavity 81

Figure 3.11 Power balances in the earplug in ATF#2 for (a) single earplug configuration and (b) DHP configuration: power spectra levels exchanged at the earplug outer surface (red); exchanged at the earplug/earcanal walls interface (blue); exchanged at the earplug/earcanal cavity interface (black); dissipated in the earplug (green). Numbers 1 – 4 correspond to the associated geometric zones where the powers are calculated. Solid line: power flowing into the earplug; dashed line: power flowing out of (or dissipated in) the earplug 83

Figure 3.12 Power balance in ATF#2 for the DHP configuration: power spectra levels exchanged at the silicone cushion/ATF interface (red); exchanged at the ATF exterior boundaries outside the earmuff (blue); exchanged at the microphone holder/ATF interface (orange); exchanged at the earcanal lateral walls (purple); exchanged at the earplug/earcanal walls interface (cyan); exchanged at the ATF boundaries under the earmuff (black); dissipated in the ATF (green). Numbers 1 – 7 correspond to the associated geometric zones where the powers are calculated. Solid line: power flowing into the ATF; dashed line: power flowing out of (or dissipated in) the ATF 84

Figure 4.1 Geometry of the IEC 60318-4 ear simulator identified from the CT scan (see Table 4.1 for geometric dimensions) 96

Figure 4.2 LPM of the IEC 60318-4 ear simulator 98

Figure 4.3 Geometry used in the FE model of the IEC 60318-4 ear simulator 101

Figure 4.4 Schematic representation of the FE model to simulate the IL of a silicone earplug. Adapted from (Viallet, Sgard, Laville & Boutin, 2014) 103

Figure 4.5 Geometry used in the complete FE model of an occluded ATF earcanal 104

Figure 4.6 IEC 60318-4 ear simulator input impedance measurements using a sound intensity probe 106

Figure 4.7 Input impedance of the IEC 60318-4 ear simulator obtained using different models: TM model (blue circles), LPM (red asterisks), FE model (dashed black). (top) modulus; (bottom) phase. Averaged simulation result together with the maximal and minimal values are plotted for each analytical model 107

Figure 4.8 Measurement and simulation results of the IEC 60318-4 ear simulator input impedance: sound intensity probe measurements (average ± standard deviation, grey), TM model (blue circles). Numerical verification result of the measurements (dashed black) is also presented. (top) modulus; (bottom) phase. Averaged simulation result together with the maximal and minimal values are plotted for the TM model 109

Figure 4.9 Different equivalent TI models of the IEC 60318-4 ear simulator: model 1 (blue circles), model 2 (red asterisks), model 3 (green squares). (top) modulus; (bottom) phase. Averaged simulation result together with the maximal and minimal values are plotted for each TI model 111

Figure 4.10 IL of the silicone earplug simulated using different equivalent TI models: model 1 (dashed blue circles), model 2 (red), model 3 (green squares). Experimental data (average ± standard deviation, grey) and simulation result using the FE model of the ear simulator (black diamonds) are also presented 112

Figure 5.1 Acoustic impedance at the reference plane measured on human subjects and simulated with the ear simulator TM model: average value (dashed blue curve) plus or minus one standard deviation (blue zone) of the experimental data in (Jønsson, Schuhmacher & Ingerslev, 2018); simulation result using the average simulator geometric dimensions (black curve); Monte

Carlo simulation results of 1000 ear simulators by varying the simulator geometric dimensions (grey curves) 117

Figure 5.2 Equivalent TI results derived from the Monte Carlo simulation of 1000 ear simulators using the RI method (grey curves). Black curve corresponds to the equivalent TI obtained from the simulator input impedance based on its average geometric dimensions. Color curves correspond to the representative maximum (solid curves) and minimum (dashed curves) TI values at 100 Hz (blue curves with circles) and 2 kHz (red curves with squares). Black diamonds and asterisks represent the extreme eardrum impedance experimental data reported in (Rosowski, Davis, Donahue, Merchant & Coltrera, 1990) and (Hudde & Engel, 1998) 119

Figure 5.3 FE model adopted to simulate the IL of a silicone earplug inserted into an earcanal of realistic geometry 121

Figure 5.4 Earplug IL results calculated using the representative maximum (solid curves) and minimum (dashed curves) TI values at 100 Hz (blue curves with circles) and 2 kHz (red curves with squares). Dotted black curve corresponds to the earplug IL obtained with the equivalent TI based on the average simulator geometric dimensions 123

LIST OF ABBREVIATIONS

AB	Airborne
ABS	Acrylonitrile butadiene styrene
ANSI	American National Standards Institute
ATF	Acoustic (or acoustical) test fixture
BC	Bone conduction
CSA	Canadian Standards Association
CT	Computed tomography
DHP	Double hearing protector
EPA	Environmental Protection Agency
FE	Finite element
IEC	International Electrotechnical Commission
IL	Insertion loss
ISO	International Organization for Standardization
ITU	International Telecommunication Union
LPM	Lumped parameter model
LRF	Low reduced frequency
MIRE	Microphone-in-real-ear
NR	Noise reduction
NSERC	Natural Sciences and Engineering Research Council of Canada

PML	Perfectly matched layer
QMA	Quasi-static mechanical analyzer
REAT	Real-ear attenuation at threshold
RI	Reduced impedance
rms	Root mean square
SB	Structure-borne
SD	Standard deviation
SPL	Sound pressure level
TI	Tympanic impedance
TM	Transfer matrix
WHO	World Health Organization

LIST OF SYMBOLS AND UNITS OF MEASUREMENTS

dB	decibel (with suffix A for A-weighted decibel)
Hz	hertz (with prefix k for kilohertz)
in	inch (equivalent to 0.0254 m)
J	joule
K	kelvin
kg	kilogram
lb	pound (equivalent to 0.45359237 kg)
m	meter (with prefix μ, m or c for micrometer, millimeter or centimeter)
N	newton
°	arc degree
°C	degree Celsius
Pa	pascal (with prefix M or G for megapascal or gigapascal)
s	second
ft	foot (equivalent to 0.3048 m)
W	watt

INTRODUCTION

0.1 Context

According to the statistical data of the World Health Organization (WHO), nearly 5% of the world population suffer from disabling hearing loss, and 16% of the disabling hearing loss is attributed to occupational noise (WHO, 2021). Auditory risks, such as occupational hearing loss due to noise exposure constitute a global issue that workers and companies are confronted with. Besides this, noise can cause other health effects, including stress, fatigue, nervousness and increase the risk of accidents at work (Nelson, Nelson, Concha-Barrientos & Fingerhut, 2005).

Occupational noise can be reduced to protect workers by (i) directly controlling noise emitting sources, (ii) isolating the noise along propagation pathways or (iii) taking actions on receivers by requiring workers to wear individual hearing protectors, such as earplugs and earmuffs (Berger & Voix, 2019). This third method remains the most commonly used short-term solution and should be used in last resort when the first two cannot be achieved. Particularly for protecting workers exposed to very high noise levels above 105 dB(A), double hearing protectors (DHPs), namely earplugs combined with earmuffs shall be used (CSA, 2014).

For evaluating the acoustic performance of commercially available or under-development hearing protectors, their sound attenuation can be measured on human subjects subjectively using the real-ear attenuation at threshold (REAT) method or objectively using the microphone-in-real-ear technique (ANSI, 2016, 2020). Alternatively, hearing protector attenuation can also be assessed on an acoustic test fixture (ATF) (ANSI, 2018, 2020), a type of artificial head that comprises an occluded ear simulator inside its earcanal (IEC, 2010; ANSI, 2014; ITU, 2021).

0.2 Common design of acoustic test fixtures

Compared to tests on human subjects, ATFs can provide repeatable results, reduce the testing time and accommodate a large variety of test signals (Berger, 1986; Schroeter, 1986). The common design of ATFs specified in the standard ANSI S12.42 (2020) consists of a manikin which includes the following features: pinnae, artificial earcanals, circumaural and interaural skin simulations, built-in heating system, sufficient self-insertion loss (IL) (Berger, 1986; Berger & Voix, 2019), instrumented occluded ear simulator inside each earcanal, etc. The ATF should be anthropometrically representative of a human head in terms of (i) geometric dimensions, e.g., head and earcanal sizes, and (ii) physical characteristics, such as the mechanical properties of the artificial skin, acoustic impedance at the eardrum (also called tympanic membrane) and temperature in the earcanal.

The ATF earcanal always embeds an occluded ear simulator which complies with the standard IEC 60318-4 (2010). If not otherwise specified, the term "ear simulator" in this thesis refers to

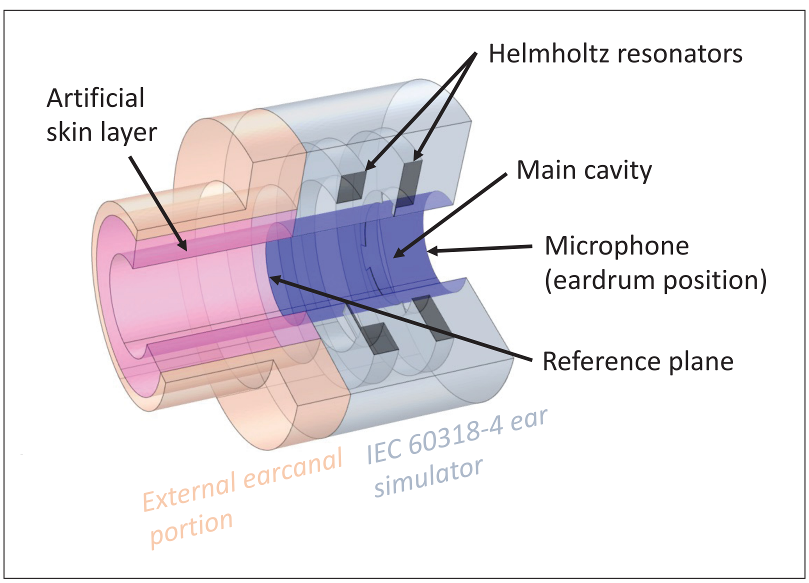

Figure 0.1 Schematic representation of an IEC 60318-4 ear simulator included in an ATF earcanal

the IEC 60318-4 ear simulator (formerly known as the IEC 711 ear simulator). It is designed such that in its working frequency range from 100 Hz to 10 kHz, its input acoustic impedance at a reference plane located at some distance ahead of the eardrum position closely resembles that of the occluded human earcanal (Lavergne, Rodrigues, Neimanns, Olsen & Barham, 2013; Rodrigues *et al.*, 2015a). The general design of the IEC 60318-4 ear simulator (see Fig. 0.1) includes (i) a cylindrical main cavity mimicking the inner portion of the earcanal, (ii) side volumes connected to the main cavity via narrow slits and (iii) a microphone at the terminal of the ear simulator where the recorded sound pressure should correspond to that perceived at the eardrum of an average human ear (Brüel, Frederiksen, Mathiasen, Rasmussen & Sigh, 1976; Jønsson, Liu, Nielsen & Schuhmacher, 2003; Jønsson, Liu, Schuhmacher & Nielsen, 2004). Especially, each side volume and the related narrow slit constitute a Helmholtz resonator. These resonators mimic the acoustic effects of the middle and inner ears on the earcanal cavity.

0.3 Research problems

ATF measurements can provide a quick assessment for product development and quality assurance of hearing protectors, and are particularly preferred for tests in high level impulsive noise where no test on human subjects is performed for ethical reasons (Kunov & Giguère, 1989; Berger & Voix, 2019). But as mentioned in (Nixon, McKinley & Steuver, 1992; ANSI, 2020), ATF measurement results cannot be used as a substitute for REAT attenuation values in a hearing protection program. Moreover, Williams (2012) has pointed out that ATFs tend to lead to a greater amount of protection than REAT tests. This indicates that the current design of ATFs specified in ANSI S12.42 (2020) is not realistic enough to closely capture the subjective sound attenuation associated with all types of hearing protectors and their fitting on a large majority of human subjects (Berger, 2005). More specifically, standardized ATFs may suffer from some limitations. First, the bone conduction (BC) is not supposed to be incorporated into the design of ATFs (Schroeter & Poesselt, 1986; Williams, 2012; Berger & Voix, 2019). It is commonly taken into account as a post-measurement mathematical correction (ANSI, 2020) such that:

$$A_{\text{BC-corrected}} = -10\log_{10}(10^{-A_{\text{uncorrected}}/10} + 10^{-BCL/10}), \tag{0.1}$$

where $A_{\text{BC-corrected}}$, $A_{\text{uncorrected}}$ and BCL correspond respectively to (i) the corrected attenuation of hearing protectors with the contribution of BC paths accounted for, (ii) the uncorrected attenuation obtained directly from the ATF, and (iii) the BC limit suggested by Berger *et al.* (2003a). Current ATFs are generally fabricated in rigid and dense materials to ensure that the airborne (AB) sound transmission in the system dominates over the structure-borne (SB) transmission (Parmentier, Dancer, Buck, Kronenberger & Beck, 2000). The latter could correspond to the vibratory energy transmitted through the ATF exterior boundaries (e.g., due to external acoustic stimulation) or through its support (e.g., as a result of room floor vibration) to the earcanal. However, for systems with a sufficiently high AB attenuation where SB transmission cannot be neglected such as DHPs (see Sec. 0.3.1), the construction of ATFs, including their geometry and materials should be adequately representative of the vibroacoustic behaviors of the human head and auditory system. Second, current ATFs do not account for the inter-individual variability in the human physical characteristics. For instance, the ear simulators in the ATF earcanals are only designed based on an average acoustic impedance measured in a group of human ears (see Sec. 0.3.2). It remains unclear (i) how the variability of the human ear impedance affects the acoustic performance of hearing protectors, and (ii) if multiple ear simulators would be necessary to grasp such a variability.

If a more realistic characterization of hearing protector sound attenuation is expected, certain aspects of the current design of ATFs need to be further investigated. In addition to experimental measurements, numerical modeling remains a good approach for efficiently evaluating the influence of some design features of ATFs while allowing for a better understanding of the related physical mechanisms. This research project seeks to experimentally and numerically address two primary problems concerning the vibroacoustic features of ATFs:

1. How the AB and SB sound transmissions are actually involved in a DHP coupled to an ATF?
2. What is the appropriate acoustic impedance of the ear simulator that should be used for measuring the hearing protector attenuation on ATFs, and should the inter-individual variability in the eardrum impedance be accounted for?

The associated specific research problems identified through a detailed literature review (see Chapter 1) are summarized in the two following subsections.

0.3.1 Sound attenuation of double hearing protectors

The sound attenuation of DHPs is difficult to predict as it is not simply equal to the algebraic sum of each single protector's attenuation when used independently but generally less (e.g., Berger, 1983; Berger *et al.*, 2003a). This phenomenon is referred to as the DHP effect in the thesis. In the literature, it has been related to certain BC paths involved in the system that bypass the AB path: (i) the sound transmitted through the head and body directly to the middle and inner ears, and (ii) the outer ear BC path which involves both the hearing protectors and earcanal together with its surrounding tissues. The AB path[1] corresponds to the direct sound transmission into the earcanal through the earmuff, the air cavity enclosed by the earmuff and the earplug. However, currently the DHP effect is poorly understood. Especially, the exact contribution of the outer ear BC path still remains unclear. Besides being seen on human subjects, this effect can also be observed on ATFs and characterized by the decrease of the earplug noise reduction (NR) (Berger, 1986; Berger & Voix, 2019) after adding the earmuff (Nélisse, Sgard, Gaudreau & Padois, 2017). Again, it is suspected to originate from the flanking SB sound transmission through the system

[1] This convention of the "direct" AB sound path is adopted throughout the thesis.

rather than the AB transmission, but the related sound paths have never been systematically investigated through experimental measurements. In addition, there is no available numerical model that can predict the DHP overall attenuation from its components and help understand the associated physical mechanisms. More specifically, numerical models of the DHP/human head system cannot be found in the literature in view of the complexity of the system. The only existing models of the DHP/ATF system based on the finite element (FE) method could not be validated against experiments because of large discrepancies found between the simulated and measured DHP attenuation (James, 2006; Nélisse *et al.*, 2017). Particularly, a few “anatomically-correct” artificial heads have been designed or fabricated in the literature to replicate the contribution of BC paths (e.g., Clavier, Wismer, Wilbur, Dietz & O’Brien, 2010b; Norris, Chambers, Kattamis, Davis & Bieszczad, 2012; Sgard *et al.*, 2018), but so far none of them has been adopted to study the sound transmission through a DHP.

0.3.2 Modeling of the ear simulator for the prediction of hearing protector sound attenuation

According to (Schroeter & Poesselt, 1986), the eardrum impedance needs to be accurately reproduced by the ear simulator for measuring the sound attenuation of earplugs, whereas it does not have a significant influence on the attenuation of earmuffs. As previously explained, the occluded ear simulators specified in the standard IEC 60318-4 (2010) are commonly designed to represent the average acoustic impedance measured in the earcanals of a panel of subjects. It still remains to be elucidated whether these ear simulators prove adequate for earplug attenuation measurements regarding the large inter-individual variability in the human eardrum impedance (e.g., Hudde, 1983; Jønsson *et al.*, 2018). Moreover, current ear simulators do not only reproduce the acoustic impedance at the eardrum but also include an earcanal portion mimicked by a main cavity. This main cavity is simply cylindrical-shaped of circular cross-section which does not have a realistic geometry. For numerically predicting the IL of earplugs inserted into an ATF earcanal in a FE model accounting for the length added by the ear simulator (Viallet *et al.*, 2013, 2014), the latter has been modeled as a cylindrical cavity terminated by an equivalent tympanic impedance (TI). The equivalent TI was determined by eliminating the components associated with the earcanal portion from a classical lumped parameter model (LPM) of the ear simulator. However, such a TI model seems not mathematically rigorous. In addition, the LPM has been commonly accepted to have inherent frequency limitations and cannot accurately describe the thermal and viscous energy losses within the narrow regions of the ear simulator (e.g., Jønsson *et al.*, 2004). The published ear simulator numerical models which can better deal with thermo-viscous effects often lack essential geometric details, and most related studies also suffer from the lack of experimental validations (e.g., Jønsson *et al.*, 2004; Sasajima, Yamaguchi, Watanabe & Koike, 2015).

0.4 Research objectives

0.4.1 General research objective

As an initial step towards ultimately improving the current design of ATFs, this doctoral research project mainly focuses on investigating the potential influence of some ATF design features related to (i) the sound attenuation prediction of DHPs which involves SB transmission through the ATF, and (ii) the impact of ear simulator acoustic impedance on the hearing protector attenuation. Prospectively, this work could serve as a foundation to guide the design and implementation of ATFs for more realistic characterization of hearing protector attenuation.

0.4.2 Specific research objectives

According to the problems summarized in Sec. 0.3, the specific research objectives concerning the two aspects of the general objective presented in the preceding subsection are defined and outlined as follows:

1. **Specific objective 1**: To study the DHP effect on an ATF (characterized by the earplug NR decrease after adding the earmuff) through experimental measurements and numerical modeling for better understanding the associated sound transmission mechanisms and improving the prediction of DHP attenuation. This is achieved through the two sub-objectives below:
   a. **Sub-objective 1.1**: To propose an experimental methodology for identifying the main sound transmission paths related to the DHP effect on a standardized commercial ATF. Attempts are made to explain this effect by the relative contributions of the AB and SB transmissions through the system. This also helps target the correct level of modeling for each component in numerical analysis.
   b. **Sub-objective 1.2**: To develop and experimentally validate a numerical model based on the FE method for predicting the DHP effect on an ATF and quantifying the contribution of each sound path involved in the system. Particularly, an in-house ATF with a simple geometry is used for more easily accounting for essential components identified from the experimental analysis carried out for sub-objective 1.1.
2. **Specific objective 2**: To investigate the influence of the IEC 60318-4 ear simulator impedance on the prediction of hearing protector sound attenuation on ATFs. As the ear simulator impedance is relatively important for assessing the attenuation of earplugs, attention is paid to simulating the IL of an earplug based on the modeling of the ear simulator. This is of additional interest for studying the impact of the inter-individual variability in the eardrum impedance on the earplug IL. The realization of this objective includes the three following steps:
   a. **Sub-objective 2.1**: To develop and experimentally validate a novel modeling approach of a commercial ear simulator based on a direct assessment of its geometric dimensions which should (i) accurately account for the thermo-viscous effects in the simulator, (ii)

represent its input acoustic impedance in a wide frequency range and (iii) allow for easily performing parametric studies on the eardrum impedance variability.

b. **Sub-objective 2.2**: To propose a model of equivalent TI based on the ear simulator impedance model developed for sub-objective 2.1, and to simulate the IL of an earplug inserted into an ATF earcanal using the proposed TI model.

c. **Sub-objective 2.3**: To study the influence of the eardrum impedance variability on the IL of an earplug inserted into an earcanal of realistic geometry with the method proposed for sub-objective 2.2 by further exploiting the ear simulator model.

0.5 Structure of the thesis

0.5.1 Chapter 1: Literature review

The literature review provided in Chapter 1 establishes the state-of-the-art on the two primary research topics concerned in this project. First, experimental studies carried out to measure the sound attenuation of DHPs on both real ears and ATFs are reviewed. The potential sound transmission paths that could be related to the DHP effect are discussed. Empirical and numerical models which have attempted to predict the DHP attenuation are also presented along with their limitations. Second, past modeling work (both analytical and numerical) of the IEC 60318-4 ear simulator impedance is reviewed. Additionally, a numerical approach proposed in the literature to simulate the earplug attenuation in an ATF earcanal based on the classical LPM of the ear simulator is discussed.

0.5.2 Chapter 2: Experimental study of earplug noise reduction of a double hearing protector on an acoustic test fixture (article n° 1)

Chapter 2 consists of a research article entitled “Experimental study of earplug noise reduction of a double hearing protector on an acoustic test fixture” published in *Applied Acoustics*. This chapter analyzes the main sound paths related to the DHP effect on a commercial ATF from an experimental point of view (sub-objective 1.1). The focus is put on measuring the NRs of the earplug alone and in the DHP. First, the potential influence of several SB sound paths through the ATF to its earcanal, and originating from the earmuff headband or ATF tripod is investigated by modifying the system coupling conditions. Second, the relative contributions of the direct AB path and possible flanking SB paths are studied by controlling the sound pressure level under the earmuff with a tiny loudspeaker placed beneath the earcup. Particular attention is paid to highlight the SB transmission through the earmuff comfort cushion with the help of a lead cushion. This work also provides the grounds for developing a numerical model to predict the DHP effect on an ATF, which constitutes the objective of Chapter 3. Additionally, following the experimental analysis of Chapter 2, a preliminary work is carried out which attempts to further evaluate the influence of SB transmission by comparing the DHP effect on the ATF to that measured on a human subject (see Appx. IV).

0.5.3 Chapter 3: A finite element model to predict the double hearing protector effect on an in-house acoustic test fixture (article n° 2)

Chapter 3 consists of a research article entitled “A finite element model to predict the double hearing protector effect on an in-house acoustic test fixture” submitted for publication in *Journal of the Acoustical Society of America*. This chapter is a continuation of Chapter 2 and proposes a 3D FE model to predict the DHP effect on an ATF (sub-objective 1.2). An in-house ATF with a geometry simpler than a commercial one is used for more easily accounting for essential components in the model. In addition, the comfort cushion of the earmuff is replaced with a silicone cushion of identical shape for better capturing its vibroacoustic behavior. First, the FE model is validated by means of NR measurements of the single earmuff, single earplug and earplug in the DHP in a diffuse sound field. Second, the model is exploited to calculate the power balances using selected configurations of the in-house ATF in order to (i) quantify the contribution of each sound transmission path, and study the effects of (ii) the artificial skin and (iii) the acoustic excitation on the ATF exterior boundaries.

0.5.4 Chapter 4: A transfer matrix model of the IEC 60318-4 ear simulator: Application to the simulation of earplug insertion loss (article n^{o} 3)

Chapter 4 contains a research article entitled "A transfer matrix model of the IEC 60318-4 ear simulator: Application to the simulation of earplug insertion loss" published in *Acta Acustica united with Acustica*. In this chapter, a transfer matrix (TM) model of a commercial IEC 60318-4 ear simulator is proposed based on the geometric dimensions assessed from computed tomography scan images (sub-objective 2.1). The thermo-viscous effects in the ear simulator are accounted for using the low reduced frequency approximation. First, the TM model is validated (i) using a FE model of the corresponding system and (ii) against measurements performed with a sound intensity probe. Second, an equivalent TI is derived from the TM model and used as a terminal impedance boundary condition in the FE model of an occluded ATF earcanal to simulate the IL of an earplug (sub-objective 2.2). The simulation result is compared to (i) that obtained using the equivalent TI retrieved from the ear simulator LPM and (ii) experimental data on an ATF.

0.5.5 Chapter 5: Influence of the inter-individual variability in the eardrum impedance on the earplug insertion loss

Chapter 5 is a complement of Chapter 4 where the TM model of the ear simulator is further exploited to investigate the potential influence of the variability in the equivalent TI on the IL of an earplug (sub-objective 2.3). This is achieved through a Monte Carlo simulation to calculate the TI values of 1000 ear simulators by varying the simulator geometric dimensions in the TM model. The Monte Carlo simulation results are deemed to be representative of the inter-individual variability in the human eardrum impedance. Two representative sets of equivalent TI are selected among these results and used as impedance boundary conditions in a FE model to simulate the corresponding earplug IL values. Particularly, instead of the ATF earcanal considered in Chapter 4, the FE model of a realistic-shaped earcanal surrounded by a skin layer is used for the IL simulation.

0.5.6 Conclusion and recommendations

The final chapter covers a synthesis of the work carried out in this thesis. The main contributions and limitations of the preceding chapters in connection with the specific research objectives are presented. Some future recommendations and perspectives are put forward. Finally, a brief general conclusion is provided which lists the potential scientific and technological impacts of the research project.

CHAPTER 1

LITERATURE REVIEW

1.1 Sound attenuation of double hearing protectors

A double hearing protector (DHP) typically provides greater protection than either of the single protectors involved (von Gierke, 1956; Dancer, Lataye & Damongeot, 1988; Berger & Voix, 2019). But double protection is a complex process, and the combined sound attenuation is not simple to predict (Mercy, Tubb & James, 2005). It generally falls short of the algebraic sum of each single protector's attenuation when used independently. This phenomenon corresponds to what is referred to as the DHP effect in the thesis (see Sec. 0.3.1). Both experimental and modeling studies have been published on assessing the DHP attenuation. These studies are reviewed in detail in the two following subsections.

1.1.1 Experimental measurements

Many past investigations have been interested in measuring the DHP attenuation on human subjects using the real-ear attenuation at threshold (REAT) or microphone-in-real-ear (MIRE) method. Most of them, such as (Berger, 1983; Abel & Armstrong, 1992; Behar & Kunov, 1999; Berger *et al.*, 2003a), have noticed the DHP effect. In the literature, this effect has been related to certain bone conduction (BC) paths in the system. Some studies have found that changing the combinations of earplugs and earmuffs can hardly improve the DHP attenuation measured subjectively at medium and high frequencies above 2 kHz (Berger, 1983; Berger *et al.*, 2003a; Mercy *et al.*, 2005; Tubb, Mercy & James, 2005; Du, Homma & Saunders, 2008). They concluded that in this frequency range, the DHP attenuation already reaches the limit imposed by the sound transmitted through the BC paths via the head and body directly to the middle and inner ears (Khanna, Tonndorf & Queller, 1976). This phenomenon has been further exhibited by some other works which achieved additional gains in the REAT results at frequencies above 1 – 2 kHz when shielding the subject's head from external acoustic stimulation (Nixon & von Gierke, 1959; Berger *et al.*, 2003a). Moreover, several studies have compared the REAT and MIRE results, and found significant differences between them around 2 kHz (Berger & Kerivan, 1983) and above 1.4 kHz (Ravicz & Melcher, 2001). This again indicates the fact that an important amount of acoustic energy directly reaches the middle and inner ears in the corresponding frequency range while bypassing the earcanal.

For the frequency range below 2 kHz, several studies have pointed out that when a DHP is worn, the primary BC path should be through the head to the walls of the earcanal (outer ear BC path) which vibrate and reradiate the sound (Berger, 1983; Berger *et al.*, 2003a; Mercy *et al.*, 2005; Tubb *et al.*, 2005; Mercy & James, 2011) probably due to the fundamental mechanisms of the occlusion effect (Stenfelt, Wild, Hato & Goode, 2003; Stenfelt & Goode, 2005). The radiated sound would be transmitted along the earcanal and finally to the middle and inner ears. Consistently, as mentioned in (Reinfeldt, Stenfelt, Good & Håkansson, 2007), the DHP attenuation measured in this frequency range actually includes the occlusion effect. Unfortunately, the real contribution of the latter to the DHP effect still remains unclear.

Mercy *et al.* (2005) and Tubb *et al.* (2005) have measured the sound attenuation of an active noise reduction earmuff both singly and in combination with a passive earplug using the MIRE method. The DHP effect was well observed by these authors, but the earmuff attenuation was found to remain the same with and without the earplug regardless of whether the active noise reduction mode was turned on or off. They hypothesized that there should be a coupling between the earplug and earmuff which modifies the overall attenuation achieved by the DHP. Besides, a number of related studies have also talked about the potential coupling between the earplug and earmuff in the DHP (Zwislocki, 1957; Berger, 1983; Ravicz & Melcher, 2001; Reinfeldt *et al.*, 2007; Mercy & James, 2011). According to these studies, the earplug and earmuff may be coupled acoustically through the air cavity under the earmuff, and mechanically through the tissues of the human head and ear. However, to the author's knowledge, there is still no evidence for supporting these hypotheses, and the related sound paths have never been explicitly analyzed in the literature. It is interesting to mention that Gorman (1982) has developed a lumped model to study the sound attenuation of an earmuff. In addition to the aforementioned outer ear BC path directly excited by external acoustic stimulation, another BC path has been accounted for by this model which corresponds to the sound transmission to the earcanal walls through the comfort cushion of the earmuff and the head due to the vibration of the earcup. The author found that this BC path can be significantly enhanced below about 1 kHz if the earcanal is occluded by an earplug, which limits the combined attenuation of the earplug and earmuff. But the model was not validated through experimental measurements, and the associated behaviors have not yet been verified by later research in the literature. Moreover, such a lumped model is limited to low frequency bands, and the high frequency behavior of the system still needs to be further investigated.

More recently, MIRE experiments have been conducted by Nélisse *et al.* (2017) to measure the noise reduction (NR) of earplugs alone and in combination with earmuffs. Nine different combinations of earplugs and earmuffs were tested. The authors confirmed the finding of (Mercy *et al.*, 2005; Tubb *et al.*, 2005) that the presence of earplugs does not significantly affect the measured attenuation of earmuffs. However, the earplug NR was found to decrease dramatically by up to about 40 dB when earmuffs were worn in combination, and such a decrease was observed in nearly the whole frequency range of interest from 125 Hz to 8 kHz. This suggests that the outer ear BC path is actually involved in the DHP effect, and its contribution seems to be important in a wide frequency band (even above 2 kHz). In addition, this work also demonstrates the earplug NR to be a good indicator for characterizing the DHP effect and studying its cause. Particularly, the same measurements were repeated by the authors on a commercial acoustic test fixture (ATF) and a similar phenomenon was discovered, indicating that the DHP effect manifests itself on both real ears and ATFs. However, standardized ATFs are not really designed to account for the BC paths of the middle and inner ears (Schroeter & Poesselt, 1986; Williams, 2012; Berger & Voix, 2019), and they are supposed to have a self-insertion loss (IL) much higher than the BC limit of human subjects (ISO, 2007; ANSI, 2018, 2020). The main sound paths that can explain the DHP effect on ATFs still remain to be identified regarding the apparent differences between ATFs and human subjects.

Particularly, "anatomically-correct" artificial heads have been designed or physically fabricated in a few studies to more or less account for the contribution of BC paths (Clavier *et al.*, 2010a; Clavier *et al.*, 2010b; Norris *et al.*, 2012; Sgard *et al.*, 2018; Xu, Sgard, Wagnac & De Guise, 2019). These artificial heads do not only have full head geometries reconstructed from computed tomography or magnetic resonance imaging datasets of human subjects, but also include components that mimic anatomical features of the human head, such as skull, brain and skin simulation parts. But none of them has ever been adopted to investigate the sound transmission paths related to the DHP effect.

1.1.2 Empirical and numerical modeling

Various empirical models have been put forward to predict the overall sound attenuation of DHPs. A rule of thumb has been proposed in (CSA, 2014) which states that a 5 dB correction factor should be added to the noise reduction rating (EPA, 1979) provided by the better of the two single protectors to estimate that of the DHP. Other studies have compared the DHP total attenuation with the individual attenuation of single protectors on either human subjects or ATFs (Behar, 1991; Behar & Kunov, 1999; Abel & Odell, 2006; Gallagher, Bjorn & McKinley, 2010; Byrne & Murphy, 2016). They pointed out that the 5 dB rule of thumb is inaccurate, and found that the correction factor actually covers a quite wide range of values depending on the combinations of earplugs and earmuffs (e.g., 2 – 14 dB reported in (Behar & Kunov, 1999)). Moreover, an empirical formula has been derived by Damongeot *et al.* (1989) from the measured attenuation of single protectors in order to calculate the global attenuation of DHPs. However, this formula cannot describe the detailed DHP attenuation as a function of frequency, and it is based on a simple regression of single protector attenuation which does not contribute to the understanding of the system physical mechanisms.

Berger (1983) has proposed an equation in the same form as Eq. (0.1) to predict the DHP attenuation as a function of frequency which depends on (i) the algebraic sum of the earplug attenuation and earmuff attenuation (equivalent to $A_{\text{uncorrected}}$ in Eq. (0.1)), and (ii) the attenuation limit imposed by the BC paths estimated using a deeply inserted foam earplug and a lead earmuff

(*BCL* in Eq. (0.1)). This equation is based on two hypotheses. First, the DHP is assumed to be a decoupled system where the attenuation achieved by the earplug and earmuff can be summed up directly. Second, the BC paths are considered to be incoherent with the airborne (AB) sound transmission through the hearing protectors. Compared to experimental data, even though the predictions based on the equation proved to be satisfactory at frequencies above 2 kHz, errors of as much as 13 dB were found at lower frequencies. The author has related these errors to the potential coupling between the earplug and earmuff in the corresponding frequency range which conflicts with the decoupled assumption but without providing any convincing evidence. In addition, as mentioned in Sec. 1.1.1, the DHP attenuation measured at low frequencies actually includes the occlusion effect which depends on the hearing protectors used and their fit (Berger & Kerivan, 1983; Reinfeldt *et al.*, 2007). It seems not rigorous enough to predict the attenuation of various DHPs with different fitting conditions (e.g., various earplug insertion depths) using the BC limit estimated with a specific DHP (i.e., deeply inserted foam earplug/lead earmuff).

Numerical modeling remains another interesting and powerful approach for predicting the DHP attenuation since all the vibroacoustic behaviors of the components involved in the system can be accurately accounted for. However, available numerical models of DHPs are scarce. James (2006) has developed a finite element (FE) model of a DHP placed on a particle board box in order to study the major behavioral mechanisms related to its noise insulation performance. Soft elastomeric components were used for certain parts of the box to mimic the interactions between the skin and earplug, and between the skin and earmuff comfort cushion. The FE model has shown that the majority of the sound pressure in the earcanal results from the vibration of the earplug, earmuff and structures between them while the air cavity enclosed by the earmuff does not have an important contribution. However, this work failed to validate the model against experimental measurements as discrepancies of up to about 40 dB were observed between the simulated and measured DHP attenuation. The author claimed that these discrepancies could be explained by the vibration of the system components incompletely accounted for in the model, such as the base structure which was simply modeled as a rigid boundary condition. More recently, Nélisse *et al.* (2017) have combined the FE models of an earplug (Viallet, 2014; Viallet *et al.*, 2014) and an earmuff (Boyer, 2015; Carillo, Sgard & Doutres, 2018) in order to predict the sound attenuation of a DHP fixed over a commercial ATF. All the acoustical couplings involved in the system were taken into account in this model but the ATF was considered to be acoustically rigid. This means that (i) there was no direct structure-borne (SB) sound transmission through the ATF into its earcanal, and (ii) the earplug and earmuff could not be coupled mechanically via the ATF components between them. Again the FE model could not be experimentally validated as significant differences between the simulation and measurement results were found. Particularly, the model failed to reproduce the DHP effect observed in the experiments using the corresponding setup. This suggests that the DHP effect on ATFs is associated with the SB sound transmission through the system and not the AB transmission, which still needs to be further investigated.

1.2 Modeling of the ear simulator for the prediction of hearing protector sound attenuation

It is believed that the acoustic impedance at the eardrum must be taken into account in ATFs for correctly assessing the sound attenuation of intra-aural devices, such as earplugs (Schroeter & Els, 1982; Schroeter & Poesselt, 1986; Hammershøi & Møller, 1996; Bockstael *et al.*, 2008). Particularly, with the help of a mathematical model of the earcanal, Schroeter & Poesselt (1986) have pointed out that the eardrum impedance is not crucial for assessing the sound attenuation of earmuffs while it has an important effect in the case of earplugs. In addition, some experimental studies have shown that the eardrum impedance measured in real ears may vary significantly from one person to another (Hudde, 1983; Rosowski *et al.*, 1990; Hudde & Engel, 1998; Jønsson *et al.*, 2018). However, standardized occluded ear simulators are commonly designed to represent an average acoustic impedance measured in the earcanals of a panel of human subjects (IEC, 2010; Lavergne *et al.*, 2013; Rodrigues *et al.*, 2015b). There is still doubt whether the earplug attenuation obtained on ATFs using these ear simulators is representative of a large majority of the population given the important inter-individual variability in the eardrum impedance.

1.2.1 Analytical and numerical modeling of the ear simulator

The IEC 60318-4 ear simulator is normally designed based on a classical lumped parameter model (LPM, see Fig. 1.1) which assimilates the ear simulator as an equivalent electrical circuit (Jønsson *et al.*, 2003, 2004; Bech, 2007). Each component in the electrical circuit (e.g., electrical inductance, capacitance or resistance) corresponds to an acoustic element of the ear simulator (e.g., acoustic mass, compliance or resistance). The LPM parameters are tuned in a manner that the input impedance of the simulator matches the average acoustic impedance measured in a group of human ears. Such an analytical model has the advantage of easily performing parametric studies for efficiently evaluating different designs of the ear simulator at an early stage (Hiipakka, 2008; Sasajima *et al.*, 2015). However, the LPM has some main drawbacks.

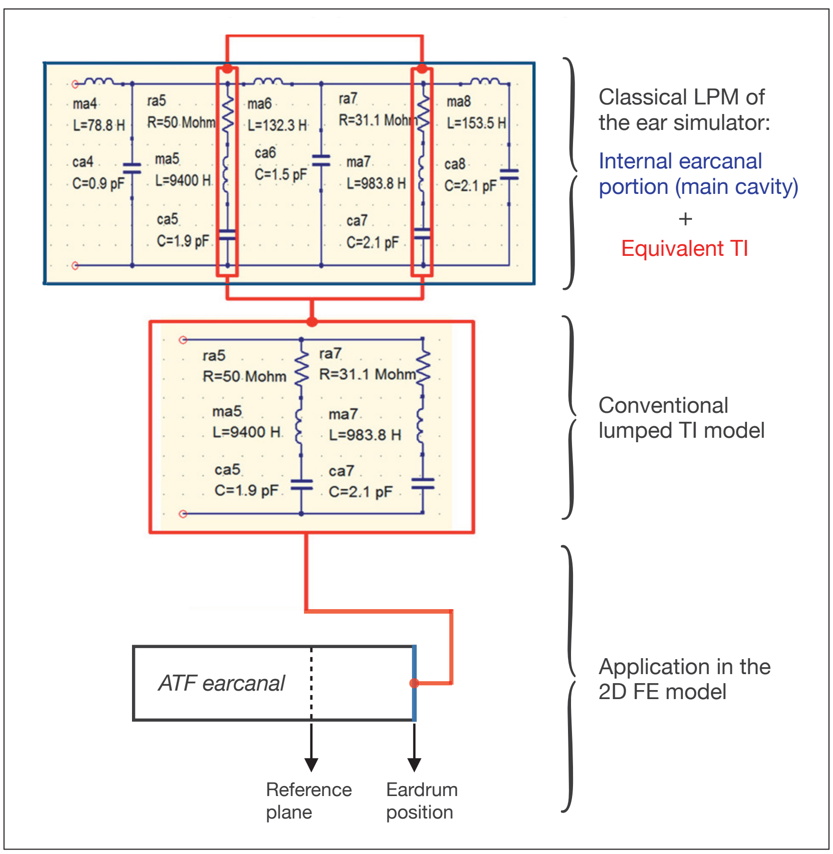

Figure 1.1 Conventional lumped TI model derived from the LPM of the IEC 60318-4 ear simulator and its application in the 2D FE model for earplug IL simulation. Adapted from (Viallet *et al.*, 2013)

First, it has been commonly recognized to be restricted to the low frequency range. Second, the thermal and viscous phenomena in the narrow areas (Bruneau, Bruneau, Herzog & Kergomard, 1987; Bruneau, Herzog, Kergomard & Polack, 1989) of the ear simulator are not negligible, but the LPM cannot appropriately deal with these phenomena (Jønsson *et al.*, 2004; Bravo *et al.*, 2008, 2012).

Alternatively, certain studies have been carried out to model the IEC 60318-4 ear simulator based on the FE or boundary element method (Jønsson *et al.*, 2003, 2004; Sasajima *et al.*, 2015; Sasajima, Yamaguchi, Hu & Koike, 2016; COMSOL, 2017). Compared to the classical LPM, these models allow for better handling thermo-viscous effects, and correctly simulating the wideband acoustic impedance of the ear simulator in its working frequency range from 100 Hz to 10 kHz (IEC, 2010; Rodrigues *et al.*, 2015a). However, to the author's knowledge, the simulations based on these models were only compared with the experimental impedance tolerances of human earcanals given in the standards (IEC, 2010; ANSI, 2014; ITU, 2021), and none of them has been experimentally validated against measurements on the corresponding ear simulators. Moreover, the essential information related to many key geometric features of the ear simulator was left unspecified in these studies, which makes it difficult for later researchers to reproduce their results. It is worth mentioning that Bravo and his colleagues have proposed a FE model of another type of ear simulator which complies with the standard IEC 60318-1 (2009) based on a direct assessment of the simulator geometric inputs using an X-ray inspection system (Bravo *et al.*, 2008, 2012). The model was validated against transfer impedance measurements on a commercial ear simulator of the same type. But this type of simulator is specifically designed for supra-aural or supra-cocha devices which does not allow for evaluating the attenuation of earplugs, and is not incorporated into the design of standardized ATFs. A comprehensive literature review of different types of ear simulators can be found in (Rodrigues *et al.*, 2015a).

1.2.2 Simulation of earplug sound attenuation based on the ear simulator acoustic impedance

Only a few numerical studies in the literature have focused on the prediction of earplug attenuation on ATFs (Sgard *et al.*, 2010; Viallet *et al.*, 2013, 2014; Viallet, 2014). These studies have proposed a 2D axisymmetric FE model to simulate the IL of earplugs inserted into an ATF earcanal accounting for the length added by the IEC 60318-4 ear simulator. In practice, the latter does not only reproduce the acoustic impedance at the eardrum but also includes the inner portion of the earcanal mimicked by a cylindrical main cavity (Brüel *et al.*, 1976; Jønsson *et al.*, 2004; IEC, 2010). This main cavity cannot be removed from the ear simulator and does not have a realistic geometry. In the 2D FE model, the ear simulator was considered as a cylindrical air cavity with an equivalent tympanic impedance (TI) imposed as a terminal impedance boundary condition at the end of the cavity (see Fig. 1.1). This allowed for simulating the sound pressure at the real microphone position in the ATF earcanal (located at the end of the ear simulator) and not at the reference plane (located at the entrance of the ear simulator). As originally proposed by Jønsson *et al.* (2003, 2004), the equivalent TI was derived from the classical LPM of the ear simulator by directly eliminating the lumped components which assimilate the earcanal portion. The use of this lumped TI model still remains questionable due to the aforementioned drawbacks of the LPM. Additionally, it seems not mathematically rigorous to represent the equivalent TI by directly extracting certain elements from the analogous electrical circuit of the ear simulator. Several studies in the literature have adopted the reduced impedance[1] method (Chaigne, 2001) to retrieve the acoustic impedance at the eardrum from that assessed at a reference plane in the earcanal using a chain matrix of the latter (Hudde, 1983; Larson, Nelson, Cooper & Egolf, 1993; Rodrigues *et al.*, 2015a,b). It proves to be a reliable approach even for human earcanals with complex geometries, and has not yet been used to determine the equivalent TI of the IEC 60318-4 ear simulator.

[1] In the literature, this is sometimes referred to as “propagated impedance”, such as in (Jønsson *et al.*, 2018). The term “reduced impedance” is used throughout the thesis.

The key points and main research problems identified from the literature review in this chapter regarding (i) the sound attenuation prediction of DHPs, and (ii) the influence of the ear simulator impedance on the hearing protector attenuation are all summarized in Sec. 0.3.

CHAPTER 2

EXPERIMENTAL STUDY OF EARPLUG NOISE REDUCTION OF A DOUBLE HEARING PROTECTOR ON AN ACOUSTIC TEST FIXTURE

Yu Luan[a] , Olivier Doutres[a] , Hugues Nélisse[b] , Franck Sgard[b]

[a] Department of Mechanical Engineering, École de Technologie Supérieure,
1100 Rue Notre-Dame Ouest, Montreal, Quebec H3C 1K3, Canada

[b] Direction Scientifique, Institut de recherche Robert-Sauvé en santé et en sécurité du travail,
505 Boulevard de Maisonneuve Ouest, Montreal, Quebec H3A 3C2, Canada

Paper published in *Applied Acoustics*, May 2021.

2.1 Abstract

Double hearing protectors (DHPs), earplugs and earmuffs worn in combination, may be needed in high level noise environments. The DHP sound attenuation is known to be less than the sum of each single protector attenuation. This effect, referred to as the DHP effect, is still not fully understood. A recent study has shown that it can be observed on an acoustic test fixture (ATF) and characterized by the decrease of the earplug noise reduction (NR) when the earmuff is added. In this paper, a measurement methodology is proposed to (i) identify the main sound paths related to the DHP effect on an ATF and (ii) explain the latter by the relative contributions of the airborne and structure-borne transmissions in the system. The focus is put on the NR values of the earplug alone and in the DHP. Measurement results suggest that the DHP effect is related to the energy transmitted from the earcup, through the earmuff cushion and finally into the earcanal via the sound radiation of the earplug and/or earcanal lateral walls. This flanking structure-borne path is found to dominate over the "direct" airborne path through the hearing protectors at frequencies above 300 Hz.

2.2 Introduction

For workers exposed to high noise levels over 105 dB(A), a mitigation solution of last resort is to wear double hearing protectors (DHPs), namely a combination of earplugs and earmuffs (CSA, 2014). A number of experimental studies (Zwislocki, 1957; Nixon & von Gierke, 1959; Berger, 1983; Abel & Armstrong, 1992; Ravicz & Melcher, 2001; Berger *et al.*, 2003a; Mercy *et al.*, 2005; Tubb *et al.*, 2005; Abel & Odell, 2006; Reinfeldt *et al.*, 2007; Du *et al.*, 2008; Gallagher *et al.*, 2010; Mercy & James, 2011; Nélisse *et al.*, 2017) have been carried out in the past to measure the sound attenuation of DHPs using the real-ear attenuation at threshold method (ANSI, 2016). Most of these studies commonly recognize that the total attenuation of the DHP is less than the sum of the attenuation of each single hearing protector. In the following, this effect is referred to as the DHP effect.

According to past investigations, the DHP effect is considered to be related to the flanking bone conduction (BC) paths that bypass the hearing protectors (Zwislocki, 1957; Nixon & von Gierke, 1959; Berger, 1983; Abel & Armstrong, 1992; Ravicz & Melcher, 2001; Berger *et al.*, 2003a; Mercy *et al.*, 2005; Tubb *et al.*, 2005; Reinfeldt *et al.*, 2007; Du *et al.*, 2008; Gallagher *et al.*, 2010; Mercy & James, 2011). The sound transmitted to the middle and inner ears through BC paths via the head and body has been shown to dominate at medium and high frequencies above 2 kHz (Zwislocki, 1957; Nixon & von Gierke, 1959; Berger, 1983; Abel & Armstrong, 1992; Ravicz & Melcher, 2001; Berger *et al.*, 2003a; Mercy *et al.*, 2005; Tubb *et al.*, 2005). Several studies have mentioned that the dominant BC path at frequencies below 2 kHz corresponds to the sound conducted through the head and body to the earcanal (due to the vibration of the earcanal walls) and finally to the middle and inner ears (outer ear BC path) (Berger, 1983; Ravicz & Melcher, 2001; Berger *et al.*, 2003a; Mercy *et al.*, 2005; Tubb *et al.*, 2005; Reinfeldt *et al.*, 2007; Mercy & James, 2011), which should be attributed to the fundamental mechanisms of the occlusion effect (e.g., Stenfelt & Goode, 2005). But the exact contribution of the latter to the DHP effect still remains unclear. In (Mercy *et al.*, 2005; Tubb *et al.*, 2005), the sound attenuation of an active noise reduction earmuff alone and in combination with an earplug was measured using the microphone-in-real-ear technique (ANSI, 2020). While observing the DHP effect, the authors found that the earmuff attenuation remained nearly the same with and without the earplug regardless of whether the active noise reduction mode was turned on or off. They hypothesized that there should be a coupling between the earplug and earmuff which modified the overall attenuation attained by the DHP, but they did not show any evidence for supporting this assumption.

As mentioned in (Berger, 1983; Ravicz & Melcher, 2001; Reinfeldt *et al.*, 2007; Mercy & James, 2011), the earplug and earmuff in the DHP might be coupled (i) acoustically through the air cavity under the earmuff and (ii) mechanically through the human body tissues. However, the related sound paths have never been explicitly analyzed due to the complexity of the system. Particularly, Gorman (1982) proposed a lumped model of an earmuff taking into account two BC paths: one related to the sound transmission to the earcanal through the head excited by the external sound field and the other related to the transmission to the earcanal through the earmuff cushion and head as a result of the earcup vibration. The author mentioned that the latter path is significantly enhanced when the earcanal is occluded and thus assumed to be the source of the DHP effect. But the corresponding behaviors still need to be verified through experimental approaches. More recently, Nélisse *et al.* (2017) measured the noise reduction (NR) of several types of earplugs and earmuffs both singly and in combination on human subjects. The authors confirmed that the presence of earplugs does not appreciably modify the sound attenuation of earmuffs (Mercy *et al.*, 2005; Tubb *et al.*, 2005) but they noticed that the earplug NR decreased considerably (up to 40 dB) in the frequency range between 125 Hz and 8 kHz when worn simultaneously with an earmuff. It implies that the DHP effect involves the outer ear BC path and extends over a broad frequency band (even above 2 kHz). In addition, similar results were obtained by the authors using an acoustic test fixture (ATF) which is supposed to have a self-insertion loss (IL) higher than the BC limit of human subjects (ANSI, 2020). This shows that the earplug NR can be used to evaluate the DHP effect, to better understand its cause, and that this effect can be observed on both real ears and ATFs.

In order to estimate the noise reduction rating (EPA, 1979) of the DHP, an empirical correction factor of 5 dB to be added to the noise reduction rating of the most attenuating single hearing protector in the system has been proposed as a rule of thumb (CSA, 2014). But it has been proved to be inaccurate in several studies (Behar, 1991; Behar & Kunov, 1999; Gallagher *et al.*, 2010; Byrne & Murphy, 2016) which found that the correction factor covered actually a quite wide range of values (2 – 14 dB). Moreover, Damongeot *et al.* (1989) derived an empirical formula to estimate the global attenuation of DHPs based on a simple regression of the measured global attenuation of single protectors. However, this formula does not contribute to the understanding of the physical mechanisms. In Berger's study (1983), an equation was proposed to predict the DHP attenuation as a function of frequency assuming that the DHP is a decoupled system where the sound attenuation of the earplug and earmuff can be summed up directly. In this equation, the sound transmission through the BC paths is also taken into account and considered to be incoherent with the airborne (AB) transmission through the hearing protectors. The attenuation for the BC paths was estimated using a very attenuating system, i.e., a deeply inserted foam earplug and a lead earmuff. Compared to experimental data, the predictions were shown to be relatively satisfactory above 2 kHz for various DHPs. But errors of as much as 13 dB were found at lower frequencies. The author attributed these errors to the presence of the coupling between the earplug and earmuff. However, no evidence was provided to further prove this hypothesis. Additionally, as mentioned in (Reinfeldt *et al.*, 2007), the BC attenuation in Berger's equation actually accounted for the occlusion effect which depends on the hearing protectors used and their fit. Thus, it seems not accurate enough to predict the attenuation of various DHPs using the BC attenuation estimated with a specific DHP. More particularly, a deeply inserted earplug such as used in (Berger, 1983) increases the AB attenuation of the DHP but may also decrease the contribution of the outer ear BC path, and thus may provide an erroneous BC correction for DHPs including shallowly inserted earplugs. This may, to some extent, explain the errors below 2 kHz observed in Berger's study. In order to offer a reliable estimate of DHP attenuation and to optimize its proper acoustical efficiency, it is important to better understand the sound transmission mechanisms through this type of hearing protector and to identify the main sound paths related to the DHP effect.

As shown in past investigations on single protectors (e.g., Viallet *et al.*, 2013, 2014; Boyer, Doutres, Sgard, Laville & Boutin, 2015; Carillo *et al.*, 2018), numerical modeling seems to be a good way for better understanding the vibroacoustic behaviors of hearing protection devices and improving the prediction of their sound attenuation. Nevertheless, few studies have focused on the numerical modeling of DHPs. Using the finite element model of a DHP placed on a heavy box, James (2006) showed that the acoustic energy in the earcanal occluded by the DHP mainly came from the vibration of the earplug/earmuff assembly together with the structures between them while the contribution of the acoustic domain enclosed by the earmuff was quite limited. However, large discrepancies between the simulation and measurement results of DHP attenuation were found and the model could not be validated. The author attributed these differences to the experimental setup which was not correctly replicated in the model, especially the vibration of the support.

Similarly, Nélisse *et al.* (2017) have tried to simulate the attenuation of a DHP fixed over an ATF by combining the finite element models of an earplug and an earmuff (Viallet *et al.*, 2014; Carillo *et al.*, 2018). In this model, all the acoustical couplings involved in the system were accounted for but the ATF was considered to be rigid so that there was no mechanical coupling between the earplug and earmuff through the ATF. Again, discrepancies between the simulation and measurement results were found. In particular, the experimentally observed DHP effect could not be reproduced by the simulation. This suggests that the DHP effect observed on ATFs should originate from the flanking structure-borne (SB) sound transmission in the system rather than the AB transmission.

The state-of-the-art reveals that at the moment, the DHP effect found on human subjects is not fully understood. More specifically, there is still considerable ambiguity with regard to the outer ear BC path which involves the complex vibroacoustic behaviors of both the hearing protectors and the earcanal together with its surrounding tissues. No available model can predict the DHP overall attenuation from its components and help understand the physics, even on a simplified system such as an ATF. In addition, there is not yet any explanation of the DHP effect observed on ATFs, and to the authors' knowledge, the related sound paths have never been investigated via experimental measurements.

As an initial step towards understanding the sound transmission mechanisms through the DHP, the present paper focuses on the experimental analysis of the DHP effect observed on an ATF. A specially designed measurement methodology is proposed to (i) identify the main sound paths related to the DHP effect characterized by the decrease of the earplug NR (when it is worn in combination with an earmuff) and (ii) explain the DHP effect by the relative contributions of the AB and SB transmissions in the system. Firstly, the potential influence of various SB paths through the ATF to its earcanal (outer ear path), and originating from the earmuff headband and ATF tripod is investigated by modifying the system coupling conditions. Secondly, the relative contributions of the "direct" AB transmission via the earmuff cavity and possible flanking SB paths involved are studied by controlling the sound pressure level (SPL) under the earmuff using a tiny loudspeaker placed beneath the earcup. Particular attention is given to the analysis of the SB transmission through the earmuff cushion with the help of a lead cushion. Ultimately, this analysis will also allow for targeting the correct level of modeling for each component in prospective numerical investigations.

The paper is organized as follows. Inspired by the predictive formula in Berger's study (1983), an analytical model of the DHP is developed in Sec. 2.3 in order to support the investigation of the DHP effect and the proposed measurement methodology. Section 2.4 presents the experimental setup, the selected sound attenuation indicators and the measurement methodology using multiple configurations. The corresponding results are shown and discussed in Sec. 2.5.

2.3 Analytical model of the double hearing protector

2.3.1 Transmission paths

Possible sound transmission paths through a DHP worn on a typical ATF (ANSI, 2020) are presented in Fig. 2.1. It is worth noting that these paths all involve both AB and SB components.

For the sake of conciseness, the term AB (or SB) path refers to an AB-dominant (or SB-dominant) sound path in the system. These sound paths are explained below:

1. AB path corresponds to the "direct" sound transmission to the earcanal through the earmuff, the air cavity under the earmuff and the earplug. According to (Berger, Royster, Royster, Driscoll & Layne, 2003b; Boyer, Doutres, Sgard, Laville & Boutin, 2014), the sound pressure under the earmuff is primarily governed by (i) the earmuff pumping motion at low frequencies and (ii) the sound transmitted via the cushion walls and earcup at medium and high frequencies.
2. SB path SB1 denotes the sound transmission to the earcanal through the ATF due to the vibration of the earmuff headband.
3. SB path SB2 is related to the sound transmission to the earcanal through the ATF excited by the external sound field.
4. SB path SB3 corresponds to the sound transmitted to the earcanal via the ATF and its support due to the room floor vibration.
5. SB path SB4 refers to the sound path through the earmuff cushion and the built-in part of the ATF mimicking the human face flesh to the earcanal as a result of the earcup vibration. A similar sound path in the DHP has been pointed out and accounted for in Gorman's lumped model (1982). James (2006) also identified this path using his numerical model of a DHP/box system.

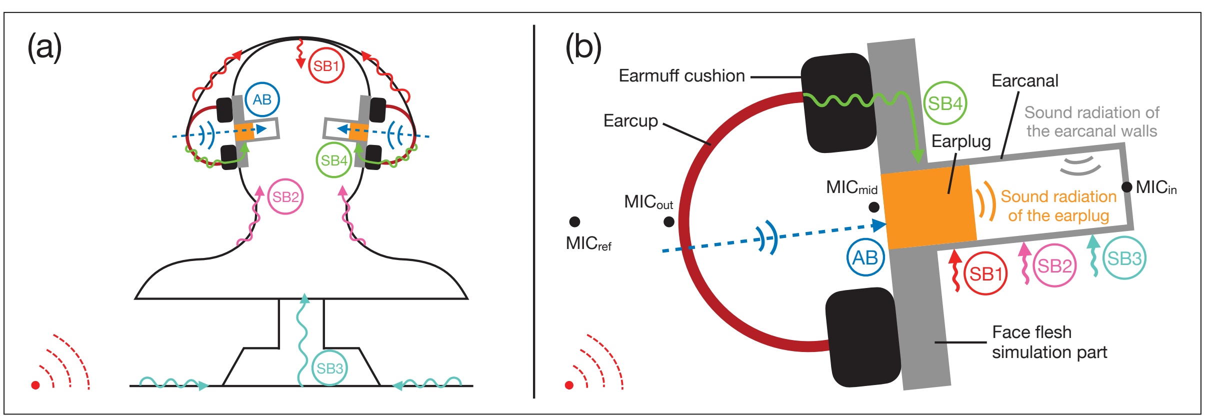

Figure 2.1 Possible sound transmission paths through the DHP/ATF system

The acoustic energy in the earcanal results from the sound radiation of (i) the non-obstructed part of the earcanal lateral walls caused by the SB paths (SB1 to SB4) and (ii) the inner face of the earplug (facing the eardrum) (James, 2006; Viallet *et al.*, 2014). In the latter case, the earplug is excited both acoustically on its outer face due to the AB path and mechanically by the earcanal walls owing to the SB paths (see the zoomed-in view in Fig. 2.1(b)). It is worth noting that the ear simulator together with its recording microphone (IEC, 2010) connected to the ATF earcanal (not presented in Fig. 2.1 for the sake of conciseness) can be excited mechanically. The vibration of the former may directly affect the microphone response or contribute to the sound radiation into the earcanal. This is accounted for in the SB paths.

2.3.2 Prediction of the DHP effect

As mentioned before, the DHP effect observed on the ATF can be characterized by the decrease of the earplug NR when the latter is combined with the earmuff, which should be related to the flanking SB paths in the system (SB1 to SB4). In order to demonstrate this effect, the quantity ΔNR_{DHP} is defined. It expresses how the NR of the DHP departs from the one obtained when only the "direct" AB transmission through the hearing protectors is considered. Similarly to Berger's study (1983), assuming that the DHP is a decoupled system where the energy transmitted via the AB and SB paths into the earcanal can add incoherently, ΔNR_{DHP} can be written as the difference between the NR values of either the DHP or earplug without and with the contributions of the SB paths:

$$\Delta NR_{\mathrm{DHP}} = NR_{\mathrm{DHP}}^{\mathrm{AB}} - NR_{\mathrm{DHP}} = NR_{\mathrm{EP}}^{\mathrm{DHP,\,AB}} - NR_{\mathrm{EP}}^{\mathrm{DHP}}. \tag{2.1}$$

$NR_{\mathrm{DHP}}^{\mathrm{AB}}$ refers to the NR of the DHP considering only the AB transmission and NR_{DHP} denotes the overall NR of the DHP when all the possible sound paths (AB and SB1 to SB4) are accounted for. Similarly, $NR_{\mathrm{EP}}^{\mathrm{DHP,\,AB}}$ and $NR_{\mathrm{EP}}^{\mathrm{DHP}}$ denote respectively the NR of the earplug in the DHP only due to the AB path and that resulting from both the AB and SB paths. In this study, $NR_{\mathrm{EP}}^{\mathrm{DHP}}$ is directly measured with the earplug and earmuff in place and $NR_{\mathrm{EP}}^{\mathrm{DHP,\,AB}}$ is estimated using the NR of the single earplug NR_{EP} (see Sec. 2.4.3). The superscript "DHP" is used to identify the earplug in the DHP configuration. The other acoustic indicators introduced in this section are not measured but are rather used to support explanations. Detailed descriptions of essential indicators are provided in Appx. I. In the case of the single earplug, the contribution of the SB transmission is expected to be of minor importance and the earplug NR is considered to be mainly due to the AB transmission ($NR_{\mathrm{EP}} \approx NR_{\mathrm{EP}}^{\mathrm{AB}}$). In addition, it is assumed that the presence or not of the earmuff does not significantly modify the AB attenuation of the earplug ($NR_{\mathrm{EP}}^{\mathrm{AB}} \approx NR_{\mathrm{EP}}^{\mathrm{DHP,\,AB}}$).

According to the aforementioned assumptions, it is straightforward to show that the DHP effect ΔNR_{DHP} can also be expressed in terms of the ratio between the root mean square (rms) sound pressure in the earcanal ($\mathrm{MIC_{in}}$ in Fig. 2.1(b)) caused by the SB paths $p_{\mathrm{in}}^{\mathrm{DHP,\,SB}}$ and AB path $p_{\mathrm{in}}^{\mathrm{DHP,\,AB}}$ such as:

$$\Delta NR_{\mathrm{DHP}} = 10\log_{10}\left(1 + \frac{{p_{\mathrm{in}}^{\mathrm{DHP,\,SB}}}^2}{{p_{\mathrm{in}}^{\mathrm{DHP,\,AB}}}^2}\right). \tag{2.2}$$

This expression simply shows that the DHP effect increases as the contributions of the SB paths outweigh that of the AB path. The mean square sound pressure ratio in Eq. (2.2) can be calculated using the NR of the DHP due to the SB paths $NR_{\mathrm{DHP}}^{\mathrm{SB}}$ and the NR values of the earplug and earmuff considered to be decoupled (i.e., $NR_{\mathrm{EP}} \approx NR_{\mathrm{EP}}^{\mathrm{AB}} \approx NR_{\mathrm{EP}}^{\mathrm{DHP,\,AB}}$ and $NR_{\mathrm{EM}} \approx NR_{\mathrm{EM}}^{\mathrm{AB}} \approx NR_{\mathrm{EM}}^{\mathrm{DHP,\,AB}}$):

$$\frac{{p_{\mathrm{in}}^{\mathrm{DHP,\,SB}}}^2}{{p_{\mathrm{in}}^{\mathrm{DHP,\,AB}}}^2} = 10^{(NR_{\mathrm{EP}}+NR_{\mathrm{EM}}-NR_{\mathrm{DHP}}^{\mathrm{SB}})/10}. \tag{2.3}$$

The latter assumption, $NR_{\mathrm{EM}} \approx NR_{\mathrm{EM}}^{\mathrm{AB}} \approx NR_{\mathrm{EM}}^{\mathrm{DHP,\,AB}}$, is supported by the fact that the NR of the earmuff in the DHP nearly equals that of the single earmuff (Mercy *et al.*, 2005; Tubb *et al.*, 2005; Nélisse *et al.*, 2017). Combining Eqs. (2.1) – (2.3) returns an equation (not shown here) that resembles Berger's predictive formula (1983) where $NR_{\mathrm{DHP}}^{\mathrm{SB}}$ is similar to the BC attenuation in the formula estimated using the deeply inserted earplug and lead earmuff. It should be noted that the BC attenuation in Berger's formula is associated with the flanking BC paths on human subjects while in this work $NR_{\mathrm{DHP}}^{\mathrm{SB}}$ accounts for all the potential SB paths contributing to the acoustic energy in the earcanal of the ATF. According to Eqs. (2.2) and (2.3), it is expected that the DHP effect arises ($\Delta NR_{\mathrm{DHP}} > 3$ dB) when:

$$NR_{\mathrm{EP}} + NR_{\mathrm{EM}} > NR_{\mathrm{DHP}}^{\mathrm{SB}}, \tag{2.4}$$

i.e., the cumulative AB attenuation of the earplug and earmuff in the DHP is higher than the attenuation of the flanking SB paths. $NR_{\mathrm{DHP}}^{\mathrm{SB}}$ is difficult to assess directly from experimental measurements due to the complexity of the system. But the impact of various SB paths (through $NR_{\mathrm{DHP}}^{\mathrm{SB}}$) can be investigated indirectly by measuring ΔNR_{DHP} which is inclined to vary with the coupling conditions between the system components (e.g., ATF, earmuff cushion, headband, etc.). Moreover, Eqs. (2.2) and (2.3) also indicate that the DHP effect increases with (i) the AB attenuation of the single protectors (i.e., $p_{\mathrm{in}}^{\mathrm{DHP,\,SB}}$ increases and dominates over $p_{\mathrm{in}}^{\mathrm{DHP,\,AB}}$ as NR_{EP} and/or NR_{EM} increases) and (ii) the contribution of the outer ear SB path (i.e., $p_{\mathrm{in}}^{\mathrm{DHP,\,SB}}$ increases and dominates over $p_{\mathrm{in}}^{\mathrm{DHP,\,AB}}$ as $NR_{\mathrm{DHP}}^{\mathrm{SB}}$ decreases). In order to study the relative contributions of the AB path and potential flanking SB paths, it is possible to control the ratio on the left-hand side of Eq. (2.3) using a small sound source added beneath the earcup of the earmuff which is driven independently from the external source. The internal source can be operated alone or in combination with the external one. This allows for assessing the corresponding changes in ΔNR_{DHP} by artificially tuning NR_{EM} in Eqs. (2.3) and (2.4). Since the rms sound pressure generated by the internal source p_{spk} and the sound pressure under the earmuff ($\mathrm{MIC_{mid}}$) resulting from the AB transmission $p_{\mathrm{mid}}^{\mathrm{DHP,AB}}$ are incoherent and assuming that p_{spk} does not contribute to the SB transmission (see Eq. (A I-7)), Eq. (2.3) can be rewritten as:

$$\frac{{p_{\mathrm{in}}^{\mathrm{DHP,\,SB}}}^2}{{p_{\mathrm{in}}^{\mathrm{DHP,\,AB}}}^2} = \frac{10^{(NR_{\mathrm{EP}}+NR_{\mathrm{EM}}-NR_{\mathrm{DHP}}^{\mathrm{SB}})/10}}{1 + p_{\mathrm{spk}}^2 / {p_{\mathrm{mid}}^{\mathrm{DHP,\,AB}}}^2}. \tag{2.5}$$

The internal source is used to evaluate (i) the contributions of some SB paths (while shunting the others) and (ii) the relative contributions of the AB path and SB paths in terms of the SPL under the earmuff (see Sec. 2.4.4.1).

2.4 Experimental setup and methodology

2.4.1 Hearing protection devices of interest

The experimental analysis is carried out on a specific DHP consisting of a homemade passive earplug and a commercial passive earmuff. The earplug is made of silicone rubber and specifically molded to best fit the shape of the ATF earcanal (see Fig. 2.2(a)). This typical earplug is chosen since it ensures good sound insulation during the experiments without sound leaks. In addition, its numerical model has been shown to provide satisfactory attenuation simulation results compared to experimental data (Viallet *et al.*, 2013, 2014), which could be helpful for future numerical investigations. The earmuff is the EAR-MODEL-1000 (3M^{TM} E-A-R^{TM}, Indianapolis, USA) whose comfort cushion is composed of foam wrapped with a thin polymer sheath (see Fig. 2.2(b)). The numerical model of this type of earmuff is detailed in published studies (Boyer *et al.*, 2015; Carillo *et al.*, 2018). More details about the constitution of the EAR-MODEL-1000 can be found in Boyer *et al.*'s work (2014).

2.4.2 Acoustical test bench

Throughout the experimental tests, an ATF (G.R.A.S. 45CB, G.R.A.S. Sound & Vibration AS, Denmark) is adopted to objectively assess the sound attenuation of the studied hearing protectors.

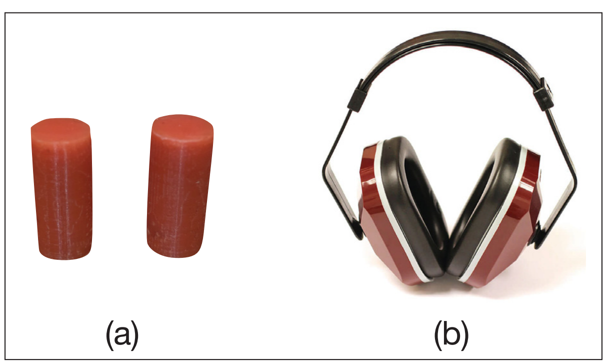

Figure 2.2 Studied hearing protection devices: (a) silicone earplug; (b) EAR-MODEL-1000 earmuff

Indeed as mentioned in the introduction, the DHP effect has been clearly observed on this test bench (Nélisse *et al.*, 2017). The ATF allows for easily making modifications to the system in order to favor one sound path while reducing the others. It is always supported by a tripod as shown in Fig. 2.3(a). The tripod is completely rigid in construction without any isolation mounts and rests on the floor. The floor is on suspension to prevent potential vibration of the building that could be transmitted into the room. In order to better demonstrate the SB sound transmission through the system, certain parts have been made more rigid. First, the soft elastomeric pinna simulator of the ATF is removed as in Nélisse *et al.*'s work (2017) and is replaced with a circular aluminum plate which can be screwed onto the ATF (see Fig. 2.3(b)). Second, a cylindrical aluminum "rigid-walled" earcanal of inner diameter 7.5 mm has been fabricated to replace the silicone-layered ATF earcanal. It has the same geometry as the ATF earcanal and can be screwed to the IEC 60318-4 ear simulator (IEC, 2010) in the ATF. During the experiments, the length

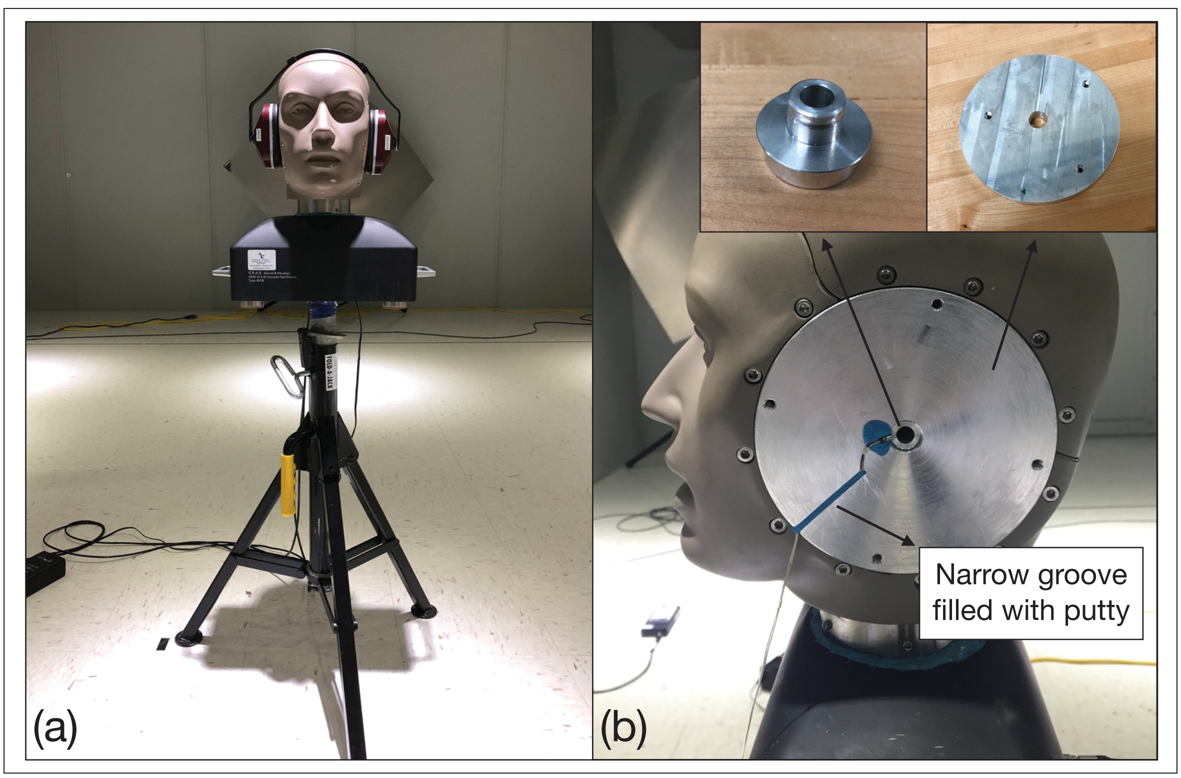

Figure 2.3 Experimental setup: (a) G.R.A.S. 45CB ATF supported by a tripod; (b) "rigid-walled" earcanal and aluminum plate with a groove

of the earmuff headband is kept unchanged so that the clamping force applied to the earmuff remains constant when it is worn over the ATF. According to Boyer *et al.*'s work (2014), the clamping force induced by the span of the ATF is about 11.5 N. Measurements are performed in a diffuse sound field (white noise) of about 110 dB in overall SPL generated by four loudspeakers (MACKIE HD1531, MACKIE®, USA) positioned at each corner of a reverberant room equipped with acoustic diffusers. Different microphones are used to measure the SPLs at four specific locations as shown in Fig. 2.1(b). The SPL at the eardrum position in the ATF earcanal is measured using the microphone (MIC_{in}) included in the ear simulator (G.R.A.S. 40AG, G.R.A.S. Sound & Vibration AS, Denmark). Two miniature microphones (FG-23329-D65, Knowles®, USA) are respectively (i) placed close to the earcanal entrance (MIC_{mid}) and (ii) suspended outside in the vicinity of the earmuff (MIC_{out}). The second miniature microphone is not directly glued to the earmuff to avoid the effect of the earcup vibration on the microphone response. In addition, a $\frac{1}{2}$ in. reference microphone (MPA231, BSWA Technology Co., China) is located at about 1 m from the earcanal entrance (MIC_{ref}) to measure the SPL in the room. Special attention is paid to ensure a good sealing condition of the system. A narrow groove has been made on the aluminum plate to pass the wire of the microphone under the earmuff (MIC_{mid}). This groove is then filled with mounting putty as shown in Fig. 2.3(b) in order to avoid possible sound leaks between the wire and earmuff cushion. Mounting putty is also used to cover the gap between the aluminum plate and ATF. Such small quantities of putty are supposed to have no significant influence on the vibroacoustic behavior of the system.

2.4.3 Sound attenuation indicators

The indicators chosen to present the sound attenuation of the studied hearing protection devices are the IL of the DHP, the NR of the single earplug and that of the earplug in the DHP. The IL of the DHP allows one to compare oneself with the standard ANSI S12.42 (2020) and is defined as the difference between the SPLs at the eardrum position (MIC_{in}) without and with the DHP:

$$IL_{\text{DHP}} = 10\log_{10}(p_{\text{in}}^{\text{open}2}) - 10\log_{10}(p_{\text{in}}^{\text{DHP}2}), \tag{2.6}$$

where $p_{\mathrm{in}}^{\mathrm{open}}$ and $p_{\mathrm{in}}^{\mathrm{DHP}}$ denote the rms sound pressure recorded at the eardrum position in the open earcanal and in the earcanal occluded by the DHP. As mentioned previously, the earplug NR has been shown to be a good indicator for the presence (or not) of the DHP effect (Nélisse *et al.*, 2017). ΔNR_{DHP} is thus evaluated experimentally by measuring the NR of the single earplug and that of the earplug in the DHP (see Sec. 2.3.2). They are calculated respectively as:

$$NR_{\mathrm{EP}} = 10\log_{10}({p_{\mathrm{mid}}^{\mathrm{EP}}}^2) - 10\log_{10}({p_{\mathrm{in}}^{\mathrm{EP}}}^2), \tag{2.7}$$

$$NR_{\mathrm{EP}}^{\mathrm{DHP}} = 10\log_{10}({p_{\mathrm{mid}}^{\mathrm{DHP}}}^2) - 10\log_{10}({p_{\mathrm{in}}^{\mathrm{DHP}}}^2), \tag{2.8}$$

where p_{mid} and p_{in} correspond to the rms sound pressure recorded at the earcanal entrance ($\mathrm{MIC_{mid}}$) and eardrum position in the case of the single earplug or DHP. Besides the sound attenuation values, special attention is paid to the SPL under the earmuff ($\mathrm{MIC_{mid}}$) in order to further analyze the sound transmission through the system.

2.4.4 Experimental methodology

2.4.4.1 Acoustical test

In order to analyze the transmission paths shown in Fig. 2.1 and their respective contributions, specially designed test configurations based on Eqs. (2.3) and (2.5) have been used which make it possible to reduce or emphasize certain paths compared to the others (see Table 2.1). The configurations that were implemented are as follows:

1. **Configuration 1**: The NR of the single earplug is measured (see Fig. 2.4). In this configuration, the sound transmission through the earplug (AB) and that through the ATF and its tripod (SB2 and SB3) are present. Configuration 1 is regarded as the reference for comparisons with DHP configurations.
2. **Configurations 2**: The NR of the earplug in the DHP is measured. The original earmuff cushion is used and the foam liner is removed from the earmuff. According to Sec. 2.3.2,

Table 2.1 Test matrix for earplug NR measurements: maximum level of the internal source is used for configurations 3.2 and 4.2; five different levels of the internal source are used for configurations 3.3 and 4.3 (referred to as 3.3a – 3.3e and 4.3a – 4.3e)

Configurations	**Hearing protectors**	**Coupling conditions**	**Cushion type**	**Foam liner**	**External source**	**Internal source**
1	Earplug	Original			✓	
2.1	Earplug + earmuff	Original	Original		✓	
2.2	Earplug + earmuff	Earmuff headband not in contact with the ATF	Original		✓	
2.3	Earplug + earmuff	ATF wrapped with soundproof material	Original		✓	
2.4	Earplug + earmuff	ATF suspended using bungee cords	Original		✓	
3.1	Earplug + earmuff	Original	Original	✓	✓	
3.2	Earplug + earmuff	Original	Original	✓		✓
3.3 (a – e)	Earplug + earmuff	Original	Original	✓	✓	✓
4.1	Earplug + earmuff	Original	Lead	✓	✓	
4.2	Earplug + earmuff	Original	Lead	✓		✓
4.3 (a – e)	Earplug + earmuff	Original	Lead	✓	✓	✓

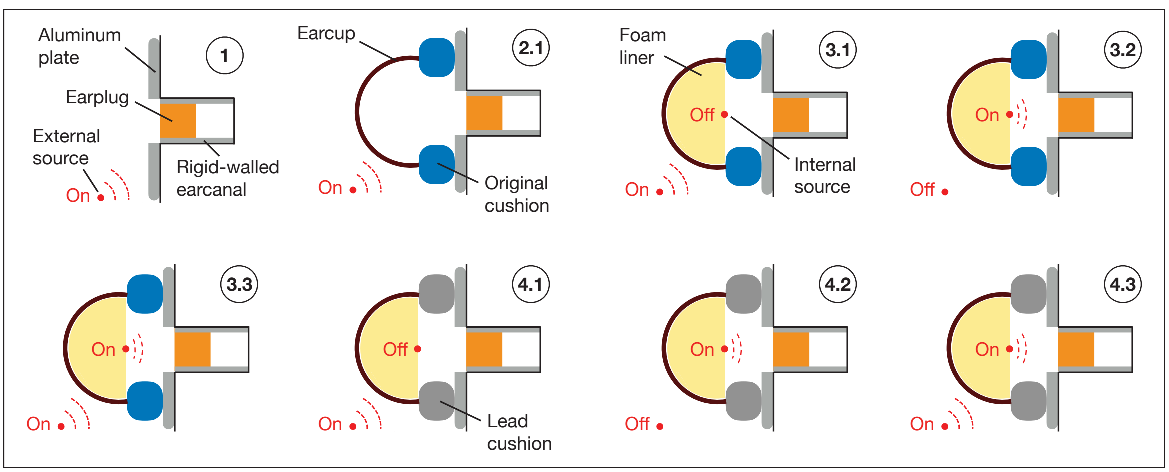

Figure 2.4 Schematic representation of test configurations

the importance of some SB sound paths (SB1, SB2 and SB3) is investigated through the changes in ΔNR_{DHP} when modifying the system coupling conditions (see Fig. 2.5).

a. **Configuration 2.1**: This configuration is similar to that adopted in Nélisse *et al.*'s work (2017) where the system's original coupling conditions are used. All the sound paths shown in Fig. 2.1 are elicited. Comparing configurations 1 and 2.1 reveals whether the DHP effect (i.e., decrease of the earplug NR) can be observed after adding the earmuff.

b. **Configuration 2.2**: First, the earmuff headband is slightly moved so that it is no longer in direct contact with the ATF, assuming that the clamping force remains the same. A small piece of fibrous material is placed between the headband and each earcup of the earmuff to ensure that the headband is always maintained in position during the experiments. By comparing the results to those of configuration 2.1, the contribution of the SB sound path due to the vibration of the headband (SB1) can be evaluated.

c. **Configuration 2.3**: The ATF is wrapped with soundproof material, a 0.375 in. thick Barymat® barrier of 1.2 lbs/sq.ft (M-100D, AcoustiGuard™, Canada), fastened using adhesive tape to reduce the incident sound power received by the ATF. A portion of the circular aluminum plate is not covered with Barymat® and is reserved for placing the earmuff to make sure that only the acoustic energy impinging on the ATF is reduced and not that exciting the earmuff. By comparing with configuration 2.1, the potential contribution of SB2 can be identified.

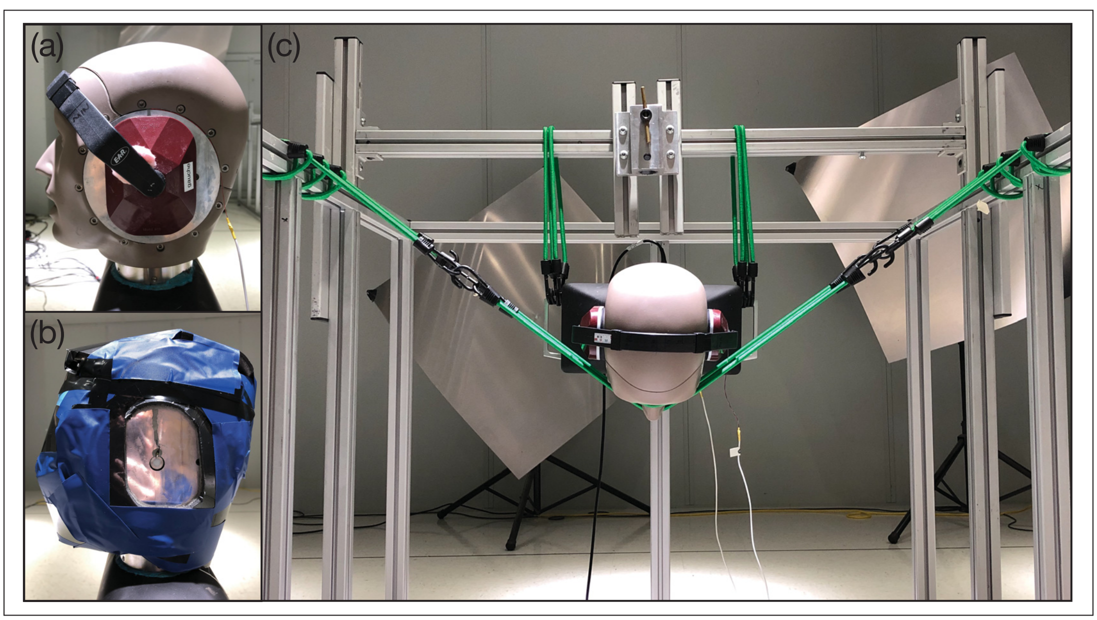

Figure 2.5 Configurations to test the effects of the earmuff headband and the sound transmission through the ATF and its tripod: (a) configuration 2.2, earmuff headband not in contact with the ATF; (b) configuration 2.3, ATF wrapped with soundproof material; (c) configuration 2.4, ATF suspended using bungee cords

d. **Configuration 2.4**: It aims at assessing the possible transmission of the room floor vibration through the tripod and ATF to the earcanal due to the acoustic excitation (SB3). To this end, the ATF is suspended on an aluminum frame using bungee cords instead of being supported by the tripod as shown in Fig. 2.3(a) so that it is vibration-isolated from the floor.

3. **Configurations 3**: Based on configuration 2.1, the foam liner is included in the earmuff inner cavity. As explained in Sec. 2.3.2, a tiny loudspeaker is used beneath the earcup of the earmuff. It is attached to the foam liner in order not to excite directly the plastic earcup and driven with a white noise uncorrelated with the external sound field (see Fig. 2.4). Its input signal is adjusted using an equalizer (iEQ-31, dbx Inc., USA) to provide a well distributed energy over the frequency range of interest under the earmuff.

   a. **Configuration 3.1**: The system is excited by the external source as in previous configurations with the internal source turned off. In this case, p_{spk} is equal to zero and Eq. (2.5) is equivalent to Eq. (2.3). All the sound paths shown in Fig. 2.1 are involved but the acoustic energy in the earmuff cavity is dissipated due to the inclusion of the foam liner. The difference between configurations 2.1 and 3.1 allows one to determine the effect of the foam liner together with the internal loudspeaker.

   b. **Configuration 3.2**: It is similar to configuration 3.1 but the system is excited by the internal source alone (the external source is turned off). The maximum level of the internal source is used which corresponds to about 103 dB in overall SPL under the earmuff. This configuration allows for shunting SB2 and SB3, and reducing SB1 and SB4 (the two may still be involved in reality since the earmuff cavity is acoustically excited). This time $p_{\text{mid}}^{\text{DHP, AB}}$ in Eq. (2.5) is equal to zero, $p_{\text{in}}^{\text{DHP, SB}}$ is negligible compared to $p_{\text{in}}^{\text{DHP, AB}}$ and the DHP effect is considered to be negligible (see Eq. (2.2)). By comparing configurations 3.1 and 3.2, the contributions of the SB paths can be analyzed.

   c. **Configuration 3.3**: It is a combination of configurations 3.1 and 3.2 where the system is excited by both the external and internal sources simultaneously. Specially, five different levels of the internal source are used (referred to as configurations 3.3a –

3.3e): the internal source level increases progressively with a 5 dB increment from a particular level corresponding to about 83 dB in overall SPL under the earmuff (configuration 3.3a) to its maximum level (configuration 3.3e). In this configuration, both p_{spk} and $p_{\mathrm{mid}}^{\mathrm{DHP,\,AB}}$ are different from zero and p_{spk} varies. This makes it possible to assess the relative contributions of the AB path and SB paths $p_{\mathrm{in}}^{\mathrm{DHP,\,SB}}/p_{\mathrm{in}}^{\mathrm{DHP,\,AB}}$ in terms of the SPL under the earmuff.

4. **Configurations 4**: They are similar to configurations 3.1 – 3.3 but the original earmuff cushion is replaced with a lead cushion in order to study the role played by the cushion in the SB sound transmission through the cushion/aluminum plate assembly (SB4). Compared to the original cushion, the use of the lead cushion is expected to change $NR_{\mathrm{DHP}}^{\mathrm{SB}}$ in Eqs. (2.3) and (2.5), and to make a difference to the DHP effect as previously explained. The same levels of the internal source as configuration 3.3 are adopted for configuration 4.3 (referred to as configurations 4.3a – 4.3e). The lead cushion was already used in Boyer *et al.*'s work (2014). Its thickness corresponds to the compressed earmuff cushion when worn over the ATF. It is attached to the back-plate of the earmuff using strong double-sided adhesive tape. To avoid sound leaks, mounting putty is used to cover the gaps between the back-plate and lead cushion, and between the lead cushion and aluminum plate.

Measurements have been repeated three times for each configuration by removing and repositioning the studied hearing protectors in order to account for the variability related to the mounting conditions. Note that, before testing the various configurations, a preliminary test has been carried out to assess the ATF self-IL. This is achieved using the EAR-MODEL-1000 earmuff and a bullet-shaped polyurethane foam earplug (Howard Leight MAX®, Honeywell, USA) according to ANSI S12.42 (2020). The ATF with the original silicone-layered earcanal is supported by the tripod and the earmuff headband is in contact with the ATF. Particularly for this test, the pinna simulation part of the ATF is present and heated to 37 °C using the built-in temperature control unit.

2.4.4.2 Mechanical test

Since SB4 involves the earmuff cushion, mechanical tests have been carried out using the experimental setup described in Sec. 2.4.2 to further assess the role played by the cushion in the SB transmission through the system. Both the original and lead cushions have been tested. Attempts have first been made to excite directly the earcup of the earmuff using an impact hammer. However, it was difficult to retain these results since hammer double hits were constantly detected when using the original cushion. Alternatively, an electrodynamic shaker (SmartShaker^{TM}, The Modal Shop Inc., USA) has been used to impose a quasi-horizontal force on the earmuff headband where an impedance head (Model 288D01, PCB Piezotronics, USA) was tightly attached using beeswax as shown in Fig. 2.6(a). The impedance head has been screwed to the shaker's stinger in order to measure the force injected by the shaker. An accelerometer (Model 356A45, PCB Piezotronics, USA) has been attached to the aluminum plate to measure the normal acceleration of the plate surface (see Fig. 2.6(b)). The transfer function between the acceleration and force (accelerance) is calculated using the estimator H_1:

$$H_1 = \frac{G_{F,a}}{G_{F,F}}, \tag{2.9}$$

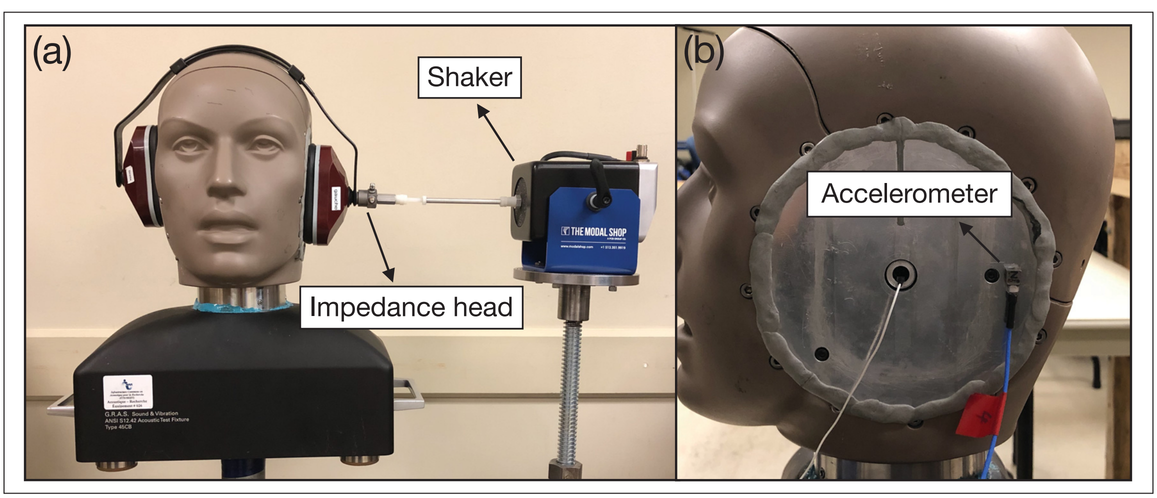

Figure 2.6 Experimental setup to test structure-borne sound transmission through the earmuff cushion

where $G_{F,a}$ is the cross-spectrum between the signals of the force and acceleration, and $G_{F,F}$ the auto-spectrum of the force signal. The test has been repeated 10 times for both the original and lead cushions. Additional tests have also been performed to measure the normal acceleration of the earcanal lateral walls by placing a miniature accelerometer in the open earcanal. However, test quality was not satisfactory due to a low coherence between the signals of the accelerometer and impedance head.

2.5 Results and discussion

2.5.1 Assessment of the ATF self-insertion loss

The measured self-IL of the ATF is displayed in Fig. 2.7 (blue curve). In this paper, results are plotted in 1/3 octave frequency bands from 125 Hz to 8 kHz. Since both ears of the ATF provide similar measurement results in the frequency range of interest, only the results obtained using the left ear are presented. The ATF self-IL is compared to the required self-IL limit given in ANSI S12.42 (2020) (black line with dots). It is found to be well above the ANSI S12.42

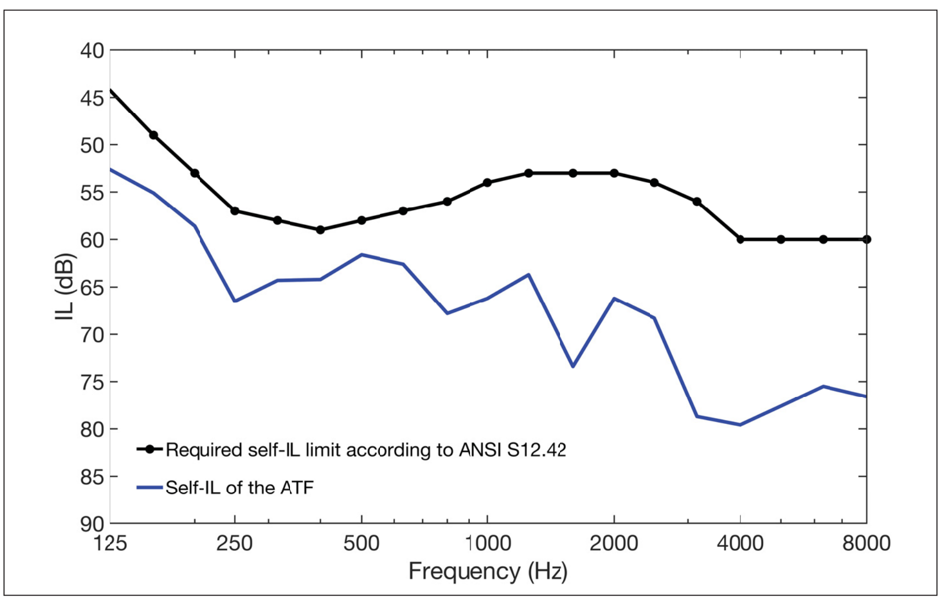

Figure 2.7 Self-IL: required self-IL limit (black dots); measured self-IL of the ATF (blue)

requirement. The high attenuation confirms satisfactory sound insulation of the adopted system and provides credits for the following measurements.

2.5.2 Observation of the DHP effect

The measured earplug NR values in the configurations where the system is excited by the external source alone are shown in Fig. 2.8(a). Results are displayed in terms of mean values and standard deviations for the three repetitions of each configuration. The grey, blue (diamonds) and red (circles) zones correspond to configurations 2.1, 3.1 and 4.1 respectively. The NR of the single earplug (configuration 1) is presented for comparison (black zone with dots). Additionally, the results in Fig. 2.8(a) are plotted in terms of ΔNR_{DHP} (see Eq. (2.1)) with reference to the NR of the single earplug in Fig. 2.8(b). The related SPLs under the earmuff are also provided in order to further analyze the sound transmission through the system (see Fig. 2.8(c)). Note that the SPLs in the earcanal in the most attenuating configurations, i.e., configurations 3.1 and 4.1 are first compared to the background noise with the hearing protectors in place and the sound source turned off (see Fig.-A II-1). Test results show that in most of the frequency range concerned, the average SPLs in the earcanal are more than 10 dB higher than the background noise. There are some exceptions around 125 Hz in configuration 4.1 and around 4 kHz in configurations 3.1 and 4.1 where the differences of the order of 5 dB are found, for which the results should be considered with care. But in the frequency range where the DHP effect occurs, this gives confidence in the measurement results that are beyond the limit of the background noise representing correctly the system vibroacoustic behavior.

In Fig. 2.8(a), a dip is found in the NR of the single earplug around 2 kHz which corresponds to the first mode of the earplug where its inner and outer faces vibrate in phase (Viallet *et al.*, 2013, 2014). Comparing configurations 1 and 2.1, the NR of the earplug is seen to drop dramatically by up to 40 dB when the earmuff is worn in combination. Moreover, the decrease in the earplug NR is observed in nearly the whole frequency range of interest. This phenomenon concurs well with the DHP effect observed in Nélisse *et al.*'s work (2017) on human subjects and on an ATF. It confirms that when an earplug is worn in combination with an earmuff, a part of acoustic energy enters the earcanal via transmission paths other than directly through the earplug. The most apparent decrease in the earplug NR in configuration 2.1 is in the frequency range [1 kHz, 2 kHz] which might be partly related to the earplug first mode (see also Fig. 2.8(b)). Another possible reason is that a local minimum of the SPL under the earmuff is observed in this frequency range (see Fig. 2.8(c)) and since the AB attenuation of the earplug alone is relatively high, $p_{\mathrm{in}}^{\mathrm{DHP,\,AB}}$ in Eq. (2.3) is small and thus $p_{\mathrm{in}}^{\mathrm{DHP,\,SB}}$ dominates. Additionally, these results reveal that even using an ATF which has a self-IL well above the required limit in the standard, the SB paths seem to play an important role in the sound transmission through the system. Moreover, differences in the earplug NR are observed when the configurations of the earmuff are modified (see configurations 2.1, 3.1 and 4.1). These differences are related to the changes in the SPL under the earmuff and the corresponding behaviors are discussed in Sec. 2.5.5.

It is necessary to note that additional measurements using a single earmuff (without earplug) under the same conditions have shown similar SPL results under the earmuff to those in configurations 2.1, 3.1 and 4.1. This is consistent with the previous finding of Tubb *et al.* (2005) and Nélisse *et al.* (2017) that the presence of the earplug makes little difference to the sound attenuation of the earmuff in a DHP. Compared to configuration 1, the evident variability in the measurement results of configurations 2.1, 3.1 and 4.1 in Fig. 2.8(a) shows that the earplug NR in the DHP is very sensitive to the mounting conditions, such as the asymmetrical compression of the earmuff cushion, relative positioning between the earplug and earcanal, etc.

2.5.3 Contributions of structure-borne paths SB1, SB2 and SB3

The earplug NR results do not exhibit significant differences between (i) configuration 2.1 and (ii) configurations 2.2, 2.3 and 2.4 (see Table-A III-1). So the latter are not included in the figure for the sake of conciseness. This indicates that the corresponding sound paths (SB1, SB2 and SB3), namely the vibration of the earmuff headband, sound transmission through the ATF or vibration transmission through the tripod do not significantly contribute to the DHP effect (increase of $p_{\mathrm{in}}^{\mathrm{DHP,SB}}$ in Eq. (2.3)) when the earplug is combined with the earmuff.

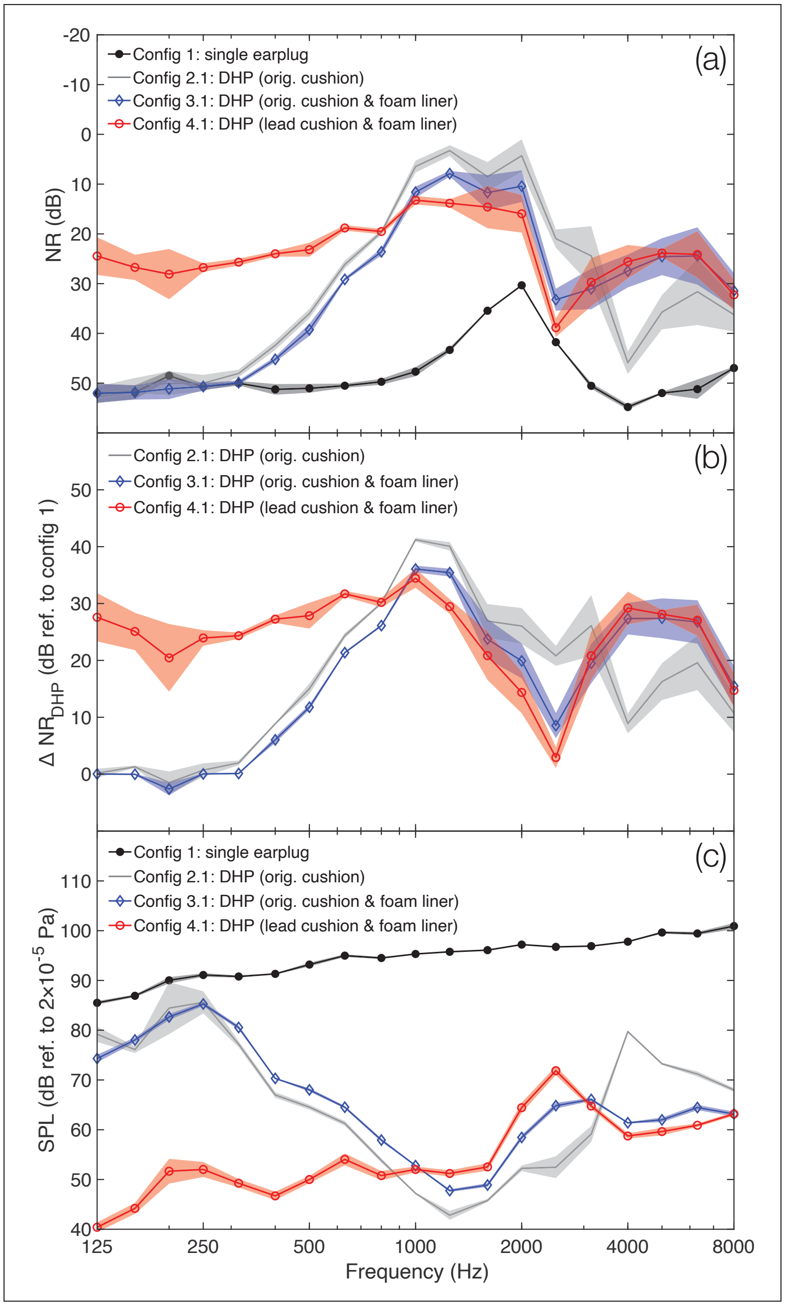

Figure 2.8 (a) Earplug NR, (b) ΔNR_{DHP} with reference to the NR of the single earplug (configuration 1) and (c) SPL measured under the earmuff excited by the external source alone: configuration 2.1 (grey), original cushion without foam liner; configuration 3.1 (blue diamonds), original cushion with foam liner; configuration 4.1 (red circles), lead cushion with foam liner. Earplug NR and SPL at the earcanal entrance in the case of single earplug are presented for comparison (black dots). Results are displayed as "mean ± standard deviation"

2.5.4 Contribution of structure-borne path SB4

The earplug NR results obtained in configurations 3.1 and 4.1 are compared (see Fig. 2.8(a)) in order to investigate the contribution of the SB sound transmission through the earmuff cushion/aluminum plate assembly (SB4). The apparent differences below 900 Hz are attributed to the use of the lead cushion which prevents the earmuff pumping motion and the sound transmission through the cushion walls (Berger *et al.*, 2003b; Boyer *et al.*, 2014) and significantly decreases the SPL under the earmuff (see Fig. 2.8(c)), i.e., increases the earmuff attenuation. As explained in Sec. 2.3.2, the DHP effect increases with the earmuff attenuation. Since it is difficult to evaluate the effect of the cushion on SB4 separately from the AB path in the frequency range controlled by the latter, mechanical test results are needed to further assess the role of the cushion in the SB transmission through the system.

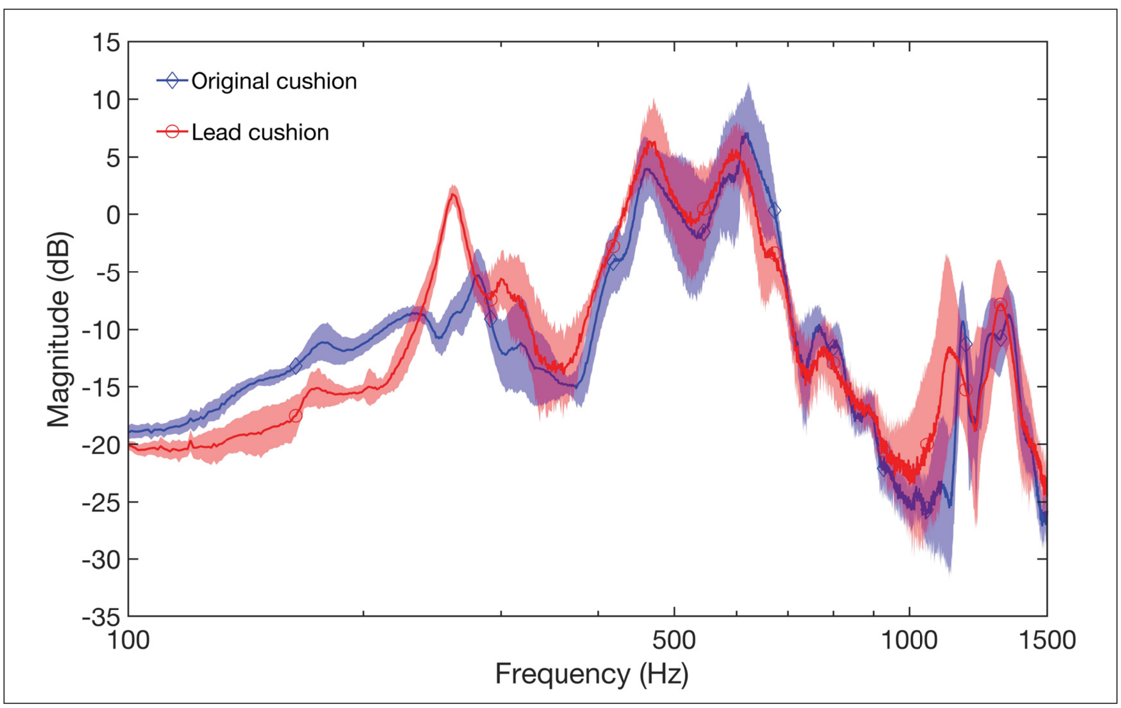

Figure 2.9 Magnitude of the measured accelerance (transfer function between the acceleration on the aluminum plate and force on the earmuff headband) in the cases of the original cushion (blue diamonds) and lead cushion (red circles). Results are displayed as “mean ± standard deviation”

Figure 2.9 displays the mean values and standard deviations of the measured accelerance magnitude for the 10 repeated tests in narrow frequency bands [100 Hz, 1.5 kHz] where the coherence between the acceleration and force signals on respectively the aluminum plate and earmuff headband is acceptable. The blue (diamonds) and red (circles) zones are related to the original and lead cushions respectively. This figure shows that the accelerance magnitude for both cushions is similar in the frequency range above 300 Hz. However, differences between the cushions observed at lower frequencies indicate that the type of cushion has an influence on the SB transmission through the DHP in the corresponding frequency range. Compared to the lead cushion, the higher accelerance magnitude of the original cushion below 250 Hz could be attributed to the mass of the earmuff cup oscillating on the springiness of the cushion. The vibration resulting from this motion is then transmitted through to the aluminum plate. The peak around 300 Hz seen from the result of the lead cushion is believed to be related to a mode of the coupled system which includes the shaker, impedance head and earmuff.

2.5.5 Relative contributions of airborne and structure-borne paths

The differences in the DHP effect induced by the changes in the SPL under the earmuff are now analyzed in more detail. As already mentioned in Sec. 2.3.2, these differences can be explained by the changes in the ratio on the left-hand side of Eq. (2.3) when NR_{EM} is modified. In Fig. 2.8(c), the resonance of the earmuff pumping motion significantly increases the SPLs under the earmuff in configurations 2.1 and 3.1 below 300 Hz. As a result, the related earplug NR values get very close to the one of the earplug alone in the corresponding frequency range and thus ΔNR_{DHP} is close to zero (see Figs. 2.8(a) and 2.8(b)). A similar phenomenon is observed in configuration 2.1 around 4 kHz where the acoustic resonance of the earmuff cavity (Pääkkönen, 1992; Boyer *et al.*, 2014) is seen. According to Eqs. (2.2) and (2.3), $p_{\mathrm{in}}^{\mathrm{DHP,\,AB}}$ increases and dominates over $p_{\mathrm{in}}^{\mathrm{DHP,\,SB}}$ as NR_{EM} decreases, and the DHP effect becomes less pronounced. This is believed to be the reason why ΔNR_{DHP} is close to zero around the resonance frequencies of the pumping motion and of the earmuff cavity. In configuration 3.1, the resonance of the earmuff cavity is evidently damped due to the addition of the foam liner. Between 300 Hz and 3

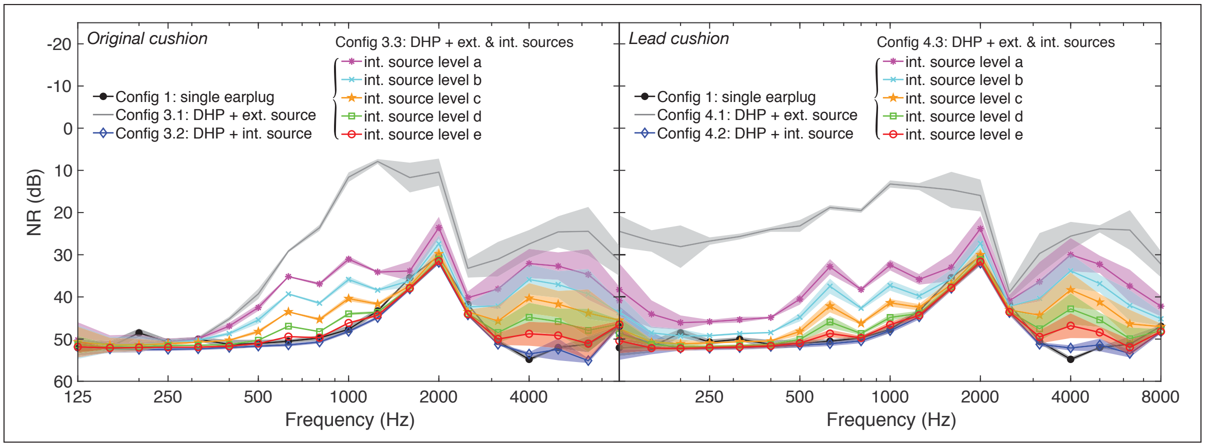

Figure 2.10 Earplug NR measured under the earmuff with the original cushion (left) and lead cushion (right): configurations 3.1 & 4.1 (grey), external source alone; configurations 3.2 & 4.2 (blue diamonds), internal source alone (level max); configurations 3.3 & 4.3 (with increasing levels a – e corresponding respectively to purple asterisks, cyan crosses, orange pentagrams, green squares and red circles), external source + internal source (five levels). NR of the single earplug (configuration 1) is presented for comparison (black dots). Results are displayed as "mean ± standard deviation"

kHz, the earplug NR in configuration 3.1 is slightly higher than that in configuration 2.1. Such a phenomenon is not found if the internal loudspeaker in configuration 3.1 is removed from the foam liner. It is due to the fact that the inclusion of the loudspeaker reduces the total volume of the earmuff cavity, which in turn increases the SPL under the earmuff and decreases NR_{EM} as previously explained. Moreover, a local maximum around 2.5 kHz is seen from the earplug NR in configuration 3.1 but not in configuration 2.1. This might be related to the mechanical resonance of the foam liner/internal loudspeaker assembly which acts as a damped mass-spring system in this frequency range and induces an increase of the SPL under the earmuff.

In order to further assess the relative contributions of the AB path and SB paths, the earplug NR results obtained from the test configurations involving the earmuff with the foam liner and internal loudspeaker (see Fig. 2.4) are displayed in Fig. 2.10. For both cushions, the grey zone corresponds to the configuration where the system is excited by the external source alone; the blue zone (diamonds) corresponds to the configuration where the system is excited by the internal source alone; the others denote the configurations where the system is excited by both

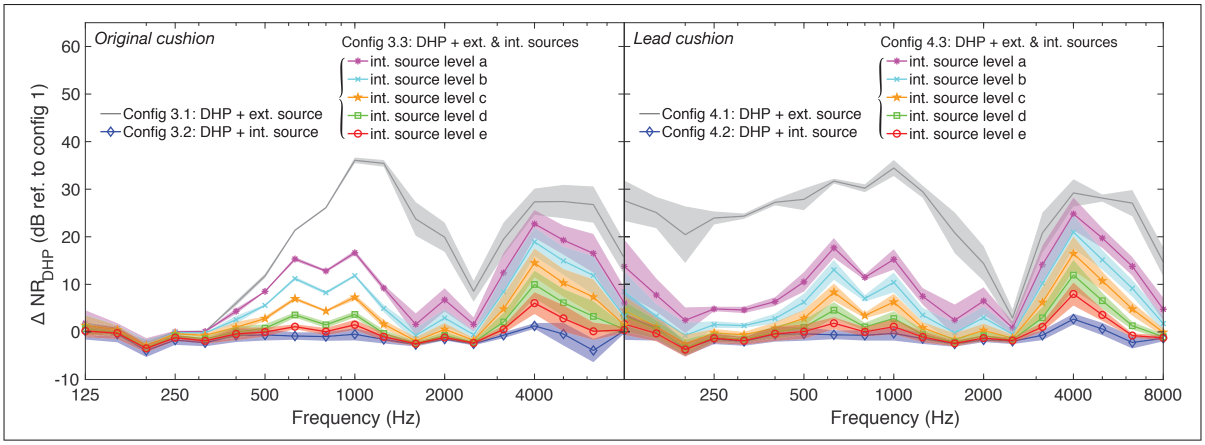

Figure 2.11 ΔNR_{DHP} with reference to the NR of the single earplug (configuration 1) with the original cushion (left) and lead cushion (right): configurations 3.1 & 4.1 (grey), external source alone; configurations 3.2 & 4.2 (blue diamonds), internal source alone (level max); configurations 3.3 & 4.3 (with increasing levels a – e corresponding respectively to purple asterisks, cyan crosses, orange pentagrams, green squares and red circles), external source + internal source (five levels). Results are displayed as "mean ± standard deviation"

the external and internal sources simultaneously with five different levels of the latter. The NR of the single earplug (configuration 1) is also presented (black zone with dots). The results in Fig. 2.10 are plotted in terms of ΔNR_{DHP} in Fig. 2.11. The corresponding SPLs under the earmuff are displayed in Fig. 2.12.

Figures 2.10 and 2.11 show that when the system is excited by the internal source alone at maximum level (configurations 3.2 and 4.2), the measured NR of the earplug in the DHP configuration is close to that of the single earplug measured with the external source and ΔNR_{DHP} is approximately equal to zero. This justifies the use of the single earplug NR (i.e., NR_{EP}) to estimate the earplug NR in the DHP due to the AB path (i.e., $NR_{\text{EP}}^{\text{DHP, AB}}$) (see Sec. 2.3.2). As described in Sec. 2.4.4.1, in this case the contributions of the SB paths are absent (SB2 and SB3) or reduced (SB1 and SB4), and only the AB path is considered to be effective. Consistently with Eqs. (2.2) and (2.5), when only the internal source is turned on, $p_{\text{mid}}^{\text{DHP, AB}}$ is equal to zero and $p_{\text{in}}^{\text{DHP, SB}}$ is negligible compared to $p_{\text{in}}^{\text{DHP, AB}}$. Thus, the DHP effect is not significant. This phenomenon again confirms that the DHP effect observed on the ATF is related to the flanking SB sound transmission through the system excited by the external sound field

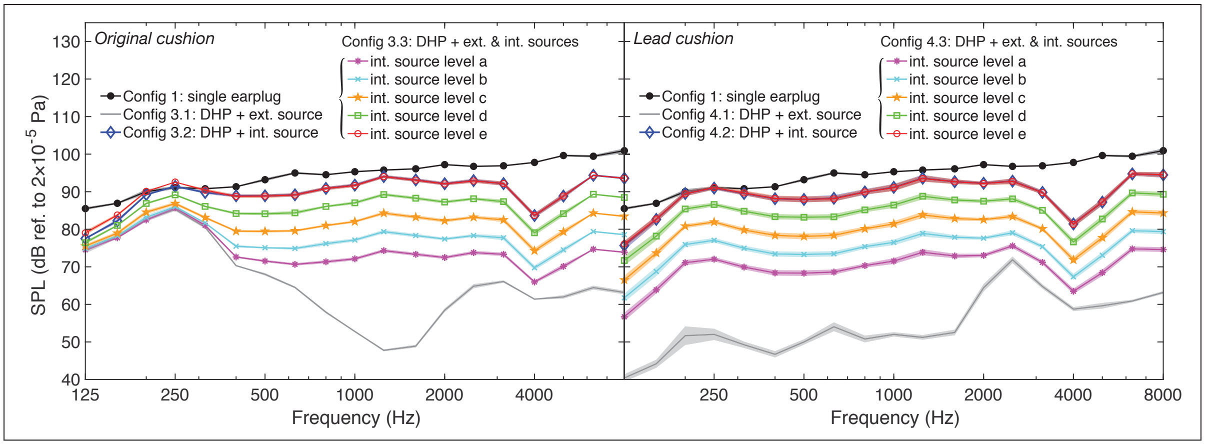

Figure 2.12 SPL measured under the earmuff with the original cushion (left) and lead cushion (right): configurations 3.1 & 4.1 (grey), external source alone; configurations 3.2 & 4.2 (blue diamonds), internal source alone (level max); configurations 3.3 & 4.3 (with increasing levels a – e corresponding respectively to purple asterisks, cyan crosses, orange pentagrams, green squares and red circles), external source + internal source (five levels). SPL at the earcanal entrance in the case of single earplug (configuration 1) is presented for comparison (black dots). Results are displayed as "mean ± standard deviation"

which is dominant over the "direct" AB transmission. In addition, it reveals that the acoustical coupling between the earplug and earmuff through the earmuff cavity does not significantly contribute to the DHP effect. This is in agreement with Nélisse *et al.*'s conclusion (2017) that the numerical model only accounting for the acoustical couplings cannot reproduce the DHP effect on the ATF. When the system is excited by both the external and internal sources (configurations 3.3 and 4.3), the measured earplug NR increases with the level of the internal source and approaches the NR of the single earplug (i.e., ΔNR_{DHP} approaches zero). This indicates that the AB sound path via the earplug becomes more and more important compared to the SB transmission as the SPL under the earmuff increases (see also Fig. 2.12). Indeed, Eq. (2.5) shows that $p_{\mathrm{in}}^{\mathrm{DHP,\,SB}}$ gets smaller compared to $p_{\mathrm{in}}^{\mathrm{DHP,\,AB}}$ as p_{spk} increases and hence the DHP effect becomes less significant. It is possible to find a particular SPL under the earmuff sufficiently high for which the AB path again becomes dominant over the SB one. The local minimum of the earplug NR around 4 kHz in configurations 3.3 and 4.3 is due to a local minimum of the SPL under the earmuff which is associated with the inherent limitation of the internal loudspeaker itself. Comparing configurations 3.3 and 4.3, the earplug NR values are found to approximately match each other above 300 Hz with similar SPLs under the earmuff. This is consistent with the mechanical test results shown in Fig. 2.9 where the effect of the earmuff cushion on the acceleration of the aluminum plate is only observed at frequencies below 300 Hz.

2.5.6 Discussion on the DHP effect

The observations in the present paper suggest that the DHP effect captured on the ATF is related to the acoustic energy transmitted from the earcup of the earmuff, through the cushion/aluminum plate assembly and finally into the earcanal via either the sound radiation of the earcanal lateral walls or the sound radiation of the earplug excited by the earcanal walls (SB4). This SB path involves (i) the mechanical coupling between the earplug and earmuff (through the cushion/plate/earcanal assembly) and (ii) the vibration of the earcanal walls which is similar to the fundamental mechanisms of the occlusion effect on human subjects. This means that the DHP effect should depend not only on the type of earplug but also on the choice of earmuff as well as the ATF used including its assembly and materials. SB4 in the DHP is found to dominate over the AB path via the earplug in most frequency bands due to the low SPL at the earcanal entrance compared to the case of the single earplug. Below 300 Hz, the contributions of both the AB path and SB4 increase due to the earmuff pumping motion. It is believed that the earmuff attenuation in this frequency range is low and the impact of the AB path is more important than the SB one (i.e., $p_{\text{in}}^{\text{DHP, SB}}/p_{\text{in}}^{\text{DHP, AB}} < 1$). As a result, the DHP effect is negligible. Between 300 Hz and 1 kHz, the earmuff attenuation increases progressively and the contribution of the AB path $p_{\text{in}}^{\text{DHP, AB}}$ decreases. The influence of SB4 is considered to remain significant and the DHP effect arises (i.e., $p_{\text{in}}^{\text{DHP, SB}}/p_{\text{in}}^{\text{DHP, AB}} > 1$). Between 1 kHz and 3 kHz, the earplug NR decreases due to the excitation of its first mode and one would expect the DHP effect to decrease. However, this is not the case. One reason could be that the earmuff attenuation is high in this frequency zone so that $p_{\text{in}}^{\text{DHP, AB}}$ remains much smaller than $p_{\text{in}}^{\text{DHP, SB}}$. Above 3 kHz, the effect of the earcanal wall vibration involved in SB4 should be reduced compared to lower frequencies. But the sound attenuation of the hearing protectors always remains relatively high which limits the contribution of the AB path, and the DHP effect is still important. Note that the experimental results obtained in the present paper do not necessarily allow for explaining the DHP effect observed on human subjects where the existing SB paths may be different from those on ATFs. But the DHP effect on human subjects could be partly related to a sound path similar to SB4 as mentioned in Gorman's work (1982), which remains to be further investigated. Prospectively, a numerical model based on a system much simpler than the ATF but accounting for the essential components together with the acoustical and mechanical couplings between them would be useful to better quantify the sound transmission mechanisms through the DHP.

2.6 Conclusion

In this paper, an objective experimental methodology has been proposed in order to (i) identify the main sound paths related to the DHP effect on an ATF and (ii) explain the latter by the relative contributions of the AB and SB transmissions in the system. The focus has been put on the NR of the single earplug and that of the earplug in the DHP configuration. Firstly, the effect of the earmuff headband and that of the sound transmission through the ATF and its tripod have been investigated by modifying the system coupling conditions. The contributions of these sound paths to the acoustic energy in the earcanal have been proved to be negligible. Secondly, the relative contributions of the "direct" AB transmission via the earplug and possible flanking SB paths have been studied using specially designed test configurations which made it possible to reduce or emphasize certain transmission paths compared to the others. The SPLs under the earmuff in these configurations have been controlled using a tiny loudspeaker placed beneath the earcup. It has been found that the acoustical coupling between the earplug and earmuff does not significantly contribute to the DHP effect. In addition, test results suggest that the DHP effect captured on the ATF is related to the acoustic energy passing from the earcup, through the cushion/aluminum plate assembly and finally into the earcanal via the sound radiation of the earplug and/or earcanal lateral walls. Particular attention has been paid to highlight this SB sound path through mechanical tests using an electrodynamic shaker. At frequencies below 300 Hz, it is believed to be controlled by the "direct" AB transmission as the presence of the pumping motion notably decreases the earmuff attenuation. In higher frequency bands, the earmuff attenuation becomes relatively high and this SB path is found to dominate over the AB path due to the low SPL at the earcanal entrance compared to the case of the single earplug. The DHP effect induced by the SB transmission is considered to be closely associated with the vibroacoustic behaviors of the hearing protectors and earcanal. This study offers some insight into the sound transmission through a DHP/ATF system and allows for better understanding the couplings between the components involved. It will also provide the grounds to develop a future numerical model to predict the sound attenuation of a DHP.

2.7 Acknowledgement

The authors gratefully acknowledge the financial support provided by the Natural Sciences and Engineering Research Council of Canada (NSERC).

CHAPTER 3

A FINITE ELEMENT MODEL TO PREDICT THE DOUBLE HEARING PROTECTOR EFFECT ON AN IN-HOUSE ACOUSTIC TEST FIXTURE

Yu Luan[a] , Franck Sgard[b] , Hugues Nélisse[b] , Olivier Doutres[a]

[a] Department of Mechanical Engineering, École de Technologie Supérieure,
1100 Rue Notre-Dame Ouest, Montreal, Quebec H3C 1K3, Canada

[b] Direction Scientifique, Institut de recherche Robert-Sauvé en santé et en sécurité du travail,
505 Boulevard de Maisonneuve Ouest, Montreal, Quebec H3A 3C2, Canada

Paper submitted for publication in *Journal of the Acoustical Society of America*, July 2021.

3.1 Abstract

The sound attenuation of double hearing protectors (DHPs), earplugs combined with earmuffs, is difficult to predict due to the DHP effect. This effect can be characterized by the earplug noise reduction decrease after adding the earmuff, and can also be observed on acoustic test fixtures (ATFs). It has been related to the relative contributions of airborne and structure-borne sound transmissions through the system, however the respective contribution of each transmission path has not been identified yet. Additionally, no available model can help understand the associated physical mechanisms. In this work, a finite element model is proposed and validated to study the DHP effect on an ATF between 100 Hz and 5 kHz. Power balances are calculated with selected configurations of the ATF in order to (i) quantify the contribution of each sound path, and study the effects of (ii) artificial skin and (iii) acoustic excitation on the ATF exterior boundaries. The DHP effect is shown to originate from the structure-borne power injected from the ATF boundaries and/or earmuff cushion. The important influence of earcanal wall vibration is highlighted when the skin is accounted for. The simulation results allow for gaining more insight into the sound transmission through a DHP/ATF system.

3.2 Introduction

Double hearing protectors (DHPs), namely earplugs combined with earmuffs, shall be used to protect workers in high noise level environments (CSA, 2014). However, it is generally recognized that their sound attenuation is difficult to predict due to the occurrence of the DHP effect (Luan, Doutres, Nélisse & Sgard, 2021). This refers to the phenomenon where the overall sound attenuation achieved by the DHP falls short of the algebraic sum of each single protector's attenuation when used independently. This effect was first observed in DHP attenuation measurements on human subjects (Berger, 1983; Berger *et al.*, 2003a; Mercy *et al.*, 2005; Tubb *et al.*, 2005) and was attributed to certain sound paths that bypass the hearing protectors: (i) the sound transmitted through the head and body directly to the middle and inner ears at frequencies above 2 kHz (Berger, 1983; Berger *et al.*, 2003a), and (ii) the occlusion effect (Stenfelt & Goode, 2005) or the acoustical and mechanical couplings between the earplug and earmuff contributing to the energy in the earcanal (outer ear bone conduction path) at frequencies below 2 kHz (Mercy *et al.*, 2005; Tubb *et al.*, 2005). However, among the aforementioned sound paths, the hypotheses regarding the contribution of the outer ear path appeared to be unsupported.

More recently, Nélisse *et al.* (2017) found that the DHP effect also occurs when DHP attenuation measurements are carried out on acoustic test fixtures (ATFs). These authors characterized the DHP effect by the decrease of the earplug noise reduction (NR) after adding an earmuff. Following Nélisse *et al.*'s work, the authors' of the present paper have conducted a series of specially designed experiments to measure the earplug NRs without and with an earmuff on a commercial ATF by controlling the sound pressure level (SPL) under the earmuff (Luan *et al.*, 2021). These experiments suggested that the DHP effect is mainly related to the structure-borne (SB) sound transmission through the system induced by external acoustic excitation. More specifically, this effect occurs when the contribution to the energy in the earcanal of the SB sound paths outweighs that of the airborne (AB) path due to the low SPL at the earcanal entrance compared to the single earplug configuration. According to the convention used, the AB path refers to the direct sound transmission into the earcanal through the earmuff, air cavity under the earmuff and earplug, while the SB paths refer to all the other sound paths through the hearing protectors and ATF. By excluding the importance of several potential SB paths which originate from the earmuff headband and ATF tripod, and focusing on the outer ear because of the use of an ATF, the authors suggested that the DHP effect on the ATF could be attributed to the SB paths involving (i) the mechanical coupling between the earplug and earmuff via the earmuff cushion/ATF assembly and (ii) the vibration of the earcanal walls which is similar to the fundamental mechanisms of the occlusion effect on human subjects. However, the respective contribution of each sound transmission path has not been identified yet.

Numerical modeling, as it has been done for single hearing protectors (Viallet *et al.*, 2013, 2014; Boyer *et al.*, 2015; Carillo *et al.*, 2018), remains a useful approach for gaining more insight into the sound transmission mechanisms through the DHP. Nevertheless, to the best of the authors' knowledge, no numerical model of the DHP/human head system can be found in the literature in view of the complexity of the system. The only existing DHP/ATF numerical models based on the finite element (FE) method could not be validated against experimental measurements due to an omission of the mechanical coupling between the earplug and earmuff via the ATF (Nélisse *et al.*, 2017) or an incomplete consideration of the SB sound paths in the system (James, 2006). A comprehensive literature review on both the experimental and numerical studies of DHP sound attenuation is available in the authors' previous work (Luan *et al.*, 2021).

This paper is a continuation of the authors' experimental analysis on the DHP effect (Luan *et al.*, 2021). Its main objective is to propose and validate a FE model in order to (i) study the DHP effect characterized by the difference between the NRs of an earplug alone and in a DHP on an ATF and (ii) better understand the sound transmission mechanisms through the DHP. First, a FE model of a DHP/ATF system is built following the modeling strategies proposed for a single earplug (Viallet *et al.*, 2013, 2014) and a single earmuff (Boyer *et al.*, 2015; Carillo *et al.*, 2018). Particularly, as the constitution of the earmuff cushion is complex and its most advanced model is accompanied with difficulties in assessing the mechanical properties (Carillo *et al.*, 2018), it is replaced by a silicone cushion of identical shape. Additionally, since the SB paths play an important role in the sound transmission through the DHP, an in-house ATF with a geometry simpler than a commercial one is used to better account for essential components in the model. The FE model is then validated by means of NR measurements of the single earmuff, single earplug and earplug in the DHP in a reverberant room. Finally, in order to quantify the contribution of each sound transmission path considered and to study the effects of the system construction, such as its material properties and boundary conditions, the FE model is exploited to calculate the power balances using selected configurations of the in-house ATF.

The paper is organized as follows. Section 3.3 describes the FE modeling strategy for the DHP/ATF system and simulation configurations, along with the geometry, boundary conditions, material properties, and the selected acoustic and vibratory indicators. Section 3.4 presents the experimental measurements of the hearing protector sound attenuation. Finally, Sec. 3.5 analyzes and discusses the simulation and measurement results for different configurations of interest.

3.3 Finite element modeling of the DHP/ATF system

3.3.1 Geometry

The system of interest is a DHP worn on an in-house ATF (see Fig. 3.1). The in-house ATF consists of an instrumented circular steel plate. It has a similar weight but a much simpler geometry compared to the G.R.A.S. 45CB ATF (G.R.A.S. Sound & Vibration AS, Denmark) used in the authors' previous work (Luan *et al.*, 2021). As explained in the introduction, this makes it possible to better account for the SB sound transmission through the system in the FE model. In addition, simple boundary conditions can be chosen for the corresponding setup to facilitate their application in the model. Inside the in-house ATF, a cylindrical earcanal has been drilled whose size is identical to the one in the G.R.A.S. 45CB. In contrast to commercial ATFs specified in the standard ANSI S12.42 (2020), certain simplifications have been made to the in-house ATF. First, the pinna simulator and artificial skin layer in the earcanal are not included. Second, there is no built-in temperature control unit. Third, the acoustic impedance produced by the ear simulator (IEC, 2010) in the earcanal is not accounted for. Moreover, as the focus is

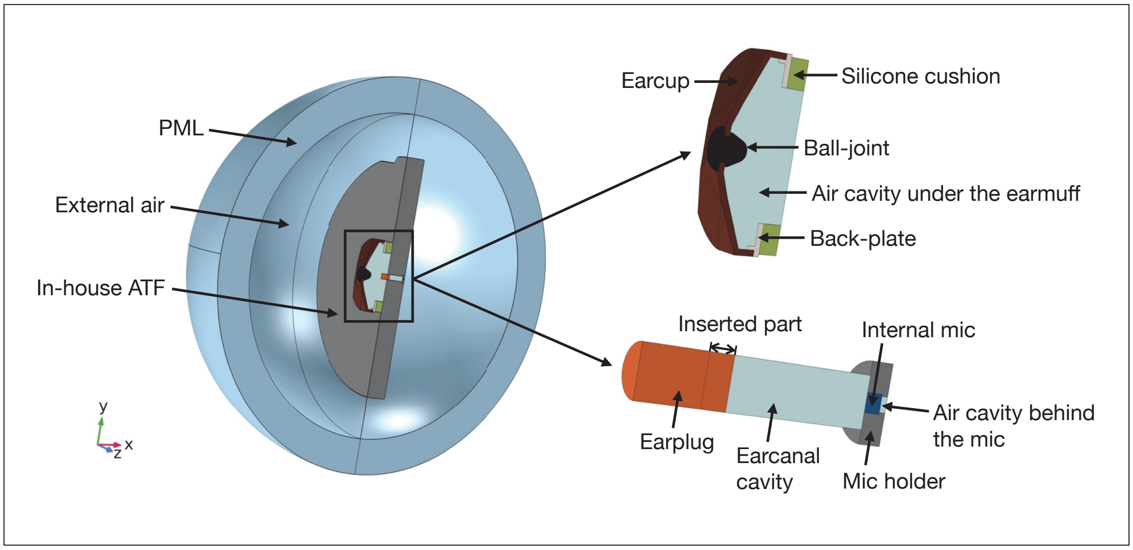

Figure 3.1 Geometry of the DHP/ATF system (symmetric view): global view (left); earmuff with a silicone cushion (upper right); earplug inserted into the earcanal (lower right)

put on the outer ear, the middle and inner ears are not included either. Actually, the terminal surface of the in-house ATF earcanal has been designed to correspond to the "eardrum position" in a commercial ATF earcanal where sound pressure is recorded (Luan, Sgard, Benacchio, Nélisse & Doutres, 2019). More specifically, an internal miniature microphone together with a microphone holder is tightly attached to the ATF so that the microphone is flush-mounted into the holder at the "eardrum position". A small cylindrical air cavity lies behind the microphone to pass the wire of the microphone. These components may still contribute to the sound pressure in the earcanal cavity but mimicking a realistic contribution of the eardrum together with the middle and inner ears is not within the scope of the present paper.

The studied DHP consists of an earplug made of silicone rubber specially molded to fit the shape of the in-house ATF earcanal and a commercial earmuff (EAR-MODEL-1000, 3M^{TM} E-A-R^{TM}, Indianapolis, USA) as used for the experiments in the authors' previous work (Luan *et al.*, 2021). Such types of single hearing protectors have already been studied numerically and experimentally (Viallet *et al.*, 2013, 2014; Boyer *et al.*, 2015; Carillo *et al.*, 2018). The total length of the earplug is 14 mm and the length of the inserted part is 4 mm which corresponds to a shallow insertion. The radius of the earplug is chosen to be 3.75 mm which is identical to that of the earcanal but in practice, its actual radius is slightly larger in order to ensure a good sealing condition (see Sec. 3.4). The foam liner inside the air cavity under the earmuff is not taken into consideration as it does not significantly modify the vibratory behavior of the system. As justified in the introduction, the original comfort cushion of the earmuff is replaced by a silicone cushion of identical shape. The thickness of the compressed silicone cushion assessed *in situ* when the earmuff is worn on the ATF is about 10.6 mm. Key geometric dimensions of the system components are provided in Table 3.1.

Two configurations of the in-house ATF are mainly studied. The first one, referred to as ATF#1 (see Fig. 3.2(a)), corresponds to the original ATF structure built to validate the FE model which includes "rigid" earcanal lateral walls as depicted in Fig. 3.1. The second ATF, referred to as ATF#2 (see Fig. 3.2(b)), is similar to ATF#1 but a silicone layer and a silicone pad mimicking the skin portions in contact with respectively the interior of the earcanal and earmuff cushion are accounted for. Their geometric dimensions are similar to the artificial skin parts of a commercial ATF and can also be found in Table 3.1. The use of ATF#2 makes the system more realistic in terms of material properties and allows for investigating the influence of the skin on the DHP effect.

3.3.2 Loading, coupling and boundary conditions

For both configurations of the in-house ATF, the simulated DHP/ATF system is supposed to be inside an infinite external air domain. It is modeled with an air-filled convex surrounded by a perfectly matched layer (PML) (Bériot & Gabard, 2019) which simulates the Sommerfeld condition (see Fig. 3.1). The system is excited by a diffuse sound field modeled as a superposition of incoming uncorrelated plane waves with equal amplitude freely propagating in multiple directions in the external air domain. Each incident plane wave with direction of propagation described by the elevation angle $\theta \in [0, \pi]$ and azimuthal angle $\varphi \in [0, 2\pi]$ (in the yz plane, see Fig. 3.1) can be written as:

$$p(\theta, \varphi) = 0.3 \exp(-\mathrm{j}(k_x x + k_y y + k_z z)), \tag{3.1}$$

Table 3.1 Key geometric dimensions of the components in the FE model

	ATF	Mic holder	Internal mic	Cavity behind the mic	Open earcanal
Radius (mm)	170	5.75	1.4	1.1	3.75
Thickness/length (mm)	30.1	3.6	2.6	1	26.5
	Occluded earcanal	**Silicone layer**	**Silicone pad**	**Cushion**	**Earplug**
Radius (mm)	3.75	5.75	57.5	–	3.75
Thickness/length (mm)	22.5	14	10	10.6	14

with $k_x = k_0 \cos\theta$, $k_y = k_0 \sin\theta \cos\varphi$, $k_z = k_0 \sin\theta \sin\varphi$ and k_0 the wavenumber. The amplitude of 0.3 Pa ensures that the overall SPL in the model is approximately the same as that measured in the room during the experiments (see Sec. 3.4). Continuity of stresses and displacements is assumed at the interfaces between solid domains. At fluid-solid interfaces, the fluid-structure coupling condition applies, i.e., continuity of tractions and normal displacements. The FE formulations associated with the problem of interest are classic and are not recalled here for the sake of conciseness. The reader can, for example, refer to Chapters 3 and 6 of Atalla & Sgard's work (2015) for details.

For ATF#1, decoupled conditions are applied to the back surface of the air cavity behind the internal microphone and that of the microphone holder (see Fig. 3.2(a)). More specifically, an

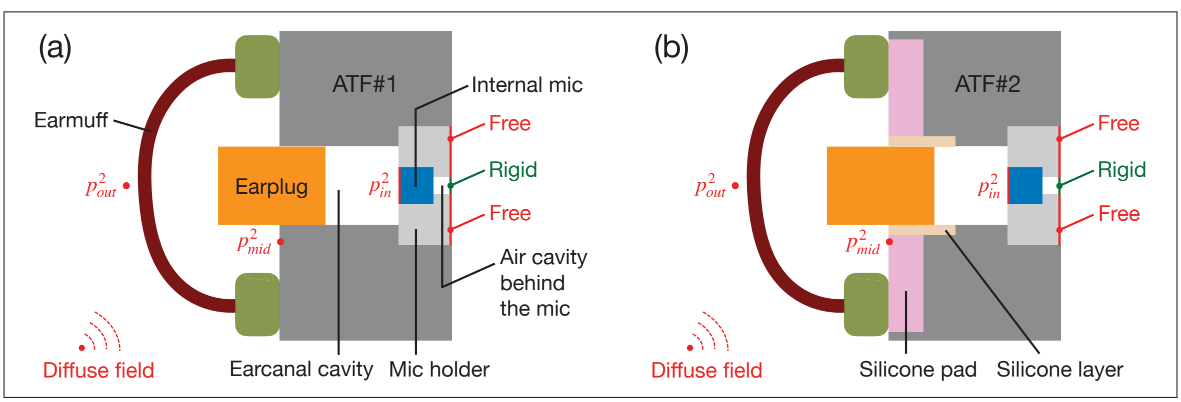

Figure 3.2 Schematic representation of the DHP worn on (a) fully "rigid" ATF#1 and (b) ATF#2 with artificial skin portions (cross-section view)

acoustically rigid boundary is used at the interface between the air cavity behind the microphone and external air domain; the microphone holder's exterior surface, which is in contact with the external air domain, is considered to be mechanically free. In other words, no acoustic excitation is applied to these boundaries. This is assumed to correspond to the setup used for the experiments (see Sec. 3.4). For ATF#2, the same decoupled conditions are adopted for the purpose of comparison (see Fig. 3.2(b)). Additionally, complementary configurations of the in-house ATF, namely ATF#3 and ATF#4 have also been investigated in which all the exterior boundaries of the ATF outside the earmuff are considered to be decoupled from the external air domain. They allow for studying the influence on the DHP effect of the acoustic excitation on the ATF exterior boundaries. These configurations together with the corresponding simulation results are described in Appx. V. Again, note that ATF#1 has been physically fabricated for experimental validation while ATF#2 – ATF#4 are devoted to numerical tests. They are all identical in terms of ATF size and earcanal geometric dimensions.

3.3.3 Material properties

The air domains (external air, air cavity under the earmuff, earcanal cavity and air cavity behind the internal microphone) are modeled as compressible perfect gas domains, defined by their density (ρ_0 = 1.2 kg/m^3) and speed of sound (c_0 = 343.4 m/s) under standard conditions for temperature (T_0 = 293.15 K) and atmospheric pressure (P_0 = 1.01e^5 Pa). No energy losses are accounted for in the external air domain while the dissipation induced by thermo-viscous effects in the air cavity under the earmuff is considered using a structural loss factor of 1% (Boyer *et al.*, 2015; Carillo *et al.*, 2018). The thermo-viscous losses in the earcanal cavity and air cavity behind the internal microphone are calculated based on the low reduced frequency model of a circular duct type (Kampinga, 2010).

The earcup and back-plate of the earmuff are made of ABS (Acrylonitrile Butadiene Styrene), and its ball-joint is made of rubber (Boyer *et al.*, 2015; Carillo *et al.*, 2018). In addition, the in-house ATF and microphone holder are made of steel, and the internal microphone is made of aluminum. These components together with the artificial skin parts are modeled as linear

Table 3.2 Mechanical properties of the components in the FE model

	ATF/mic holder	**Internal mic**	**Artificial skin**	**Earcup/back-plate**	**Ball-joint**	**Cushion**	**Earplug**
ρ_s **(kg/m^3)**	7850	2700	1150	1200	800	1170	1500
E_s **(GPa)**	200	70	$4.2e^{-4}$	2.16	0.1	–	$2.9e^{-3}$
ν_s **(1)**	0.3	0.33	0.43	0.38	0.48	0.49	0.49
η_s **(1)**	0.005	0.005	0.2	0.05	0.5	–	0.1

isotropic elastic solids whose mechanical properties are given in Table 3.2. Particularly, the properties of artificial skin are adopted from Viallet *et al.*'s work (2014).

The mechanical properties of the earplug and silicone cushion are characterized using cylindrical specimens on a quasi-static mechanical analyzer (QMA) (ISO, 2011) and calibrated according to the sound attenuation measurements of single protectors. The earplug is modeled as a linear isotropic elastic solid (Viallet *et al.*, 2014) and its properties can also be found in Table 3.2. Specifically, the silicone cushion is considered as a linear isotropic viscoelastic solid. Its frequency dependent Young's modulus and loss factor are assessed using the method proposed by Boyer *et al.* (2015) by means of curve fitting a fractional derivative Zener model based on the low frequency QMA data (see Appx. VI).

3.3.4 Meshing and solving

All the domains in the FE model are meshed using 10-noded tetrahedral elements except for the PML domain which is meshed using 15-noded quadratic triangular prisms. A meshing criterion of at least 6 elements per wavelength is selected. Preliminary simulations using refined meshes have shown that this criterion is sufficient to achieve convergence of the solution. For calculating the acoustic and vibratory indicators under a diffuse field excitation, the system equations are solved for each incident plane wave in the software COMSOL Multiphysics (v.5.6 COMSOL®, Sweden). Each diffuse field indicator can then be calculated through an integration over the entire space:

$$A^{\mathrm{d}} = \int_0^{2\pi} \int_0^{\pi} A_{(\theta,\varphi)}\, d\theta\, d\varphi, \tag{3.2}$$

with $A_{(\theta,\varphi)}$ being a mean square sound pressure or an exchanged power described in Sec. 3.3.5. In the present paper, the diffuse field indicators are all computed based on a Gauss point integration scheme of 16 Gauss points (Sgard, Atalla & Nicolas, 2000).

3.3.5 Calculation of acoustic and vibratory indicators

3.3.5.1 Sound attenuation indicators

Mean square sound pressures are computed at three different locations (see Fig. 3.2) for each incident plane wave in the FE model: (i) at a point outside but close to the center of the earcup (p_{out}^2), (ii) at a point below but close to the earcanal entrance (p_{mid}^2) and (iii) at the surface of the internal microphone, i.e., at the "eardrum position" (p_{in}^2). These locations approximately correspond to the real microphone positions in the experiments (see Sec. 3.4). The associated diffuse field results ${p_{\mathrm{out}}^{\mathrm{d}}}^2$, ${p_{\mathrm{mid}}^{\mathrm{d}}}^2$ and ${p_{\mathrm{in}}^{\mathrm{d}}}^2$ are then derived from Eq. (3.2) in order to determine the sound attenuation indicators of the hearing protectors. In the following, the abbreviations "EM", "EP" and "DHP" in the superscripts are used to identify the single earmuff, single earplug or DHP configuration.

As explained in the introduction, the NRs of the earplug alone (NR_{EP}) and in the DHP ($NR_{\mathrm{EP}}^{\mathrm{DHP}}$) are of particular interest for quantifying the DHP effect (Luan *et al.*, 2021). They are defined as the difference between the SPLs at the earcanal entrance and at the "eardrum position" when a single earplug (see Eq. (3.3)) or a DHP (see Eq. (3.4)) is worn:

$$NR_{\mathrm{EP}} = 10\log_{10}\left(\frac{{p_{\mathrm{mid}}^{\mathrm{d,EP}}}^2}{p_{\mathrm{ref}}^2}\right) - 10\log_{10}\left(\frac{{p_{\mathrm{in}}^{\mathrm{d,EP}}}^2}{p_{\mathrm{ref}}^2}\right), \tag{3.3}$$

$$NR_{\mathrm{EP}}^{\mathrm{DHP}} = 10\log_{10}\left(\frac{{p_{\mathrm{mid}}^{\mathrm{d,DHP}}}^2}{p_{\mathrm{ref}}^2}\right) - 10\log_{10}\left(\frac{{p_{\mathrm{in}}^{\mathrm{d,DHP}}}^2}{p_{\mathrm{ref}}^2}\right), \tag{3.4}$$

where $p_{\mathrm{ref}} = 2\mathrm{e}^{-5}$ Pa. In particular, the NR of the earmuff alone (NR_{EM}) is also calculated using ATF#1 in order to validate the FE modeling of the earmuff. It corresponds to the difference between the SPLs outside the earmuff and at the "eardrum position" when a single earmuff is worn:

$$NR_{\mathrm{EM}} = 10\log_{10}\left(\frac{p_{\mathrm{out}}^{\mathrm{d,EM}^2}}{p_{\mathrm{ref}}^2}\right) - 10\log_{10}\left(\frac{p_{\mathrm{in}}^{\mathrm{d,EM}^2}}{p_{\mathrm{ref}}^2}\right). \tag{3.5}$$

3.3.5.2 Exchanged powers

In order to quantify the energy transfers through the DHP/ATF system, the powers exchanged at the interfaces between different fluid and solid domains are calculated. At a fluid-solid interface, for example at the earplug medial surface towards the earcanal cavity, the exchanged power can be calculated by:

$$\Pi_{\mathrm{exch,f/s}} = \frac{1}{2}\Re\left[\int_S p\vec{n}\cdot\vec{v}^*\,\mathrm{d}S\right], \tag{3.6}$$

where p is the sound pressure in the fluid domain, $\vec{v}^*$ denotes the complex conjugate of the structural velocity, and $\vec{n}$ the normal vector to the interface. At a solid-solid interface, such as the interface between the earplug and earcanal lateral walls, the exchanged power is expressed as:

$$\Pi_{\mathrm{exch,s1/s2}} = \frac{1}{2}\Re\left[\int_S \underline{\underline{\sigma}}\vec{n}\cdot\vec{v}^*\,\mathrm{d}S\right], \tag{3.7}$$

where $\underline{\underline{\sigma}}$ denotes the structural stress tensor. In addition, the power dissipated in a solid domain due to structural damping can be calculated by:

$$\Pi_{\mathrm{diss,s}} = \frac{1}{2}\Re\left[-\mathrm{j}\omega\int_V \underline{\underline{\sigma}} : \underline{\underline{\varepsilon}}^*\,\mathrm{d}V\right], \tag{3.8}$$

where $\underline{\underline{\sigma}} : \underline{\underline{\varepsilon}}^*$ refers to the double dot product of the structural stress tensor and the complex conjugate of the structural strain tensor. The corresponding diffuse field powers $\Pi^{\mathrm{d}}_{\mathrm{exch,f/s}}$, $\Pi^{\mathrm{d}}_{\mathrm{exch,s1/s2}}$ and $\Pi^{\mathrm{d}}_{\mathrm{diss,s}}$ are obtained using Eq. (3.2) by substituting Eqs. (3.6) – (3.8) for $A_{(\theta,\varphi)}$. Finally, the diffuse field power dissipated in a fluid domain due to thermo-viscous effects is calculated using a power balance approach. The power balance for a given fluid domain writes:

$$\sum \Pi^{\mathrm{d}}_{\mathrm{exch,f/s}} + \Pi^{\mathrm{d}}_{\mathrm{diss,f}} = 0. \tag{3.9}$$

3.4 Experimental setup

In order to validate the FE model, the sound attenuation indicators of the hearing protectors (see Sec. 3.3.5.1) are measured at normal room temperature using the setup corresponding to ATF#1 (see Fig. 3.3). Measurements are carried out in a diffuse sound field generated by four loudspeakers (MACKIE HD1531, MACKIE®, USA) placed at each corner of a reverberant room. The speakers are fed with white noise of about 110 dB in overall SPL using a Minirator MR2 audio generator (NTi Audio AG, Liechtenstein). The in-house ATF is suspended on an aluminum frame in the center of the room using nylon cords via two hooks on the ATF. The center of the ATF earcanal is located at a height of about 75 cm above the floor. The earplug is shallowly inserted into the earcanal, which facilitates the removal of the earplug. The silicone cushion is attached to the back-plate of the earmuff using strong double-sided adhesive tape. The earmuff together with the silicone cushion is placed on the ATF with the help of a half headband screwed to the ATF. The half headband was already used in Boyer *et al.*'s work (2014) to reproduce the clamping force imposed by the span of a standardized commercial ATF of about 11.5 N. The hooks on the ATF and half headband are not included in the FE model (see Sec. 3.3.1) since preliminary simulations have shown that they do not significantly affect the simulated sound attenuation of the hearing protectors.

The mean square sound pressure at the "eardrum position" is measured using a miniature microphone (FG-23629-P16, Knowles®, USA) fixed by a microphone holder at the terminal of the ATF earcanal (see Fig. 3.1 lower right). A small air cavity behind this microphone has been fabricated in the microphone holder in order to pass the wire of the microphone. The back surface of this air cavity and that of the microphone holder are covered by two layers of 0.375 in. Barymat® barrier of 1.2 lbs/sq.ft (M-100D, AcoustiGuard™, Canada) with mounting putty carefully placed around them in order to minimize the influence of parasitic sound leaks. In addition, two miniature microphones (FG-23329-D65, Knowles®, USA) are attached to (i) the half headband outside the earmuff (see MIC_{out} in Fig. 3.3(b)) and (ii) the ATF front surface close to the earcanal entrance (see MIC_{mid} in Fig. 3.3(c)) to measure the mean square sound pressures at the corresponding positions. Particularly, a narrow groove has been made on

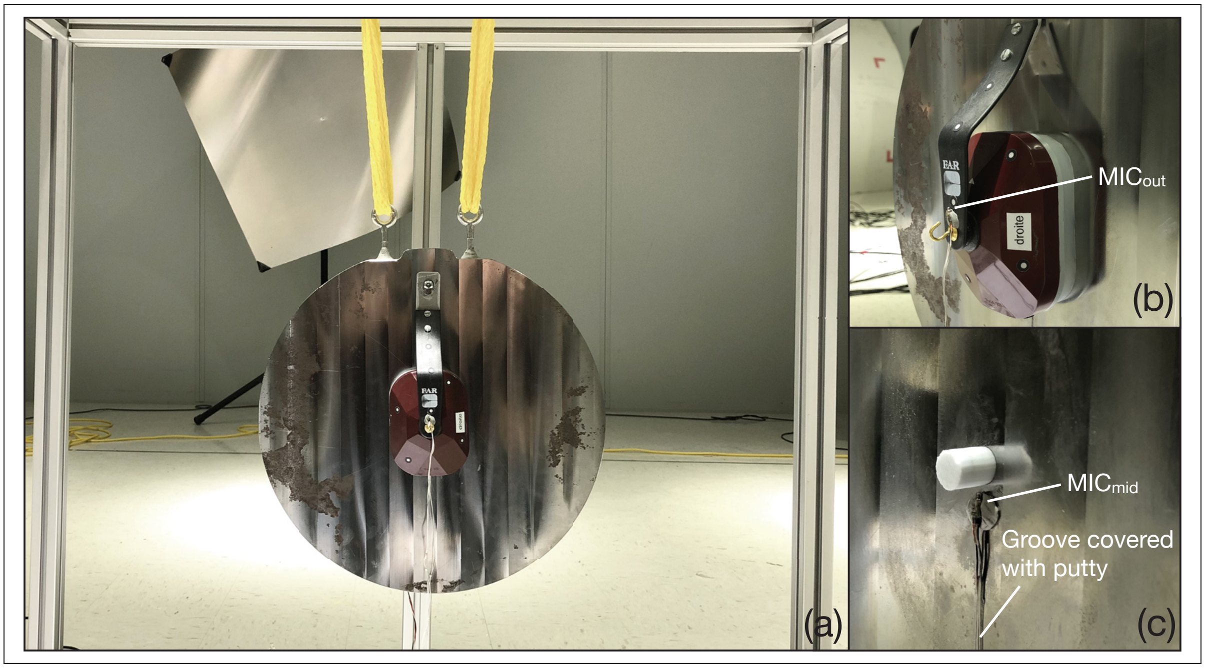

Figure 3.3 Experimental setup adopted to validate the FE model: (a) global view; (b) earmuff with a silicone cushion; (c) earplug inserted into the earcanal

the ATF front surface to pass the wire of the microphone positioned at the earcanal entrance ($\mathrm{MIC_{mid}}$) to the outside of the earmuff. This groove is filled with mounting putty in order to avoid potential sound leaks induced by the wire between the silicone cushion and ATF. A reference $\frac{1}{2}$ in. microphone (BSWA Technology Co., China) is placed at about 1 m from the earcanal entrance (not shown in Fig. 3.3) in order to obtain the transfer functions between the other three microphones and this microphone (Boyer *et al.*, 2014; Viallet *et al.*, 2014). These transfer functions are then substituted for the mean square sound pressures in Eqs. (3.3) – (3.5) to calculate the sound attenuation indicators of interest. Tests are performed using respectively the single earmuff, single earplug and DHP. Each test is repeated three times by removing and repositioning the studied hearing protectors in order to account for the variability related to the mounting conditions.

3.5 Results and discussion

3.5.1 Sound attenuation of hearing protectors

3.5.1.1 Validation of the finite element model

First, the simulated sound attenuation of the hearing protectors in both the single and DHP configurations on ATF#1 is compared with the experimental data in order to validate the FE model (see Figs. 3.4 and 3.5). In the present paper, results are plotted in narrow frequency bands between 100 Hz and 5 kHz, and the experimental data are displayed in terms of mean values and 95% confidence intervals for the three repetitions of each test. Figure 3.4 presents the single earmuff NRs in which the blue curve with dots and grey zone correspond respectively to the simulation and measurement results.

The figure shows that the simulated earmuff NR is in very good agreement with the measurement results. The earmuff with a silicone cushion is found to be capable of replicating the earmuff pumping motion (Berger *et al.*, 2003b; Boyer *et al.*, 2014; Boyer, 2015) at about 230 Hz. The trough around 380 Hz corresponds to a mechanical mode of the earmuff under acoustic excitation for which (i) the inner and outer lateral walls of the silicone cushion vibrate in phase, and (ii) the rest of the structure moves as a rigid body. A similar phenomenon has been pointed out in past studies which considered the original earmuff comfort cushion as an equivalent elastic solid (Boyer, 2015; Carillo *et al.*, 2018). At about 3 kHz, a local minimum of the earmuff NR is found. It is related to an acoustic resonance controlled by the earcanal cavity. The troughs around 4.1 kHz and 4.7 kHz correspond to the coupled modes of the earmuff controlled by the earmuff cavity (Pääkkönen, 1992; Berger *et al.*, 2003b).

The simulated and measured earplug NRs are compared in Fig. 3.5. The black and grey zones denote the measured NRs of the single earplug and of the earplug in the DHP. The DHP effect, i.e., difference between the NRs of the earplug alone and in the DHP can be observed up to 5 kHz. This confirms the ability of the proposed in-house ATF to capture this effect as already

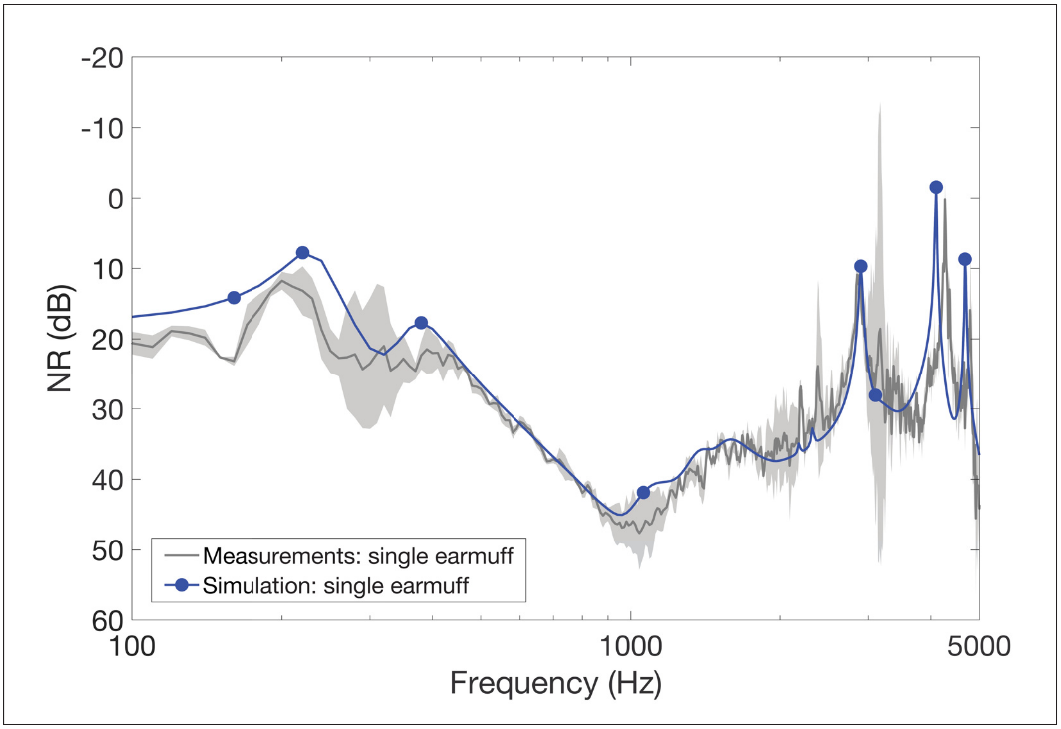

Figure 3.4 NRs of the single earmuff measured and simulated using ATF#1: measurement results (averaged value with 95% confidence interval, grey zone); simulation result (blue curve with dots)

observed on commercial ATFs and human subjects. The blue curve with dots and green curve with diamonds correspond to the associated simulation results respectively. A satisfactory agreement is seen between the simulation and measurement results in the single configuration in nearly the whole frequency range concerned, and in the DHP configuration at frequencies above 400 Hz. For the single earplug, its modes (Sgard *et al.*, 2010) at about 1 kHz and 2.5 kHz can be predicted by the FE model. A sharp trough is observed at about 2.2 kHz. It corresponds to a symmetric bending wave mode of the in-house ATF for which the central region of the ATF exhibits the highest displacement. The earcanal together with the earplug and earmuff all lies within this region. Comparing the DHP configuration to the single configuration, the DHP effect can also be correctly captured by the model at frequencies above 400 Hz. The most significant DHP effect, up to about 40 dB, occurs at medium frequencies between 2 kHz and 2.5 kHz where the bending wave mode of the ATF is observed. The DHP effect is also found to be pronounced

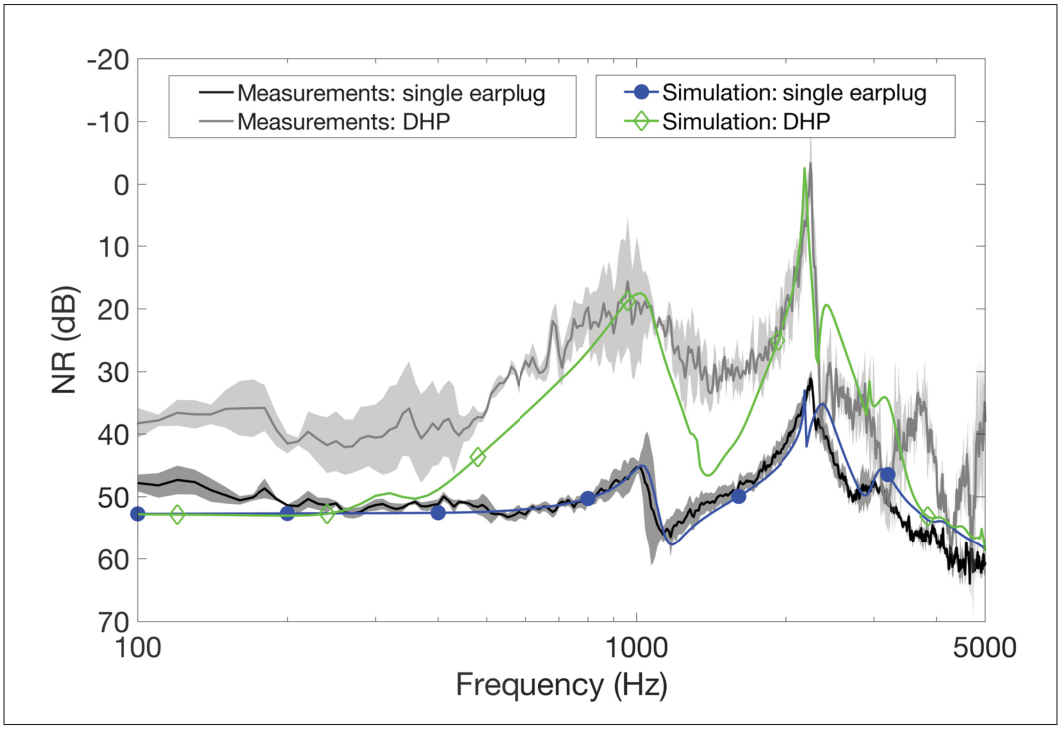

Figure 3.5 NRs of the earplug measured and simulated using ATF#1: measurement results of the single earplug (averaged value with 95% confidence interval, black zone) and earplug in the DHP (averaged value with 95% confidence interval, grey zone); simulation results of the single earplug (blue dots) and earplug in the DHP (green diamonds)

around 1 kHz probably because of the maximum earmuff attenuation that is reached in this frequency range (Luan *et al.*, 2021) (see also Fig. 3.4).

At frequencies below 400 Hz, the simulated earplug NRs in both the single and DHP configurations are similar. In other words, no significant DHP effect is shown by the FE model. This is consistent with the experimental data obtained on a commercial ATF in the authors' previous work (Luan *et al.*, 2021) and on human subjects in Nélisse *et al.*'s work (2017). It has been explained by the low earmuff attenuation in this frequency range due to the earmuff pumping motion that increases the sound pressure under the earmuff and makes the direct AB sound path through the earplug outer surface dominant over the SB paths (Luan *et al.*, 2021).

However, the measured earplug NRs in the single and DHP configurations are not close to each other at frequencies below 400 Hz, which suggests a non-negligible DHP effect. In this frequency range, the measured earplug NR in the DHP is found to be lower than the simulated one by up to about 15 dB. Supplementary tests (both experimental and numerical) suggest that this phenomenon could be explained by potential SB sound transmission through the earcanal terminal portion, which is not accurately captured by the model. This behavior might contribute directly to the sound pressure in the earcanal cavity, or facilitate the sound radiation of the earcanal lateral walls without evidently changing the sound pressure at the earcanal entrance, and in turn decreases the earplug NR. As the DHP has a much higher AB attenuation compared to the single earplug, it is more sensitive to SB transmission, and thus the decrease of the earplug NR is only pronounced in the DHP configuration. Such a phenomenon is also found to have an effect around 1.5 kHz where a difference of about 15 dB is observed between the simulated and measured earplug NRs in the DHP. Moreover, as the AB attenuation of the earmuff is even lower than that of the earplug alone, especially at frequencies below 400 Hz (due to the pumping motion and transverse mode of the silicone cushion previously explained), such a phenomenon is not detectable in Fig. 3.4.

According to the results above, despite some local discrepancies between the simulations and measurements in the DHP configuration due to potential SB transmission that is difficult to fully control in practice, the FE model is deemed capable of capturing the over behavior of the DHP/ATF system in the frequency range between 100 Hz and 5 kHz where the DHP effect mainly occurs. In the following simulations, the model is exploited to analyze different sound transmission paths, and study the impacts of material properties and boundary conditions on the DHP effect in an ideal system without the influence of undesirable SB sound.

3.5.1.2 Analysis of the contribution of the ATF on the DHP effect

Now that the FE model is considered to have been validated against experimental measurements, it is used to simulate the earplug NRs in the single and DHP configurations on both ATF#1 and ATF#2 in order to study the impact of the skin on the DHP effect. The NRs of the single earplug and of the earplug in the DHP on ATF#1 are plotted in Fig. 3.6(a) using the black curve with dots and dotted black curve with crosses. The corresponding simulation results on ATF#2 are presented by the blue curve with diamonds and dotted blue curve with pentagrams. For the purpose of a clearer comparison, results on each ATF are also displayed in terms of ΔNR_{DHP} in Fig. 3.6(b) using the black curve with dots and blue curve with diamonds. This indicator was already used in the authors' previous work (Luan *et al.*, 2021) to characterize the DHP effect. It is defined as the difference between the NRs of the earplug alone and in the DHP (see Sec. 3.3.5.1): $\Delta NR_{\mathrm{DHP}} = NR_{\mathrm{EP}} - NR_{\mathrm{EP}}^{\mathrm{DHP}}$.

From the single earplug NR on ATF#2 (see Fig. 3.6(a)), a mechanical mode of the earplug/skin assembly is found around 350 Hz. This mode is mainly dominated by the behavior of the earplug which exhibits the highest displacement. It is shifted to lower frequencies and becomes more spread out over the frequency zone compared to the earplug resonances found on ATF#1 (see Sec. 3.5.1.1). The fact that the artificial skin has a much lower Young's modulus and higher loss factor than those of the earplug can explain this phenomenon (see Table 3.2). From a mechanical point of view, the skin plays an important role around the earplug lateral walls which reduces the overall stiffness of the earplug/ATF system. As a result, it is expected to have more sound energy radiated into the earcanal cavity by the earplug and earcanal walls. This also explains the significant decrease of the single earplug NR by up to 45 dB on ATF#2 compared to ATF#1 at frequencies below 1.5 kHz where the system is mainly controlled by its stiffness (Viallet *et al.*, 2014). The lowest single earplug NR on ATF#2 is observed around 800 Hz which could be attributed to multiple coupled modes of the earplug/skin assembly excited in this frequency range. Moreover, compared to ATF#1, the frequency of the symmetric bending wave mode of ATF#2 is slightly reduced to about 2 kHz again due to the inclusion of the artificial skin that decreases the system overall stiffness. It is interesting to mention that both the NRs of the single earplug and of the earplug in the DHP on ATF#2 are of a similar order of magnitude to the experimental data obtained on human subjects in Nélisse *et al.*'s work (2017). This indicates the importance of taking into account the skin for predicting the DHP attenuation in a more realistic way.

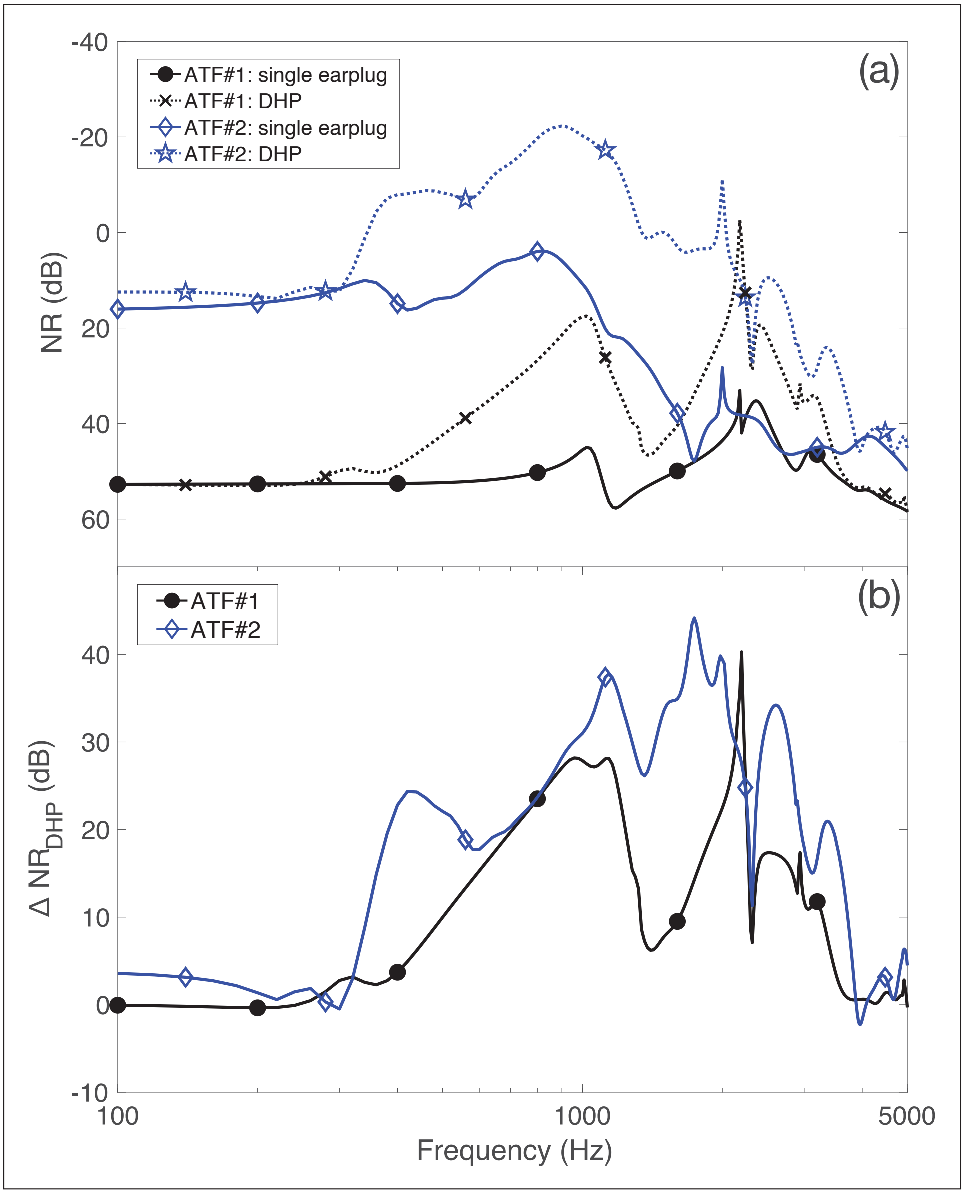

Figure 3.6 Simulation results of (a) earplug NRs: results of the single earplug on ATF#1 (black dots) and ATF#2 (blue diamonds), and results of the earplug in the DHP on ATF#1 (dotted black crosses) and ATF#2 (dotted blue pentagrams); (b) ΔNR_{DHP}: results on ATF#1 (black dots) and ATF#2 (blue diamonds)

Figure 3.6(b) shows that ΔNR_{DHP} is close to zero at frequencies below 300 Hz for both ATF#1 and ATF#2. As explained in Sec. 3.5.1.1, the direct AB sound path through the earplug outer surface is dominant over the SB paths in this frequency range due to the pumping motion and silicone cushion transverse mode, which hence decreases the DHP effect. In most frequency bands, the DHP effect on ATF#2 is found to be higher than that on ATF#1. This could result from the use of the artificial skin which raises the vibration of the earcanal walls (in contact with the non-occluded part of the earcanal cavity), increases the acoustic volume velocity imposed by the latter, and therefore favors the outer ear SB path.

Additionally, the simulation results of ΔNR_{DHP} are also compared between ATF#1 – ATF#2 and ATF#3 – ATF#4 in Fig.-A V-2(b) in order to investigate the influence on the DHP effect of the acoustic excitation on the ATF exterior boundaries. A notable DHP effect on ATF#3 is only observed around 2.2 kHz where the bending wave mode of the ATF occurs. It is found to be lower than the DHP effect on ATF#1 at most frequencies below 2 kHz and above 2.5 kHz. This means that the acoustic excitation on the ATF exterior boundaries has an important influence in these configurations within the corresponding frequency zones. On the opposite, the comparison between ATF#2 and ATF#4 shows that the acoustic excitation on the ATF boundaries does not make a great difference to the DHP effect when the artificial skin is accounted for. This is further studied through power balances in the following section.

3.5.2 Analysis of the contribution of each sound path using power balances

This section presents the simulation results of power balances. The results for ATF#1 (fully "rigid") and ATF#2 (with artificial skin) are discussed in the two following subsections respectively. For each of them, the power balances are calculated in three chosen domains, namely the earcanal cavity, earplug and ATF. The power balances in the earcanal cavity and earplug are compared between the single earplug and DHP configurations. This makes it possible to study the relative contributions of different sound paths without and with the earmuff. The power balance in the ATF is shown only for the DHP configuration for which SB sound transmission is considered to be significant. Main sources of the SB paths in the system are then identified. Additionally, the simulated power balances for ATF#3 and ATF#4 are presented in Appx. V.3.

3.5.2.1 ATF#1: fully "rigid" ATF

Figure 3.7 illustrates the calculated power balances in the earcanal cavity of ATF#1. Figures 3.7(a) and 3.7(b) correspond to the single earplug and DHP configurations, respectively. Numbers 1 – 4 denote the power spectra levels exchanged between the earcanal cavity and (1) the earplug medial surface, (2) the earcanal lateral walls, (3) the earcanal terminal surface, and (4) the power spectrum level dissipated in the earcanal cavity due to thermo-viscous effects. In the following figures of power balances, a solid curve indicates an amount of power flowing into a domain of interest (e.g., earcanal cavity for Fig. 3.7) through an associated boundary while a dashed curve indicates the power flowing out of (or dissipated in) this domain.

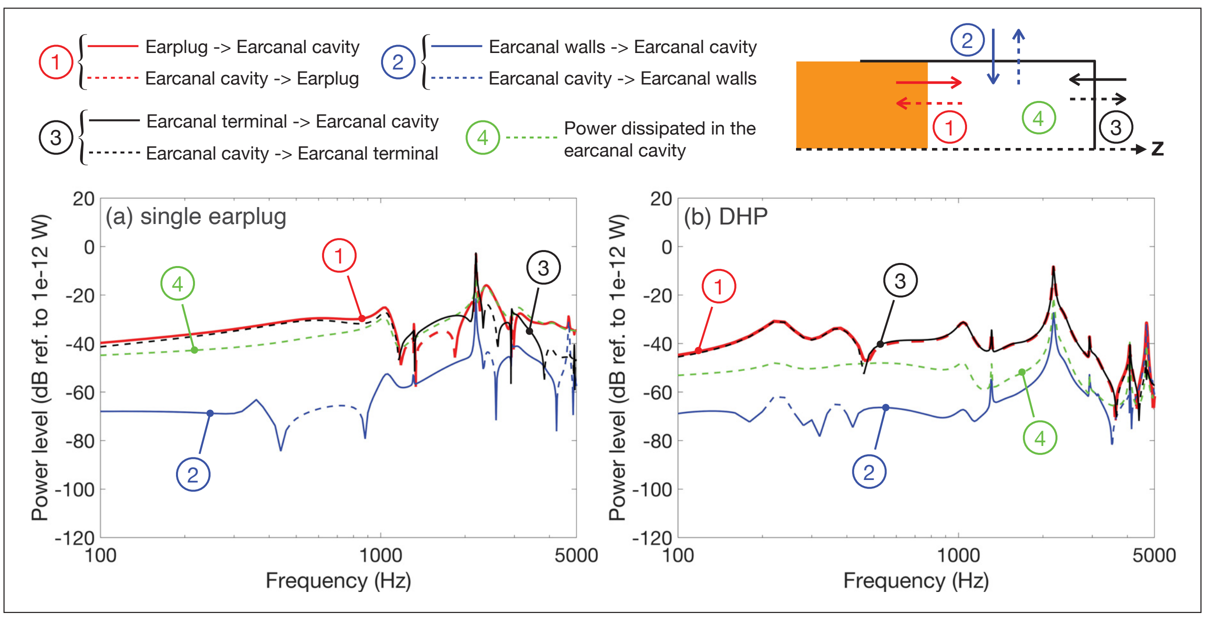

Figure 3.7 Power balances in the earcanal cavity of ATF#1 for (a) single earplug configuration and (b) DHP configuration: power spectra levels exchanged at the earplug/earcanal cavity interface (red); exchanged at the earcanal lateral walls (blue); exchanged at the earcanal terminal surface (black); dissipated in the earcanal cavity (green). Numbers 1 – 4 correspond to the associated geometric zones where the powers are calculated. Solid line: power flowing into the earcanal cavity; dashed line: power flowing out of (or dissipated in) the earcanal cavity

As expected, for most frequency bands in the single earplug configuration (see Fig. 3.7(a)), the direct AB sound transmission is dominant. More specifically, most power flows into the earcanal cavity due to the sound radiation of the earplug medial surface (solid red curve). The highest sound radiations of the earplug around 1 kHz and 2.5 kHz are related to its modes (see Sec. 3.5.1.1). This part of power is either dissipated internally (dashed green curve), or flows out of the earcanal cavity through the earcanal terminal surface (dashed black curve). At certain frequencies (i.e., around 1.3 kHz, 2.2 kHz and 2.9 kHz), the earcanal terminal surface is found to inject power into the earcanal cavity (solid black curve). These frequencies correspond to different bending wave modes of the ATF. Additional simulations of mechanical fluxes (not presented here) show that these modes facilitate the vibration transmission from the ATF to the microphone holder and thus the sound radiation from the latter into the earcanal cavity. The mode at 2.2 kHz contributes the most to the injected power since it leads to the highest displacement within the central region of the ATF (see Sec. 3.5.1.1). The contributions of the other modes are relatively small since they correspond to asymmetric vibrations of the ATF for which the displacement within the region close to the earcanal is not significant. In general, the earcanal lateral walls do not play an important role in the power transfers through the earcanal cavity (blue curve) except at certain resonance frequencies of the ATF (i.e., around 2.2 kHz and 4.7 kHz).

In the DHP configuration (see Fig. 3.7(b)), a majority of the power injected into the earcanal cavity at most frequencies between 450 Hz and 3.6 kHz originates from its terminal surface, i.e., the SB transmission is dominant. As expected, the highest power injected through this boundary is observed around 2.2 kHz as a result of the ATF mode. Most of the injected power flows out of the earcanal cavity through the earplug medial surface (dashed red curve). Conversely, in the frequency ranges below 450 Hz and above 3.6 kHz, power enters the earcanal cavity mainly through the earplug medial surface (AB transmission dominates). This is due to either the resonances of the earmuff at frequencies below 450 Hz and around 4.1 kHz (see Sec. 3.5.1.1), or another bending wave mode of the ATF which coincides with the acoustic resonance controlled by the earmuff cavity around 4.7 kHz. These phenomena are further explained when analyzing the power balances in the earplug. Again, the earcanal lateral walls do not significantly contribute to the power in the earcanal cavity. It is important to note that even though the main boundaries

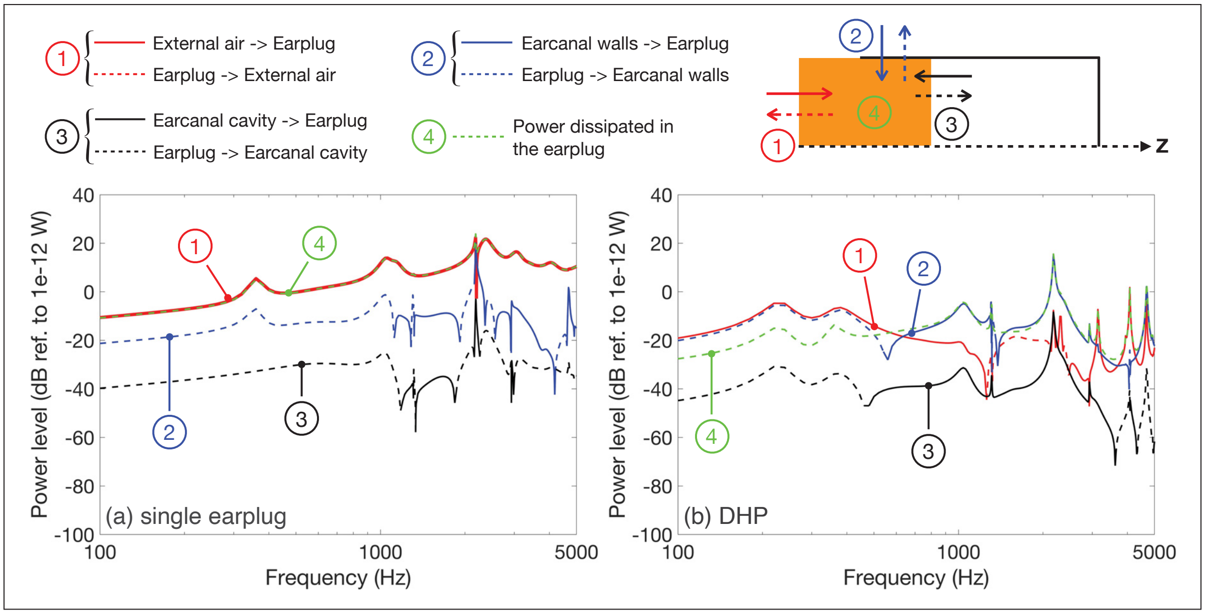

Figure 3.8 Power balances in the earplug in ATF#1 for (a) single earplug configuration and (b) DHP configuration: power spectra levels exchanged at the earplug outer surface (red); exchanged at the earplug/earcanal walls interface (blue); exchanged at the earplug/earcanal cavity interface (black); dissipated in the earplug (green). Numbers 1 – 4 correspond to the associated geometric zones where the powers are calculated. Solid line: power flowing into the earplug; dashed line: power flowing out of (or dissipated in) the earplug

for the power injected into the earcanal cavity are switched in the single and DHP configurations, their contributions are comparable in terms of power levels in the frequency range studied.

Figure 3.8 illustrates the power balances in the earplug for the single earplug and DHP configurations on ATF#1. Numbers 1 – 4 denote respectively the power spectra levels exchanged at (1) the earplug outer surface, (2) the interface between the earplug and earcanal walls, (3) the earplug medial surface towards the earcanal cavity, and (4) the power spectrum level dissipated in the earplug due to mechanical damping. If not otherwise specified, the earplug outer surface refers to all the exterior boundaries of the non-inserted part of the earplug in contact with the external air domain in the single earplug configuration (or with the air cavity under the earmuff in the DHP configuration).

In the single earplug configuration (see Fig. 3.8(a)), power enters the earplug mainly through its outer surface in nearly the whole frequency range of interest (solid red curve). Besides the local maximum related to the ATF bending wave mode at about 2.2 kHz, the highest levels of the injected power are found around the resonance frequencies of the earplug (i.e., 1 kHz and 2.5 kHz). A noticeable amount of power exchanged at the interface between the earplug and earcanal walls is only observed around 2.2 kHz (solid blue curve). In other frequency bands, the contribution of this boundary is relatively limited compared to the amount of power that is injected from the earplug outer surface. The injected power is mostly dissipated inside the earplug (dashed green curve) with a minor remaining part transferred into the earcanal cavity (dashed black curve) as already shown in Fig. 3.7(a).

In the DHP configuration (see Fig. 3.8(b)), the mechanical resonances of the earmuff (i.e., pumping motion and transverse motion of the silicone cushion) increase the sound pressure under the earmuff at frequencies below 600 Hz, which makes power continue to flow into the earplug through its outer surface as in the single earplug configuration (AB transmission dominates). Most of the injected power is transmitted into the ATF via the earplug/earcanal walls interface (dashed blue curve). Conversely, at frequencies above 600 Hz, the earcanal walls turn into the dominating boundaries for the power injected into the earplug (solid blue curve) with most of the injected power dissipated internally (SB transmission dominates). The largest contribution of these boundaries is seen around the ATF resonance frequency at 2.2 kHz. Another local maximum of the power injected through the earcanal walls at about 4.7 kHz corresponds to the ATF mode that coincides with an acoustic resonance of the earmuff previously explained. This mode appears to favor the vibration transmission from the ATF to the earplug via the earcanal walls, while an important amount of power is still injected through the earplug outer surface. Exceptions are found around 3.2 kHz and 4.1 kHz where most power restarts to enter the earplug through its outer surface due to other acoustic resonances controlled by the earmuff cavity which again induce an increase in the sound pressure under the earmuff.

The power balance in ATF#1 for the DHP configuration is displayed in Fig. 3.9. Numbers 1 – 7 denote respectively the power spectra levels exchanged between (1) the silicone cushion and ATF,

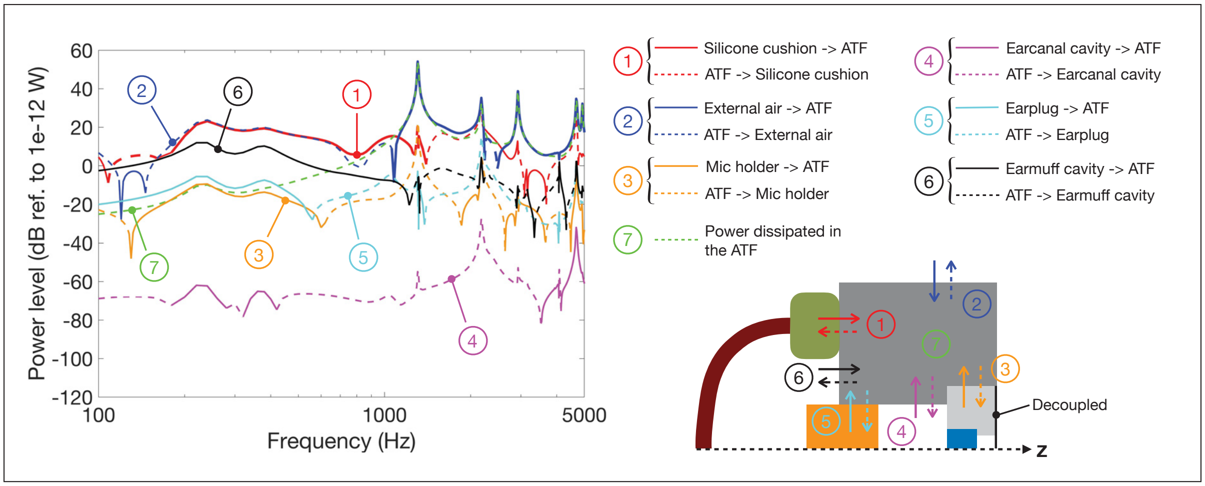

Figure 3.9 Power balance in ATF#1 for the DHP configuration: power spectra levels exchanged at the silicone cushion/ATF interface (red); exchanged at the ATF exterior boundaries outside the earmuff (blue); exchanged at the microphone holder/ATF interface (orange); exchanged at the earcanal lateral walls (purple); exchanged at the earplug/earcanal walls interface (cyan); exchanged at the ATF boundaries under the earmuff (black); dissipated in the ATF (green). Numbers 1 – 7 correspond to the associated geometric zones where the powers are calculated. Solid line: power flowing into the ATF; dashed line: power flowing out of (or dissipated in) the ATF

(2) the ATF exterior boundaries outside the earmuff and external air, (3) the microphone holder and ATF, (4) the earcanal lateral walls and earcanal cavity, (5) the earcanal walls and earplug, (6) the ATF boundaries under the earmuff and earmuff cavity, and (7) the power spectrum level dissipated in the ATF.

Two main regimes can be identified from the power balance in ATF#1. First, below about 1 kHz, power mainly flows into the ATF from the silicone cushion (solid red curve), and most of it is radiated into the external air domain through the ATF exterior boundaries (dashed blue curve). This is probably due to the fact that the system is governed by the earmuff mechanical resonances controlled by the silicone cushion, which promotes the vibration transmission from the cushion to the ATF. It is worth noting that in this frequency range, a non-negligible amount of power also gets into the ATF through its boundaries under the earmuff (solid black curve). As explained before, the earmuff resonances concurrently raise the sound pressure under the earmuff and thus the power transmitted into the ATF from the earmuff cavity.

Second, at frequencies above 1 kHz, the exterior boundaries emerge as the dominant ones for the power injected into the ATF (solid blue curve). In this frequency range, the bending wave modes of the ATF are excited (i.e., around 1.3 kHz, 2.2 kHz, 2.9 kHz, 4.7 kHz and 4.9 kHz). They increase the power transmitted into the ATF directly from the external air domain. Most of the power is dissipated in the ATF (dashed green curve). Around certain ATF resonance frequencies (i.e., 2.2 kHz and 4.7 kHz), the injected power flows from the ATF into the silicone cushion (dashed red curve). The remaining part of power is redirected towards other surrounding domains, such as the earplug, earcanal cavity and microphone holder. Consistently with the results shown in Fig. 3.7(b), more power is transmitted from the ATF into the microphone holder around 2.2 kHz (dashed orange curve). In the case of ATF#1 with "rigid" earcanal lateral walls, the power exchanged at the earcanal walls (purple curve) is found to be of minor importance in comparison to the total injected power.

3.5.2.2 ATF#2: ATF with artificial skin

Similarly to Sec. 3.5.2.1, the calculated power balances in the earcanal cavity, earplug and ATF#2 are presented respectively in Figs. 3.10 – 3.12. In the single earplug configuration (see Fig. 3.10(a)), the earplug medial surface remains the primary boundary for the power injected into the earcanal cavity as on ATF#1 at frequencies below 900 Hz, or between 2.5 kHz and 4 kHz (solid red curve). The highest levels of the injected power are detected around 350 Hz and 800 Hz which correspond to the coupled modes of the earplug/skin assembly (see Sec. 3.5.1.2). The remaining power is dissipated internally (dashed green curve), and mostly transferred into the ATF through the earcanal lateral walls (dashed blue curve). It is necessary to note that compared to ATF#1, the power injected through the earplug medial surface is approximately 20 – 60 dB higher in the related frequency ranges on ATF#2. At frequencies between 900 Hz and 2.5 kHz, or above 4 kHz, a pronounced contribution of the earcanal lateral walls to the power in the earcanal cavity is observed when the artificial skin is accounted for (solid blue curve). This agrees with the finding of Viallet *et al.*'s work (2014) which considered the skin layer for predicting the sound attenuation of single earplugs inserted into an ATF earcanal. The power

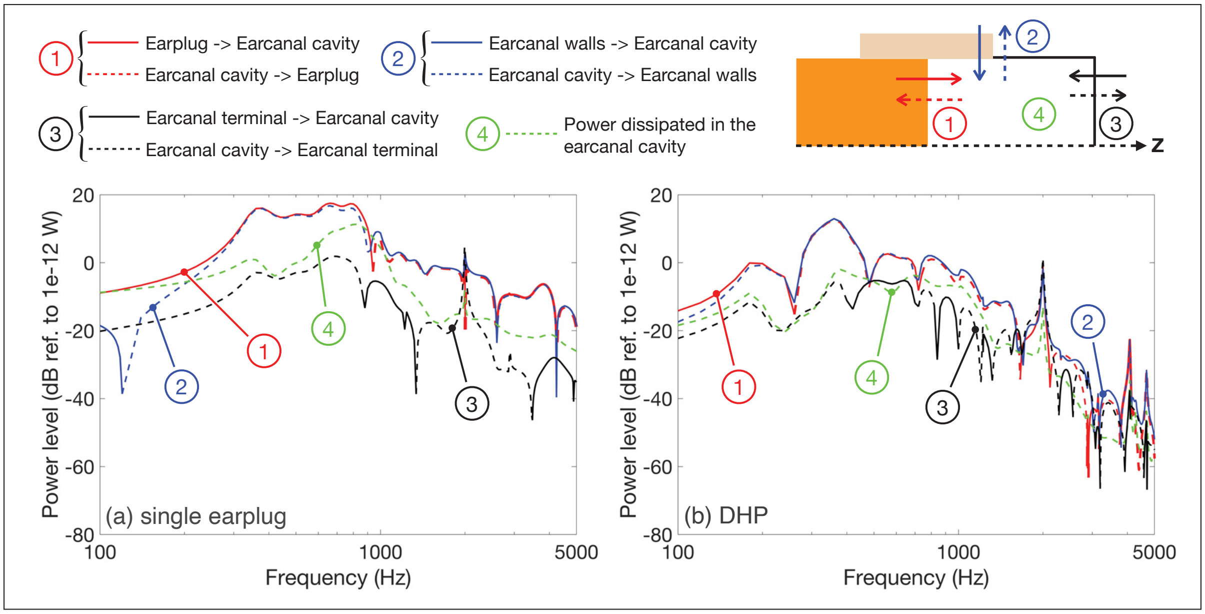

Figure 3.10 Power balances in the earcanal cavity of ATF#2 for (a) single earplug configuration and (b) DHP configuration: power spectra levels exchanged at the earplug/earcanal cavity interface (red); exchanged at the earcanal lateral walls (blue); exchanged at the earcanal terminal surface (black); dissipated in the earcanal cavity (green). Numbers 1 – 4 correspond to the associated geometric zones where the powers are calculated. Solid line: power flowing into the earcanal cavity; dashed line: power flowing out of (or dissipated in) the earcanal cavity

injected through the earcanal walls mainly flows out of the earcanal cavity via the earplug medial surface (dashed red curve). In opposition to ATF#1, generally no significant contribution of the earcanal terminal surface is found. Particularly around 2 kHz where the symmetric bending wave mode of ATF#2 occurs (see Sec. 3.5.1.2), both the earplug medial surface and earcanal walls are found to transmit power into the earcanal cavity. At this frequency, the terminal surface turns to be an important boundary through which power flees the earcanal cavity (dashed black curve).

In the DHP configuration (see Fig. 3.10(b)), power mainly flows into the earcanal cavity through the earplug medial surface at frequencies below about 300 Hz (AB transmission dominates). This is due to the earmuff pumping motion shifted to around 200 Hz when the artificial skin pad is accounted for, which increases the sound pressure under the earmuff and the power transmitted into the earplug from the earmuff cavity as explained earlier. The injected power is mostly transferred out of the earcanal cavity through its lateral walls. A similar phenomenon is observed around 4.1 kHz where an acoustic resonance of the earmuff takes place (see Sec. 3.5.1.1). But in most frequency bands studied, power mainly enters the earcanal cavity through its lateral walls (SB transmission dominates). At frequencies around 350 Hz, or between 750 Hz and 1.6 kHz, the coupled modes of the earplug/skin assembly seem to facilitate the entry of power through the earcanal walls and the exit of power through the earplug medial surface. Similarly to the single earplug configuration, both the earplug medial surface and earcanal walls transmit power into the earcanal cavity around 2 kHz which mainly flows out of the latter via its terminal surface. The local maximum of the power injected through the earcanal walls at about 4.7 kHz could be explained by another earmuff acoustic resonance which increases the direct acoustic excitation on the skin boundaries under the earmuff, and thus the sound radiation of the skin into the earcanal cavity. In general, the power dissipation and earcanal terminal surface are involved to a relatively lesser extent for the power balance in the earcanal cavity compared to the other boundaries considered.

Figure 3.11(a) reveals that for the single earplug configuration on ATF#2, the earplug outer surface, and the interface between the earplug and earcanal walls remain the two major boundaries for the power balance in the earplug. In general, they behave alternatively as the dominant boundary for the power injected into the earplug. The power injected through one boundary is mostly transmitted out of the earplug through the other or dissipated internally (dashed green curve). At frequencies below 750 Hz, most power flows into the earplug via its outer surface (solid red curve) probably because of the coupled mode controlled by the earplug behavior at about 350 Hz (see Sec. 3.5.1.2). At frequencies between 750 Hz and 1.2 kHz, the coupled modes of the earplug/skin assembly seem to be dominated by the behavior of the skin, and hence power principally enters the earplug through the earcanal walls (solid blue curve). At frequencies below 1 kHz, or between 2.5 kHz and 4 kHz, the remaining power in the earplug (about 20 dB less than the injected power on average) is found to flow into the earcanal cavity through the earplug medial surface (dashed black curve) as already shown in Fig. 3.10(a).

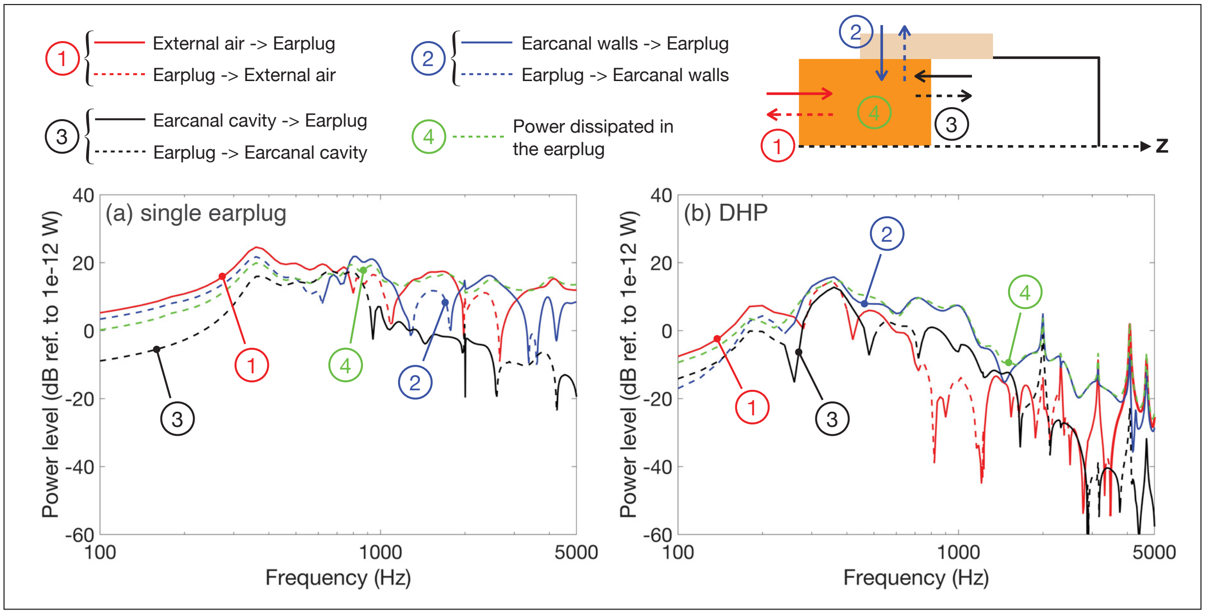

Figure 3.11 Power balances in the earplug in ATF#2 for (a) single earplug configuration and (b) DHP configuration: power spectra levels exchanged at the earplug outer surface (red); exchanged at the earplug/earcanal walls interface (blue); exchanged at the earplug/earcanal cavity interface (black); dissipated in the earplug (green). Numbers 1 – 4 correspond to the associated geometric zones where the powers are calculated. Solid line: power flowing into the earplug; dashed line: power flowing out of (or dissipated in) the earplug

Consistently with the power balance in the earcanal cavity shown in Fig. 3.10(b), in the DHP configuration (see Fig. 3.11(b)), a majority of power enters the earplug through its outer surface at frequencies below about 300 Hz due to the pumping motion (AB transmission dominates). At frequencies above 300 Hz, the power in the earplug is mainly attributed to that transmitted through the earcanal walls (SB transmission dominates). Most of the injected power is dissipated inside the earplug. Around the resonance frequency of ATF#2 at 2 kHz, a local maximum of the power injected through the earcanal walls is observed. At this frequency, a noticeable amount of power is transferred into the earcanal cavity through the earplug medial surface. Around certain resonance frequencies controlled by the earmuff cavity (i.e., 2.3 kHz, 3.2 kHz, 4.1 kHz and 4.7 kHz), besides the power injected through the earcanal walls, large amounts of power also flow into the earplug through its outer surface. These resonances seem to increase simultaneously the

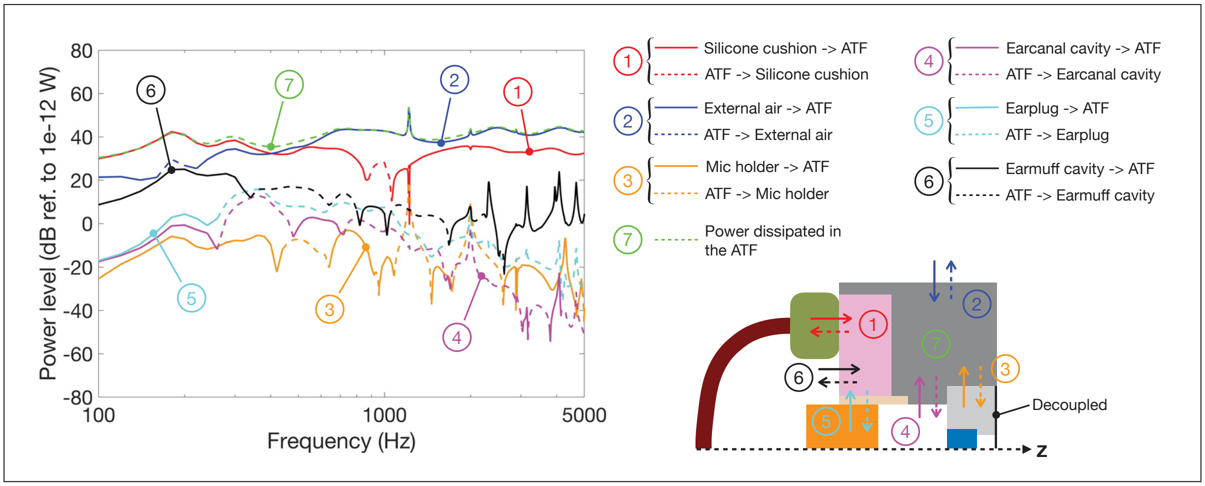

Figure 3.12 Power balance in ATF#2 for the DHP configuration: power spectra levels exchanged at the silicone cushion/ATF interface (red); exchanged at the ATF exterior boundaries outside the earmuff (blue); exchanged at the microphone holder/ATF interface (orange); exchanged at the earcanal lateral walls (purple); exchanged at the earplug/earcanal walls interface (cyan); exchanged at the ATF boundaries under the earmuff (black); dissipated in the ATF (green). Numbers 1 – 7 correspond to the associated geometric zones where the powers are calculated. Solid line: power flowing into the ATF; dashed line: power flowing out of (or dissipated in) the ATF

acoustic excitation on the earplug outer surface and skin boundaries under the earmuff, and thus the power transmitted into the earplug from the earmuff cavity and surrounding skin layer.

Similarly to ATF#1, the power balance in ATF#2 exhibits two major regimes (see Fig. 3.12). First, below about 400 Hz, the silicone cushion emerges as the major source for the power injected into the ATF (solid red curve). Besides the pumping motion which takes place at about 200 Hz, another earmuff resonance governed by the silicone cushion transverse motion is shifted to around 300 Hz. They naturally facilitate the vibration transmission from the cushion to the ATF. In the same frequency band, a noticeable amount of power also gets into the ATF through its exterior boundaries outside the earmuff, especially between 300 Hz and 400 Hz (solid blue curve).

Second, the power injected through the exterior boundaries of the ATF becomes dominant at frequencies above 400 Hz. The highest level of the power injected through these boundaries is observed around another resonance frequency of ATF#2 at 1.2 kHz. It should be noted that at 1.5 kHz and above, a non-negligible amount of power still flows into the ATF from the silicone cushion. In the whole frequency range of interest between 100 Hz and 5 kHz, the injected power is mostly dissipated in the ATF (dashed green curve) probably due to the presence of the artificial skin which increases the overall mechanical damping of the system. The power transmitted through the other boundaries appears to be less important which is roughly 50 – 60 dB lower than the injected power in terms of power levels.

3.5.2.3 Summary on power balances

The previous observations generally show that for the single earplug configuration on ATF#1, power mainly flows from the earplug into the earcanal cavity through the direct AB sound path in the frequency range of interest. When the earmuff is worn in combination, the DHP effect occurs at frequencies between 450 Hz and 3.6 kHz (see also Fig. 3.6). In this frequency range, the sound pressure at the earcanal entrance is low due to a relatively high earmuff attenuation, and a significant amount of SB sound power is transmitted from the silicone cushion and ATF exterior boundaries into the earcanal cavity via the microphone holder. At frequencies below 450 Hz and above 3.6 kHz, the DHP effect tends to be negligible as the acoustical and mechanical resonances of the earmuff lead to an increase in the sound pressure at the earcanal entrance.

The power balances for ATF#2 highlight the important contribution of the earcanal lateral walls to the power in the earcanal cavity when the artificial skin is accounted for, even in the single earplug configuration at frequencies between 900 Hz and 2.5 kHz, or above 4 kHz. In the DHP configuration, the power in the earcanal cavity is dominated by the sound radiation of its lateral walls especially at frequencies between 300 Hz and 4 kHz again due to the SB sound power injected from the silicone cushion and ATF exterior boundaries. This agrees with the significant DHP effect observed in the associated frequency range in Fig. 3.6. Moreover, an indirect SB sound path can be identified at frequencies between 500 Hz and 700 Hz, or around 2 kHz which corresponds to the sound radiation of the earplug excited by the surrounding earcanal walls. At frequencies below 300 Hz and above 4 kHz, the DHP effect is not significant as the earmuff resonances raise the direct acoustic excitation on the earplug outer surface and skin boundaries under the earmuff, which makes the AB sound transmission dominant over the SB one.

Additionally, the comparison between the power balances for ATF#1 and ATF#3 (see also Appx. V.3.1) reveals that blocking the acoustic excitation on the ATF exterior boundaries in the DHP configuration generally leads to a lower amount of power injected into the ATF, and thus relatively smaller contributions of the SB paths (i.e., earcanal lateral walls and terminal surface) to the power in the earcanal cavity especially at frequencies between 450 Hz and 1 kHz, or above 3 kHz. This explains why the DHP effect is mainly observed in the frequency range between 1 kHz and 3 kHz on ATF#3 (see Fig.-A V-2). The power injected into ATF#3 mostly comes from its boundaries under the earmuff at frequencies below 800 Hz and from the silicone cushion at higher frequencies (see Fig.-A V-5).

Compared to ATF#2, ATF#4 shows no significant overall differences in the power exchanged at the earcanal lateral walls or earplug/earcanal walls interface (in terms of power levels and hierarchization of the sound paths) maybe for the reason that the presence of the artificial skin greatly elevates the contributions of these SB paths, even without the acoustic excitation on the ATF exterior boundaries (see Appx. V.3.2). An exception is found around the ATF resonance frequency at 2 kHz where the power injected through these boundaries is somehow reduced in the DHP configuration. Besides, the decoupled condition on the ATF boundaries also decreases the power exchanged at the earcanal terminal surface, which is however involved to a lesser extent in the power transfers through the system. This is consistent with the similar DHP effects on ATF#2 and ATF#4 displayed in Fig.-A V-2. It is interesting to note that the SB power injected into ATF#4 mainly comes from the silicone cushion in the whole frequency range studied (see Fig.-A V-8). Because of space limitation, the system behaviors on ATF#3 and ATF#4 are not discussed in detail here.

3.5.3 Discussion

The numerical simulations in the present paper confirm some main conclusions drawn from the authors' previous experimental work (Luan *et al.*, 2021). First, the DHP effect indeed originates from the SB sound transmission through the system and can be explained by the relative contributions of the direct AB path and SB paths involved. Second, the sound radiation of the earcanal lateral walls or that of the earplug excited by the earcanal walls constitutes a primary SB path that contributes to the sound pressure in the earcanal cavity (when ATF#2 and ATF#4 with the skin are considered). But the contributions of these SB paths may vary with the earplug insertion depth which can alter the interaction between the earcanal walls and earplug, or between the earcanal walls and earcanal cavity. Third, the earmuff cushion emerges as an important source for the SB sound power injected into the system. These conclusions depend certainly on the construction of the system (e.g., assembly, materials and boundary conditions) and frequency range studied as demonstrated in this work.

It should be kept in mind that compared to a commercial ATF or a human head, the simplifications made for the in-house ATF can influence the DHP effect observed. First, the ear simulator in the earcanal of a commercial ATF plays an important dissipative role (Viallet *et al.*, 2014), and may evidently reduce the sound radiation of the earcanal terminal surface in ATF#1 and ATF#3. Second, the human middle ear ossicular resonances above 1 kHz (Brüel *et al.*, 1976) are expected to increase the mid-frequency contribution of the earcanal terminal portion to the power injected into the earcanal cavity. Additionally, Berger *et al.* (2003a) have achieved additional gains in the measured DHP attenuation at frequencies above 1 – 2 kHz when shielding the human head from acoustic stimulation, whereas for the simulation configurations with the skin (i.e., ATF#2 and ATF#4), blocking the acoustic excitation on the ATF exterior boundaries does not lead to significant overall differences in the contributions of the SB paths or in the DHP effect. This suggests that more realistic modifications need to be made to the system for better capturing the DHP attenuation on human subjects. However, despite some limitations, the present paper has demonstrated the use of a computational model for predicting the DHP effect on an ATF, which also helps understand the related physical mechanisms. The model can be further improved by increasing the complexity of the system in terms of geometry and material properties for ultimately studying the DHP effect on human subjects.

3.6 Conclusion

In the present paper, a FE model has been proposed in order to study the DHP effect on an in-house ATF. This effect has been characterized by the difference between the NRs of the single earplug and of the earplug in the DHP. The comfort cushion of the earmuff was replaced by a silicone cushion for better capturing its vibroacoustic behavior in the model. First, the model has been validated against NR measurements of the single earmuff, single earplug and earplug in the DHP in the frequency range between 100 Hz and 5 kHz. Second, exploited simulation configurations of the ATF have been used to simulate and analyze the power balances in the system for (i) quantifying the contribution of each sound path, and studying the effects of (ii) the artificial skin and (iii) the acoustic excitation on the ATF exterior boundaries.

On the fully "rigid" ATF, the DHP effect arises between 450 Hz and 3.6 kHz due to a large amount of SB sound power transmitted into the earcanal cavity through its terminal surface. In other frequency bands, the DHP effect tends to be negligible as the earmuff resonances increase the sound pressure at the earcanal entrance, and make the AB sound transmission through the earplug dominant over the SB one. On the ATF with artificial skin components, the earcanal lateral walls are proved to be the major SB path responsible for the evident DHP effect occurring between 300 Hz and 4 kHz. A relevant indirect SB path can also be identified which corresponds to the sound radiation of the earplug excited by the earcanal walls. This configuration highlights the importance of taking into account the skin if a more realistic prediction of the DHP attenuation is desired. Additionally, the acoustic excitation on the ATF exterior boundaries is found to have a non-negligible influence on the DHP effect on the "rigid" ATF especially below 1 kHz or above 3 kHz, whereas it does not significantly affect the DHP effect on the ATF with the skin. The SB power injected into the system is shown to mainly come from the earmuff silicone cushion and/or the ATF exterior boundaries depending on the materials, boundary conditions and frequency range studied. This work has allowed for gaining more insight into the sound transmission mechanisms through a DHP/ATF system. Prospectively, it will also provide a useful tool for more realistic DHP attenuation predictions based on legitimate increases in the system complexity.

3.7 Acknowledgement

The authors wish to acknowledge the Natural Sciences and Engineering Research Council of Canada (NSERC) for funding this research.

CHAPTER 4

A TRANSFER MATRIX MODEL OF THE IEC 60318-4 EAR SIMULATOR: APPLICATION TO THE SIMULATION OF EARPLUG INSERTION LOSS

Yu Luan[a] , Franck Sgard[b] , Simon Benacchio[a] , Hugues Nélisse[b] , Olivier Doutres[a]

[a] Department of Mechanical Engineering, École de Technologie Supérieure,
1100 Rue Notre-Dame Ouest, Montreal, Quebec H3C 1K3, Canada

[b] Direction Scientifique, Institut de recherche Robert-Sauvé en santé et en sécurité du travail,
505 Boulevard de Maisonneuve Ouest, Montreal, Quebec H3A 3C2, Canada

Paper published in *Acta Acustica united with Acustica*, December 2019.

4.1 Abstract

The IEC 60318-4 ear simulator is used to measure the insertion loss (IL) of earplugs in the earcanal of an acoustical test fixture (ATF) and is designed to represent an average acoustic impedance (in a reference plane) of the human ear. The ear simulator is usually modeled using a lumped parameter model (LPM) which has frequency limitations and inadequately accounts for the thermo-viscous effects in the simulator. The simulator numerical models that can better deal with the thermo-viscous phenomena often lack essential geometric details. Most related studies also suffer from the lack of experimental validation of the models. Therefore, a transfer matrix (TM) model of the IEC 60318-4 simulator is proposed based on a direct assessment of its geometric dimensions. Such a model is of particular interest for designing artificial ear simulators. The variability in the simulator impedance due to the geometric uncertainties is quantified using the Monte Carlo method. The TM model is validated using (i) a finite element (FE) model of the simulator and (ii) impedance measurements with a sound intensity probe. It is found to better describe the simulator impedance above 3 kHz compared to the LPM. The TM model is then coupled to a FE model of an occluded ATF earcanal to simulate the IL of an earplug in the frequency range [100 Hz, 10 kHz]. In the model, the simulator is considered as a cylindrical cavity terminated by an equivalent tympanic impedance which is determined from

the TM model to simulate the sound pressure measured at the real microphone position (not at the reference plane) in the ATF earcanal. The simulated IL is validated against (i) that obtained with a complete FE model of the corresponding system and (ii) measurements using an ATF. The TM model is shown to better agree with the simulator FE model than the LPM above 6 kHz regarding the earplug IL simulated using this method.

4.2 Introduction

Acoustical test fixtures (ATFs) (ANSI, 2018) can be used instead of human subjects to measure the sound attenuation of individual hearing protection devices, such as earplugs (ANSI, 2020) since they can provide repeatable results and accommodate a large variety of test signals (Berger, 1986). One of the indicators of the earplug attenuation is the insertion loss (IL), which corresponds to the difference between the sound pressure levels measured close to the position of the eardrum (also called tympanic membrane) with and without the earplug (ANSI, 2020). The ATF generally consists of an acoustically rigid artificial head and a cylindrical earcanal of constant circular cross-section (ANSI, 2020). The inner portion of this earcanal is normally included in an IEC 60318-4 occluded ear simulator (formerly known as IEC 711 ear simulator). The latter is fabricated using acoustic resonant elements tuned in a manner that the acoustic impedance at its entrance represents an average input impedance of the inner part of the human earcanal at a reference plane[1] up to 10 kHz (IEC, 2010; ANSI, 2014). A microphone is placed at the output of the simulator where the recorded sound pressure would be as close as possible to that measured at the eardrum of an average human ear (Brüel *et al.*, 1976). Such simulator contains the information about the average eardrum acoustic properties which may be beneficial for designing more realistic artificial ear simulators in the field of hearing protectors.

The IEC 60318-4 ear simulator was originally designed with the help of a lumped parameter model (LPM) which assimilates the simulator as an analogous electrical circuit whose parameters are associated with the acoustic properties of the simulator components (Jønsson *et al.*, 2003, 2004).

[1] Due to the difficulty of directly assessing the eardrum impedance, measurements of the acoustic impedance of the human ear are practically performed at a reference plane in the earcanal between the canal entrance and eardrum where earplugs (or ear moulds) normally end (Brüel *et al.*, 1976).

A reliable analytical impedance model is of particular interest in terms of easily performing parametric studies to design artificial ear simulators. However, the LPM is commonly accepted to be limited to the low frequency range and often inadequately accounts for the thermo-viscous effects due to the sound propagation through the narrow regions of the simulator (Jønsson *et al.*, 2004; Bravo *et al.*, 2008).

Several numerical models of the IEC 60318-4 simulator based on the finite element (FE) or boundary element method have been proposed to better account for the thermo-viscous phenomena involved in the system (Jønsson *et al.*, 2003, 2004; Sasajima *et al.*, 2015; COMSOL, 2017). But most of the existing simulator numerical models (Sasajima *et al.*, 2015; COMSOL, 2017) were validated against experimental impedance data taken from international standards (IEC, 2010; ANSI, 2014) which were obtained using simultaneously an insert earphone and a probe microphone fixed in the human earcanal (e.g., Brüel *et al.*, 1976; Keefe, Ling & Bulen, 1992; Sanborn, 1998; Farmer-Fedor & Rabbitt, 2002). They suffer from the lack of experimental validation of the models using the corresponding ear simulators. In addition, these studies either rely upon the adjusted component dimensions to acquire the closest impedance simulation results to the measurement data on human subjects or lack essential details associated with the simulator geometric parameters.

To the authors' knowledge, the only study on the modeling of an ear simulator based on a direct determination of its geometric inputs was conducted by Bravo *et al.* (2008; 2012). It proposed a FE model to calculate the transfer impedance of an IEC 60318-1 simulator (IEC, 2009) whose geometry was constructed using an X-ray inspection system. However, the uncertainties related to the simulator geometry were only considered using the maximal and minimal values of two particular component dimensions, which seems not sufficient to represent the large variability in the simulator impedance that could be induced by different combinations of the geometric inputs. Moreover, this kind of simulator is designed for supra-aural or supra-cocha devices and cannot be adopted to evaluate the attenuation of earplugs (IEC, 2009; Rodrigues *et al.*, 2015a). A comprehensive review about different types of ear simulators can be found in (Rodrigues *et al.*, 2015a).

Besides the direct impedance simulation of the IEC 60318-4 simulator, it is relevant to assess how the simulator impedance model affects the simulated IL of earplugs inserted in an ATF earcanal. A 2D axisymmetric FE model of the corresponding system has been proposed in a few studies to precisely capture the vibroacoustic behavior of a silicone earplug (Viallet *et al.*, 2013, 2014). In the model, the ear simulator was considered as a cylindrical cavity terminated by an equivalent tympanic impedance (TI) in order to simulate the sound pressure measured at the real microphone position (not at the reference plane) in the ATF earcanal. The equivalent TI was determined by eliminating the components associated with the earcanal portion from the LPM of the simulator as originally proposed in (Jønsson *et al.*, 2003). But there is still doubt with regard to the validity of this traditional lumped TI model since it seems not mathematically rigorous to represent the TI by extracting directly certain elements from the simulator equivalent circuit. Several published investigations have adopted the reduced impedance (RI) method (Chaigne, 2001) to retrieve the eardrum impedance from the acoustic impedance measured at a reference plane in the human earcanal using a chain matrix of the canal considered as a stepped duct (e.g., Hudde, 1983; Larson *et al.*, 1993; Rodrigues *et al.*, 2015a). It proves to be a reliable method but has not yet been applied to calculate the equivalent TI of the IEC 60318-4 simulator. In addition, one can wonder whether it is valid to consider such a simulator as a cavity with a locally reacting terminal impedance condition for simulating the sound pressure in an ATF earcanal occluded by an earplug.

To address the above-mentioned lacks in the literature, the main objective of this work is to propose a reliable analytical impedance model of the IEC 60318-4 simulator and apply it to the IL simulation of earplugs in an ATF earcanal. This objective is achieved via a three-step methodology detailed hereafter. Firstly, the geometry of a commercial model of the IEC 60318-4 occluded ear simulator is identified from a micro-computed tomography (micro-CT) scan. A transfer matrix (TM) model of the simulator is proposed based on the component dimensions assessed from CT scan images and compared to the LPM. The variability in the model output (simulator impedance) due to the uncertainties on the geometric inputs is quantified using the Monte Carlo method. The proposed model is validated using (i) a FE model of the scanned simulator which includes full and detailed modeling of the thermo-viscous phenomena involved in the system and (ii) measurements carried out with a sound intensity probe. Secondly, the equivalent TI is determined from the TM model and LPM using the RI method and compared to that obtained from the traditional lumped TI model. Thirdly, TI results are used as a boundary condition in a FE model of an occluded ATF earcanal to simulate the IL of a silicone earplug. A typical silicone earplug is chosen because it has already been studied in the literature and its FE model has been shown to provide satisfactory attenuation simulation results compared to experimental data (Viallet *et al.*, 2013, 2014). The simulated IL based on the TM model is validated against (i) that obtained with a complete FE model of the corresponding system and (ii) measurements using an ATF. The validity of considering the ear simulator as a cylindrical cavity terminated by an equivalent TI is verified and the effects of the TI models on the IL simulation are discussed.

4.3 Modeling of the IEC 60318-4 ear simulator

This section presents different modeling strategies to simulate the input impedance of the IEC 60318-4 simulator and is organized as follows. The simulator geometry and key dimensions determined from a CT scan are given in Sec. 4.3.1. Section 4.3.2 recalls the principles of the LPM of the ear simulator. Section 4.3.3 provides the details of a TM model of the simulator. To validate the TM model, a FE model of the scanned simulator is constructed and described in Sec. 4.3.4. Note that in this paper the pressure-volume velocity analogy is adopted so that the term “impedance” refers to acoustic impedance.

4.3.1 Geometry

The IEC 60318-4 ear simulator studied in this work is the G.R.A.S. RA0045 (G.R.A.S. Sound & Vibration AS, Denmark) which complies with the requirements of IEC 60318-4 (2010). The geometry of the simulator is identified from a micro-CT scan with a 15.4 µm isotropic resolution (XT H 225 micro-CT X-Ray Scanner, Nikon Metrology, United States) (see Fig. 4.1). It is made of hard nonporous material and consists of a cylindrical tube of constant circular cross-section

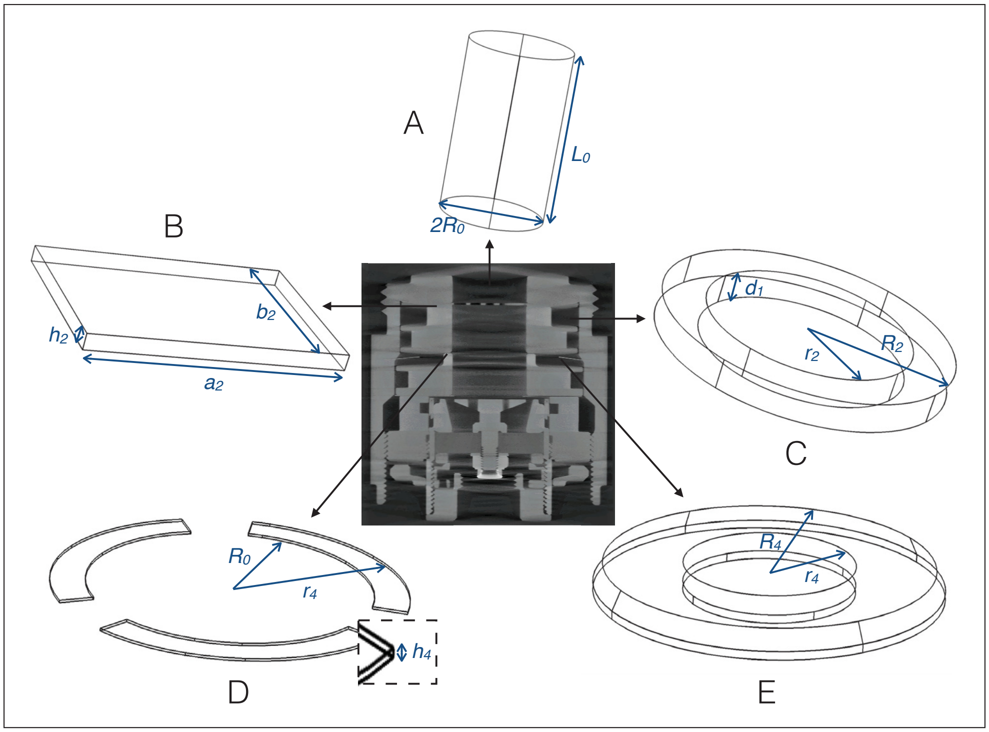

Figure 4.1 Geometry of the IEC 60318-4 ear simulator identified from the CT scan (see Table 4.1 for geometric dimensions)

(main cavity) (component A) attached to two annular side volumes (components C, E) via two narrow slits (components B, D). The main cavity of the simulator approximates the human earcanal portion and is divided into three sections by the narrow slits. The latter include thin air layers in which thermo-viscous boundary effects cannot be neglected, mimicking the energy losses at the human eardrum and those in the middle and inner ears. Each narrow slit and the corresponding side cavity constitute a Helmholtz resonator.

The first slit is of parallelepipedic shape (component B) while the second one consists of three identical annular parts (component D). The second side cavity[2] (component E) comprises a conical part containing a ring-shaped sheet metal. The IEC 60318-4 simulator is generally terminated by a recording microphone at its output (eardrum position). In this study, it is

[2] The second side cavity is simplified to a pure annular form in the TM model since it has been proved that only the volume of the cavity affects the simulated impedance of the ear simulator. An equivalent thickness that preserves the same volume of this cavity is provided in Table 4.1.

Table 4.1 Component geometric dimensions of the IEC 60318-4 ear simulator

Notation	**Parameter**	**Average ± standard deviation**
R_0	Radius of the main cavity	3.77 ± 0.03 mm
L_0	Total length of the main cavity	12.56 ± 0.29 mm
L_1	Length: 1st section of the main cavity	3.12 ± 0.10 mm
L_3	Length: 2nd section of the main cavity	4.75 ± 0.04 mm
L_5	Length: 3rd section of the main cavity	4.69 ± 0.14 mm
a_2	Length of the rectangular slit	2.53 ± 0.06 mm
b_2	Width of the rectangular slit	2.35 ± 0.03 mm
h_2	Thickness of the rectangular slit	0.16 ± 0.06 mm
r_2	Inner radius of the 1st annular cavity	6.30 ± 0.06 mm
R_2	Outer radius of the 1st annular cavity	9.01 ± 0.03 mm
d_1	Thickness of the 1st annular cavity	1.91 ± 0.08 mm
r_4	Outer radius of the annular slit (Inner radius of the 2nd annular cavity)	4.66 ± 0.04 mm
α_2	Angle of each part of the annular slit	95.33 ± 1.09°
h_4	Thickness of the annular slit	0.05 ± 0.02 mm
R_4	Outer radius of the 2nd annular cavity	9.01 ± 0.03 mm
d_2	Equivalent thickness of the 2nd annular cavity	1.40 ± 0.11 mm

replaced by a rigid boundary (infinite terminal impedance) for simplicity because the impedance of the microphone is very high compared to that of the system in front (IEC, 2010).

The dimensions of the identified acoustic elements (i.e., main cavity, narrow slits and side cavities) have been assessed by measurements on micro-CT scan images using VGSTUDIO (Volume Graphics, Germany). Different measurements were performed by three members of the research team to obtain the average and standard deviation for each geometric dimension of interest (see Table 4.1[2]).

4.3.2 Lumped parameter model

If the wavelength is sufficiently large compared to the dimensions of the acoustic components in the IEC 60318-4 simulator, these components can be modeled as lumped acoustic elements. In

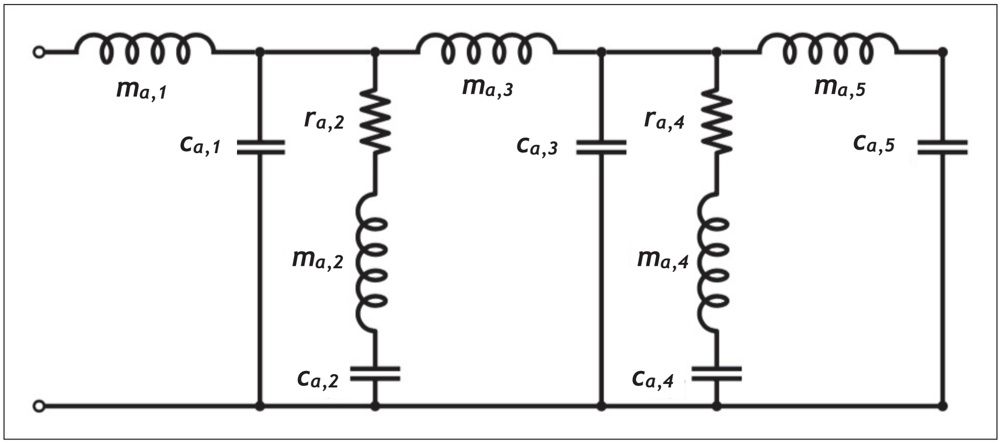

Figure 4.2 LPM of the IEC 60318-4 ear simulator

this case, the simulator can be considered as an analogous electrical circuit or lumped parameter model (LPM).

Figure 4.2 presents the LPM of the studied ear simulator built according to (Jønsson *et al.*, 2004), the principles of which are recalled as follows. In this model, each section of the simulator main cavity is represented by an LC circuit where the electrical inductance and capacitance correspond respectively to the acoustic mass and compliance of the cavity portion. The latter can be derived from (Jønsson *et al.*, 2004):

$$\begin{cases} m_{\mathrm{a},m} = \dfrac{\rho_0 L_m}{S_0}, \\ c_{\mathrm{a},m} = \dfrac{V_m}{\rho_0 c_0^2}, \end{cases} \tag{4.1}$$

where m = 1, 3 and 5 correspond to each section of the simulator main cavity, L_m denotes the length of each section, V_m the volume of the section correspondingly and S_0 is the cross-section area of the simulator main cavity equal to πR_0^2. ρ_0 is the density of air and c_0 is the speed of sound in air. Parameters of the thermo-viscous fluid adopted in the models are derived from the standard atmospheric pressure and normal room temperature, and are specified in Table 4.2. In the same way, each RLC circuit in the LPM corresponds to a Helmholtz resonator in which the electrical resistance and inductance match the acoustic resistance and mass of the resonator's neck (narrow slit), and the electrical capacitance matches the acoustic compliance of

Table 4.2 Parameters of the thermo-viscous fluid

Parameter	**Value**	**Unit**
Static pressure P_0	1.01×10^5	Pa
Temperature T_0	293.15	K
Density ρ_0	1.20	kg/m^3
Speed of sound c_0	343.90	m/s
Shear dynamic viscosity μ	1.82×10^{-5}	Pa·s
Thermal conductivity λ	24.80×10^{-3}	W/(m·K)
Ratio of specific heats γ	1.40	-
Specific heat coefficient at constant pressure per unit of mass C_p	1.00×10^3	J/(kg·K)

the resonator's cavity. Thus, the input impedance of the Helmholtz resonator (Jønsson *et al.*, 2004) can be calculated by:

$$Z_{\mathrm{HR},n} = r_{\mathrm{a},n} + \mathrm{j}\omega m_{\mathrm{a},n} + \frac{1}{\mathrm{j}\omega c_{\mathrm{a},n}}. \tag{4.2}$$

$n = 2$ and 4 correspond respectively to the first and second Helmholtz resonators. $c_{\mathrm{a},n}$ can be determined as Eq. (4.1) and $r_{\mathrm{a},n}$, $m_{\mathrm{a},n}$ are obtained from the simulator geometric properties (Jønsson *et al.*, 2004) by:

$$\begin{cases} r_{\mathrm{a},n} = \dfrac{12\mu a_n}{b_n h_n^3}, \\ m_{\mathrm{a},n} = \dfrac{6\rho_0 a_n}{5S_{\mathrm{slit},n}}, \end{cases} \tag{4.3}$$

where a_n, b_n and h_n are respectively the length, width and thickness of the narrow slit, $S_{\mathrm{slit},n}$ corresponds to the cross-section area of the rectangular or annular slit, and μ denotes the shear dynamic viscosity of air.

4.3.3 Transfer matrix model

When considering each acoustic element in the IEC 60318-4 simulator as a two-port system, the acoustic pressure and volume velocities at the inlet and outlet of the element can be related using a transfer matrix. For each section of the simulator main cavity, one has:

$$\boldsymbol{T_m} = \begin{bmatrix} \cos(k_0 L_m) & \mathrm{j} Z_1 \sin(k_0 L_m) \\ \mathrm{j}\sin(k_0 L_m)/Z_1 & \cos(k_0 L_m) \end{bmatrix}. \tag{4.4}$$

m = 1, 3 and 5 correspond respectively to each section of the main cavity, k_0 denotes the wavenumber and Z_1 denotes the characteristic impedance of the main cavity equal to $\rho_0 c_0/S_0$. For each Helmholtz resonator:

$$\boldsymbol{T_n} = \begin{bmatrix} 1 & 0 \\ 1/Z_{\mathrm{HR},n} & 1 \end{bmatrix}. \tag{4.5}$$

n = 2 and 4 correspond to the first and second Helmholtz resonators. $Z_{\mathrm{HR},n}$ corresponds to the impedance at the input of the first or second resonator. The input impedance of the rectangular and annular slits is derived using the low reduced frequency (LRF) model in which the thermal and viscous energy losses in the fluid are taken into account in a homogeneous way using the complex wavenumber and characteristic impedance (Rodrigues, Guianvarc'h, Durocher, Bruneau & Bruneau, 2008; Kampinga, 2010). The detailed calculation process of $Z_{\mathrm{HR},n}$ based on the LRF model is provided in Appx. VII.

The global transfer matrix of the IEC 60318-4 simulator can be obtained by assembling the one related to each element of the system:

$$\boldsymbol{T^{\mathrm{ES}}} = \begin{bmatrix} T_{11}^{\mathrm{ES}} & T_{12}^{\mathrm{ES}} \\ T_{21}^{\mathrm{ES}} & T_{22}^{\mathrm{ES}} \end{bmatrix} = \boldsymbol{T_1}\,\boldsymbol{T_2}\,\boldsymbol{T_3}\,\boldsymbol{T_4}\,\boldsymbol{T_5}. \tag{4.6}$$

The reflection coefficient of the simulator in the case of an infinite terminal impedance can be determined by:

$$R_s = \frac{T_{11}^{\mathrm{ES}} - T_{21}^{\mathrm{ES}} Z_1}{T_{11}^{\mathrm{ES}} + T_{21}^{\mathrm{ES}} Z_1}. \tag{4.7}$$

The input impedance of the ear simulator is derived from Eq. (4.7):

$$Z_s = Z_1 \frac{1 + R_s}{1 - R_s}. \tag{4.8}$$

4.3.4 Finite element model

To validate the TM model, a detailed FE model of the G.R.A.S. RA0045 simulator is constructed in COMSOL Multiphysics (v.5.3a COMSOL®, Sweden) following the modeling strategy of (COMSOL, 2017) based on its scanned geometry (see Fig. 4.1). The entrance of the simulator (reference plane) is marked in Fig. 4.3. The sound propagation in the main cavity and side volumes of the simulator is governed by Helmholtz equation in which energy losses are not considered. This choice is made since the thermo-viscous effects in these regions are negligible and those around the ring-shaped sheet metal in the second side cavity have been proved to have very little influence on the simulated impedance of the simulator. These domains are meshed using quadratic 10-noded tetrahedral elements based on a meshing criterion of at least 6 elements per wavelength. On the other hand, thermo-viscous acoustic domains are adopted for the narrow slits where the sound propagation is governed by linearized Navier-Stokes equations with viscous and heat conduction effects taken into account (Blackstock, 2000). These domains are meshed

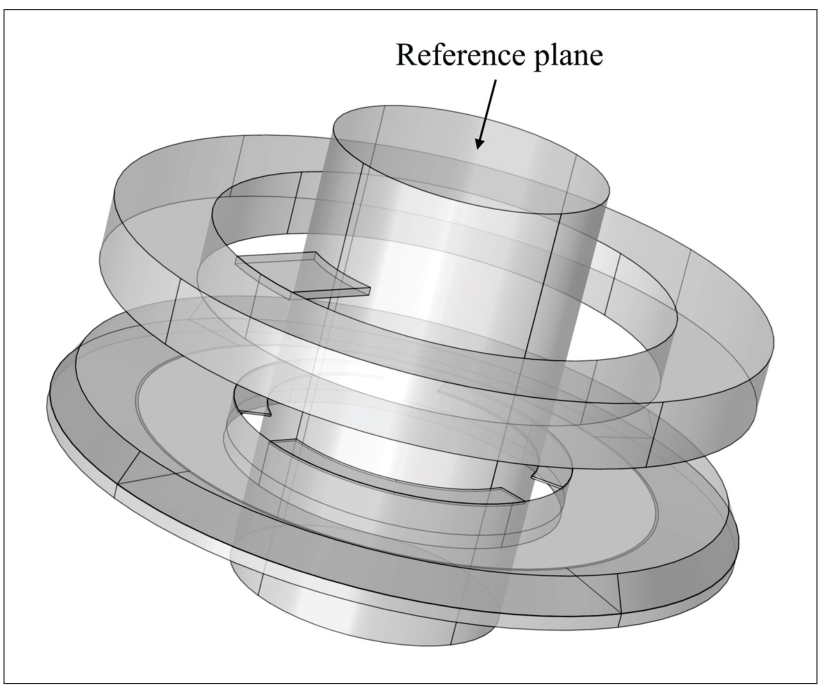

Figure 4.3 Geometry used in the FE model of the IEC 60318-4 ear simulator

using a dense element distribution in the normal direction along the horizontal walls of the slits to accurately resolve the acoustic boundary layers within which thermal and viscous dissipation is significant. The sound pressure, particle velocity and temperature are computed at each node of the domains. The coupled problem is solved using the built-in *Acoustics/Thermoviscous Acoustics Multiphysics* boundary coupling condition in COMSOL Multiphysics. An acoustically rigid condition is introduced to the outlet of the simulator and a displacement excitation of 10^{-5} m is imposed at the reference plane. The input impedance of the simulator is calculated using the sound pressure p and particle velocity $\vec{v}$ determined at each node of the simulator entrance:

$$Z_s = \frac{1}{S_0} \frac{\int_{S_0} p \, \mathrm{d}S}{\int_{S_0} \vec{v} \cdot \vec{n} \, \mathrm{d}S}. \tag{4.9}$$

4.4 Modeling of the open and occluded ATF earcanals

4.4.1 Insertion loss of the earplug

The IL of a 6.6 mm long silicone custom-molded earplug inserted into the earcanal of an ATF is simulated using a 2D axisymmetric FE model in COMSOL Multiphysics (see Fig. 4.4) following the modeling strategy of (Viallet *et al.*, 2013). The ATF earcanal consists of a rigid-walled cylinder of constant circular cross-section terminated by an IEC 60318-4 simulator. In the model, the simulator is considered as a cylindrical air cavity terminated by an equivalent TI (see Sec. 4.4.2) in order to simulate the sound pressure at the eardrum position rather than that at the reference plane. The elastic isotropic mechanical properties of the silicone earplug adopted in the simulation are assessed using a quasi-static mechanical analyzer: density (1500 kg·m^{-3}), Young's modulus (1.7 MPa), Poisson's ratio (0.48) and isotropic loss factor (0.18). A blocked pressure of 2 Pa induced by a normal incident plane wave is imposed at $z = 0$. In the specific case of the open ear, a normal acoustic particle acceleration condition is introduced at $z = 0$ which depends simultaneously on the blocked pressure and the radiation impedance of a baffled circular piston to account for the interaction with the external fluid (Schroeter & Poesselt, 1986).

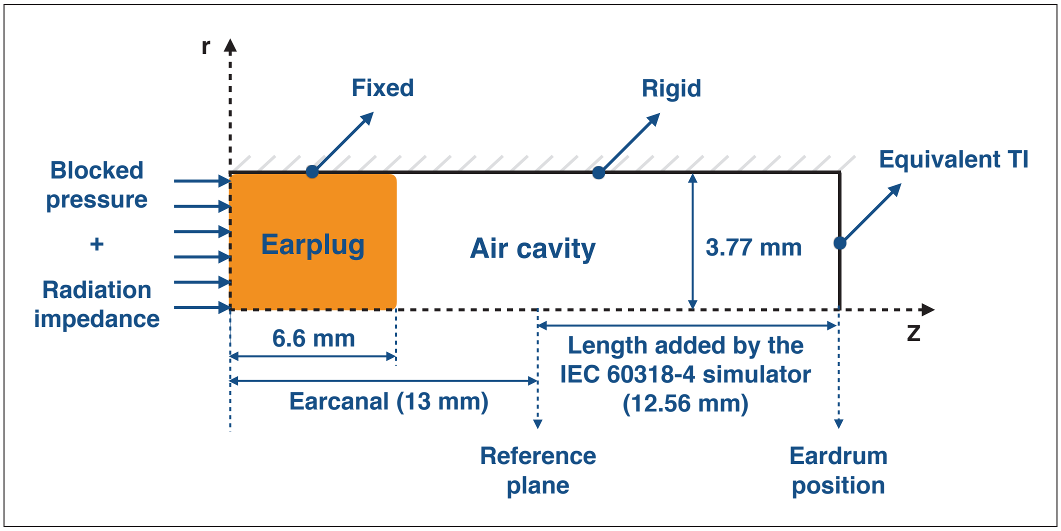

Figure 4.4 Schematic representation of the FE model to simulate the IL of a silicone earplug. Adapted from (Viallet *et al.*, 2014)

The calculation of the earplug IL requires the simulation of the sound pressure at the eardrum position in the open earcanal and that in the earcanal occluded by the earplug:

$$IL = 20\log_{10}\left(\left|p_{\text{open}}\right|\right) - 20\log_{10}\left(\left|p_{\text{occluded}}\right|\right) . \tag{4.10}$$

Additionally, the earplug IL simulated with a complete FE model of the corresponding system (see Fig. 4.5) which uses the detailed FE model of the IEC 60318-4 simulator (see Fig. 4.3) is taken as the reference. The same modeling process as the 2D axisymmetric FE model is followed and the sound pressure at the output of the ear simulator (eardrum position) is simulated in order to calculate the earplug IL using Eq. (4.10).

4.4.2 Equivalent tympanic impedance

A traditional way to obtain the equivalent TI of the IEC 60318-4 simulator is to extract the two RLC circuits in parallel from the LPM of the simulator (see Fig. 4.2) which correspond to the Helmholtz resonators (Viallet *et al.*, 2013). In this study, another approach based on the RI method is adopted to determine the TI from the input impedance of the simulator. Considering

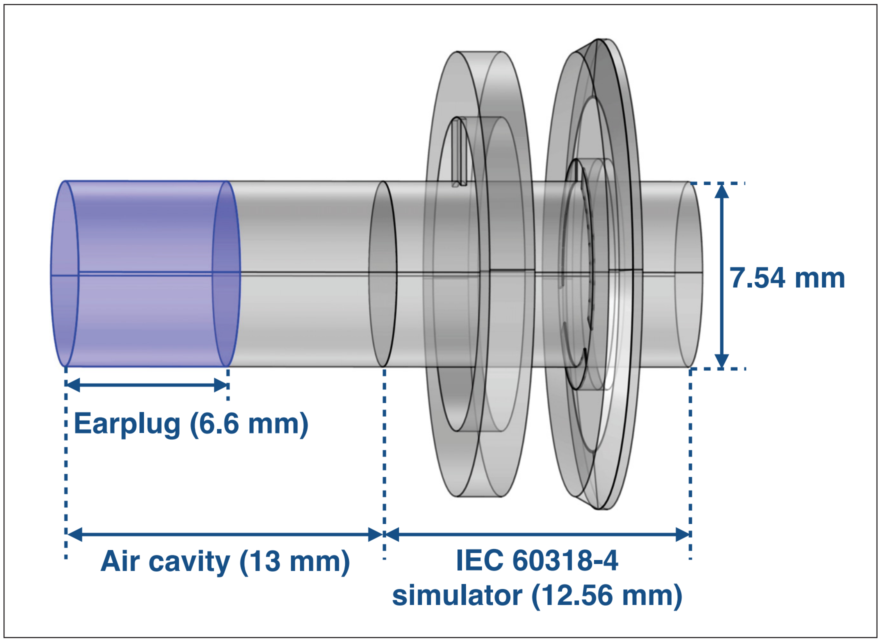

Figure 4.5 Geometry used in the complete FE model of an occluded ATF earcanal

the entire ear simulator as a two-port system, the acoustic pressure and volume velocities at the reference plane (p_{rp}, u_{rp}) and eardrum position (p_{ep}, u_{ep}) can be related by a transfer matrix (Hudde, 1983; Larson *et al.*, 1993; Rodrigues *et al.*, 2015a):

$$\begin{pmatrix} p_{\mathrm{rp}} \\ u_{\mathrm{rp}} \end{pmatrix} = \begin{bmatrix} T_{11} & T_{12} \\ T_{21} & T_{22} \end{bmatrix} \begin{pmatrix} p_{\mathrm{ep}} \\ u_{\mathrm{ep}} \end{pmatrix}, \tag{4.11}$$

with $T_{11} = \cos(k_0 L_0)$, $T_{12} = \mathrm{j} Z_1 \sin(k_0 L_0)$, $T_{21} = \mathrm{j}\sin(k_0 L_0)/Z_1$ and $T_{22} = \cos(k_0 L_0)$. L_0 is the length between the reference plane and microphone position (eardrum position) of the simulator (see Fig. 4.4). The equivalent TI is then given by:

$$Z_{\mathrm{ep}} = \frac{T_{22} Z_{\mathrm{rp}} - T_{12}}{T_{11} - T_{21} Z_{\mathrm{rp}}}, \tag{4.12}$$

where $Z_{\mathrm{rp}} = p_{\mathrm{rp}}/u_{\mathrm{rp}}$ denotes the impedance at the reference plane. This method allows for calculating the TI once the input impedance of the simulator and its length are provided.

Specifically in this work, one is interested in three equivalent TI models based on the analytical impedance models of the IEC 60318-4 simulator: model 1 corresponds to the TI derived from the TM model of the simulator using the RI method, model 2 and model 3 are related to the TI obtained from the LPM of the simulator respectively with the RI method and in the traditional way using the RLC circuits in parallel.

4.5 Experimental measurements

4.5.1 Measurements of the IEC 60318-4 ear simulator input impedance

In order to validate the proposed TM model, the simulator impedance was measured using a sound intensity probe (PU Match-PTN, Microflown Technologies, Netherlands) which allows for determining the acoustic pressure and particle velocity in the frequency range from 100 Hz to 10 kHz (see Fig. 4.6). The system was excited acoustically in a semi-anechoic chamber with a white noise of 97 dB in overall sound pressure level generated by a loudspeaker (model K162 SN, dB Technologies, Italy). The center of the speaker was located at the same height (about 1 m) as the center of the simulator and at a distance of about 2 m. The floor around the simulator was covered with sound-absorbing foam to minimize ground reflections. The dust protector at the inlet of the simulator was removed and the intensity probe was placed as close as possible to the entrance of the simulator in order to precisely calculate the input impedance of the latter using the experimental data. Four successive measurements were performed on three G.R.A.S. RA0045 simulators of different serial numbers to account for the possible variability associated with the probe position and orientation.

4.5.2 Measurements of the earplug insertion loss using an ATF

The IL of the silicone earplug was assessed at normal room temperature using an ATF (G.R.A.S. 45CB, G.R.A.S. Sound & Vibration AS, Denmark) without pinna simulators which comprises a rigid-walled cylindrical earcanal terminated by an IEC 60318-4 simulator. The system was excited by a white noise of around 110 dB in overall sound pressure level in a reverberant room

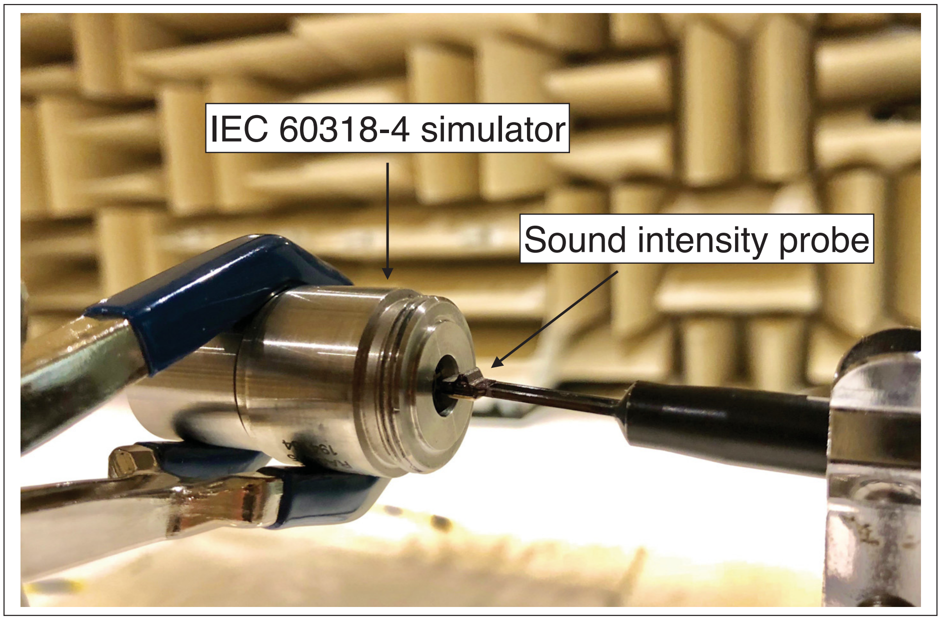

Figure 4.6 IEC 60318-4 ear simulator input impedance measurements using a sound intensity probe

(diffuse field). The sound pressure levels in the open and occluded earcanals were measured using the recording microphone in the ear simulator (G.R.A.S. 40AG, G.R.A.S. Sound & Vibration AS, Denmark). A reference microphone (MPA231, BSWA Technology Co., China) was positioned at about 1 m from the earcanal entrance in order to obtain the corresponding transfer functions between the two microphones which are used to calculate the earplug IL. The measurements were repeated three times to evaluate the variability related to the mounting conditions. The details of the earplug IL measurements can be found in (Viallet *et al.*, 2014).

4.6 Results and discussion

4.6.1 Input impedance of the IEC 60318-4 ear simulator

Figure 4.7 illustrates the input impedance of the IEC 60318-4 ear simulator obtained from different models: the blue zone (circles) corresponds to the TM model, the red zone (asterisks) corresponds to the LPM and the dashed black line is related to the FE model of the simulator.

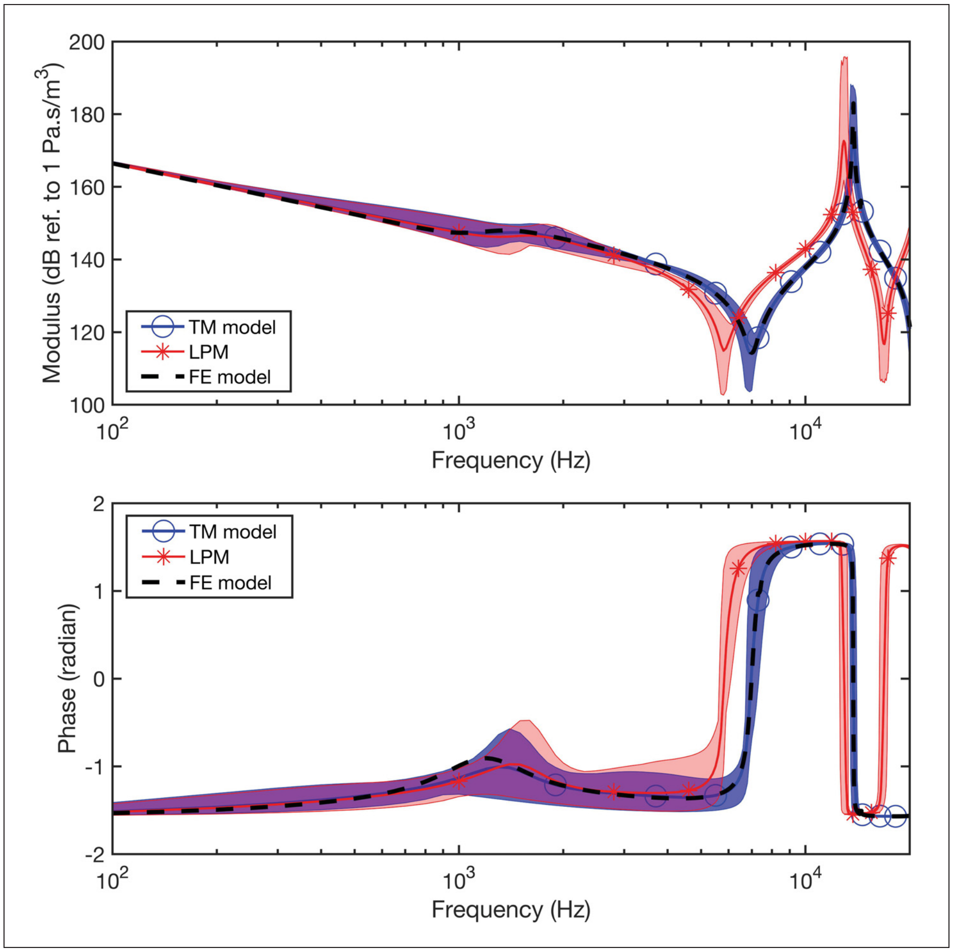

Figure 4.7 Input impedance of the IEC 60318-4 ear simulator obtained using different models: TM model (blue circles), LPM (red asterisks), FE model (dashed black). (top) modulus; (bottom) phase. Averaged simulation result together with the maximal and minimal values are plotted for each analytical model

For the analytical models, the uncertainty propagation of the simulator geometric dimensions is taken into account using the Monte Carlo method. 1000 evaluations have been run for each model in which a uniform distribution is chosen for any dimension concerned based on the corresponding average and standard deviation in Table 4.1. A convergence study has shown that this number of evaluations is sufficient to capture the variability in the simulator impedance (or equivalent TI) induced by its geometric uncertainties. The FE model is based on the mean component dimensions of the simulator. Results are presented in the frequency range from

100 Hz to 20 kHz as all the relevant studies (Jønsson *et al.*, 2003, 2004; Sasajima *et al.*, 2015; COMSOL, 2017) in order to exhibit the first resonance of the simulator main cavity around 13.5 kHz. In the following, results are displayed in the working frequency range of the ear simulator (100 Hz – 10 kHz) beyond which it does not necessarily represent the acoustic impedance of the human ear (IEC, 2010). The figure shows that all the models are able to provide similar impedance simulation results up to nearly 3 kHz. A frequency offset is observed from the LPM at medium and high frequencies (over 3 kHz) compared to the other models. In this frequency range, the LPM fails to precisely describe the behavior of the IEC 60318-4 simulator. This is consistent with previous findings of (Bravo *et al.*, 2008, 2012) which used the LPM to calculate the acoustic impedance of an IEC 60318-1 simulator. Additional results not presented in the paper have shown that the LPM of the simulator main cavity does not satisfy the low frequency approximation, which is the reason for the observed frequency offset. The TM model is found in perfect agreement with the FE model of the simulator in the whole frequency range of interest, which proves the validity of the former. It is necessary to mention that the Helmholtz resonators of the IEC 60318-4 simulator have resonant frequencies at about 1400 Hz and 3800 Hz, covering the behavior of the system in the mid-frequency range. The simulated simulator impedance (especially phase values) is shown to be very sensitive to the resonator geometric parameters in the associated frequency ranges. Around 1500 Hz, the TM model is found to be slightly closer to the FE model than the LPM. This is probably due to the fact that the impedance of the first resonator's neck (rectangular narrow slit) is better captured by the LRF model than the LPM.

Figure 4.8 displays the measurement results using the sound intensity probe (grey zone) together with the simulator input impedance calculated by the TM model. Even though there do exist some discrepancies in certain frequency bands, a satisfactory agreement is seen between the simulation and measurements of the simulator impedance, which further gives confidence in the TM model of the simulator in the frequency range from 100 Hz to 10 kHz. The differences observed between the model and sound intensity probe measurements (mainly below 700 Hz and above 7 kHz) are partly associated with the sound diffraction of the probe positioned in front of the simulator all along the experiments as shown in Fig. 4.8 (dashed black line). This curve has

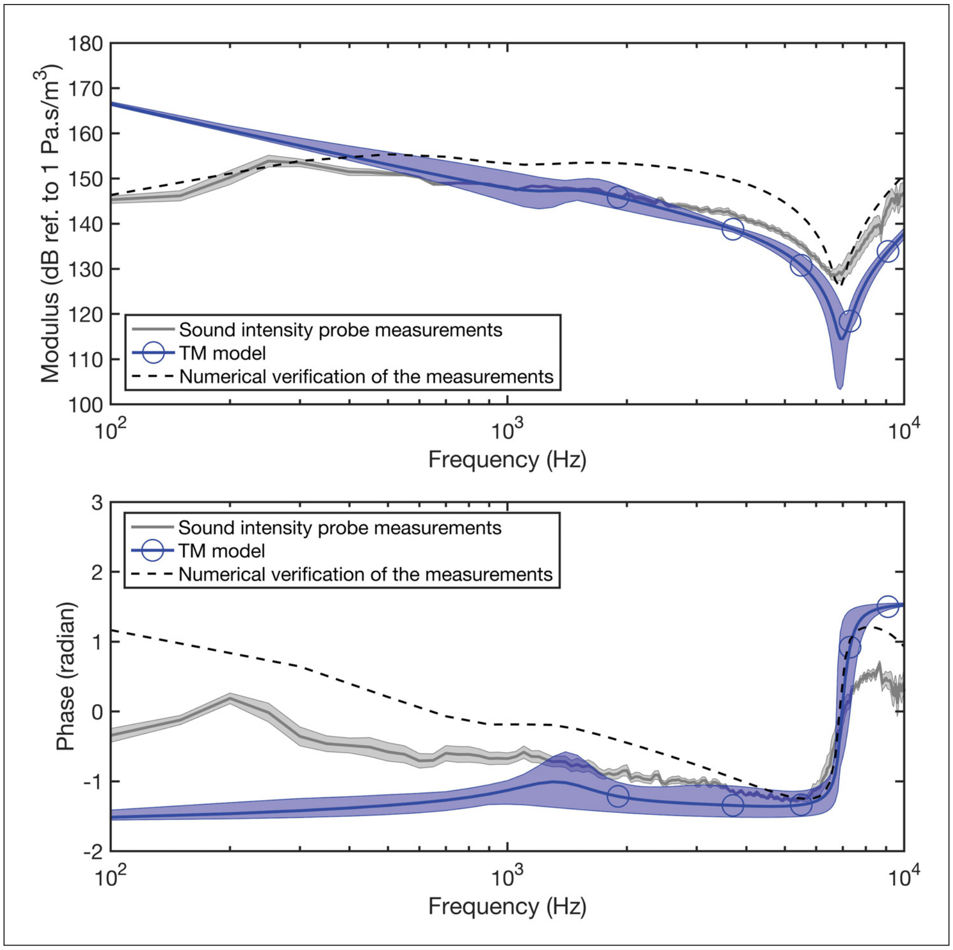

Figure 4.8 Measurement and simulation results of the IEC 60318-4 ear simulator input impedance: sound intensity probe measurements (average ± standard deviation, grey), TM model (blue circles). Numerical verification result of the measurements (dashed black) is also presented. (top) modulus; (bottom) phase. Averaged simulation result together with the maximal and minimal values are plotted for the TM model

been obtained by accounting for the scattering from the sound intensity probe in the FE model of the ear simulator (see Fig. 4.3). Note that in the simulation, a simplified shape of the probe has been considered and the probe sensor has been positioned approximately at the same place as in the experiments. Another possible reason is that the sound intensity probe was difficult to be placed right at the input surface of the simulator when performing the measurements and the interaction with the external sound field is not taken into account in the TM model.

4.6.2 Equivalent tympanic impedance

Figure 4.9 illustrates different equivalent TI models of the IEC 60318-4 simulator accounting for its dimension uncertainties: the blue zone (circles) corresponds to model 1 (TM model - RI), the red zone (asterisks) corresponds to model 2 (LPM - RI) and the green zone (squares) corresponds to model 3 (traditional TI model). A wide variation due to the simulator geometric uncertainties is exhibited in the calculated TI at frequencies over 1 kHz. Below 3 kHz, all the models provide similar TI simulation results which however become rather different at higher frequencies. Particularly, the obvious differences between model 2 (LPM - RI) and the first TI model (TM model - RI) over 3 kHz could originate from the inconsistencies already seen in Fig. 4.7 between the LPM and TM model of the simulator. These inconsistencies are due to the fact that the sound propagation in the simulator main cavity is better captured by the TM model than the LPM. Furthermore, model 3 (traditional TI model) even though not mathematically rigorous, seems not far from model 1 (TM model - RI) up to 7 kHz.

4.6.3 Insertion loss of the earplug

Figure 4.10 presents the silicone earplug IL simulated using the various TI models: the dashed blue curve (circles) corresponds to model 1 (TM model - RI), the red curve corresponds to model 2 (LPM - RI) and the green line (squares) is related to model 3 (traditional TI model). In addition, the earplug IL calculated using the FE model of the ear simulator (see Fig. 4.5) is displayed as the reference (black curve with diamonds), together with the measurement results using the ATF (grey zone). All the models are based on the mean component dimensions of the simulator (see Table 4.1). From Fig. 4.10, no remarkable effect of the TI models on the earplug IL simulation is observed up to 6 kHz. In this frequency range, the system is mainly controlled by the first resonance of the earplug around 1.9 kHz which corresponds to a rigid body mode of the earplug with elastic boundary conditions (Viallet *et al.*, 2013, 2014). In accordance with Fig. 4.7, model 1 (TM model - RI) compares well with the reference model (FE model of the simulator) in the whole frequency range of interest with regard to the simulated IL. This finding confirms that considering the IEC 60318-4 simulator as a cylindrical cavity terminated by an

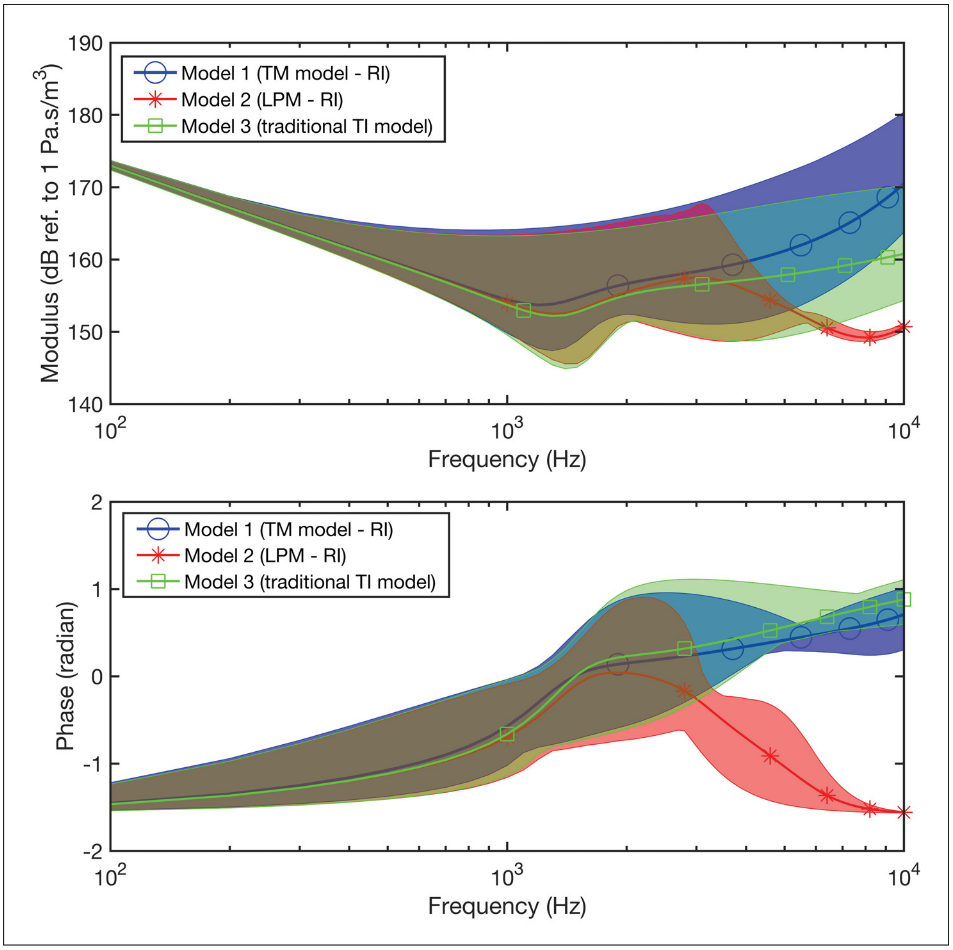

Figure 4.9 Different equivalent TI models of the IEC 60318-4 ear simulator: model 1 (blue circles), model 2 (red asterisks), model 3 (green squares). (top) modulus; (bottom) phase. Averaged simulation result together with the maximal and minimal values are plotted for each TI model

equivalent TI to simulate the IL of earplugs in an ATF earcanal is valid up to 10 kHz. Above 6 kHz, the simulated IL based on model 2 (LPM - RI) differs significantly from those obtained using the other TI models. This could be supported by the fact that the equivalent TI derived from model 2 (LPM - RI) correlates poorly with that obtained from the others from 6 kHz especially in phase (see Fig. 4.9) in view of the sound propagation in the simulator main cavity poorly described by the LPM. At higher frequencies (over 8.5 kHz), a mismatch is seen between the IL simulated using model 3 (traditional TI model) and that using model 1 (TM model - RI) (see the “zoomed-in” view of Fig. 4.10). This indicates that the adoption of the traditional TI

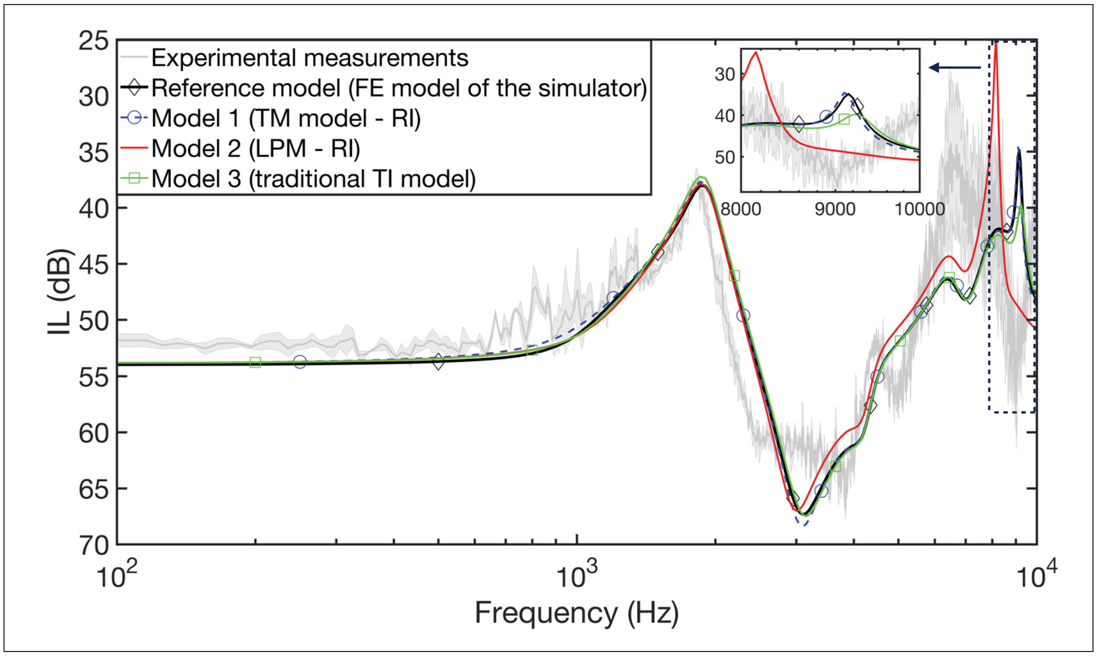

Figure 4.10 IL of the silicone earplug simulated using different equivalent TI models: model 1 (dashed blue circles), model 2 (red), model 3 (green squares). Experimental data (average ± standard deviation, grey) and simulation result using the FE model of the ear simulator (black diamonds) are also presented

model to calculate the IL of earplugs might be limited to the frequency range below 8.5 kHz if accurate IL simulation is desired. All the IL simulation results in Fig. 4.10 are in satisfactory agreement with the experimental data up to 6 kHz. The evident inconsistency between the simulation based on the reference model (FE model of the simulator) and measurements at higher frequencies (above 6 kHz) is believed to be related to the simplified materiel model of the earplug adopted in the simulation.

4.7 Conclusion

In this work, a TM model of an IEC 60318-4 occluded ear simulator has been proposed based on the geometric information identified from micro-CT scan images. It was established using the LRF model to calculate the impedance of the simulator narrow slits where thermo-viscous energy losses should be taken into account. The TM model was validated using (i) a FE model of the scanned simulator in the frequency range [100 Hz, 20 kHz] and (ii) impedance measurements with a sound intensity probe (100 Hz – 10 kHz). The uncertainty propagation of the simulator component dimensions was accounted for using the Monte Carlo method. The TM model was found to better describe the simulator input impedance above 3 kHz compared to the LPM. The equivalent TI was derived from the simulator analytical impedance models (TM model and LPM) using the RI method, and compared to that obtained from the traditional lumped TI model. The various TI models have then been exploited to simulate the IL of a silicone earplug using a FE model of an occluded ATF earcanal (100 Hz – 10 kHz). The IL obtained using the TI derived from the TM model (model 1) was found in very good agreement with that acquired using the complete FE model of the simulator (reference model) in the whole frequency range of interest. It confirms that considering the IEC 60318-4 simulator as a cylindrical cavity with a locally reacting terminal impedance condition (equivalent TI) to simulate the IL of earplugs in an ATF earcanal is valid up to 10 kHz. In addition, the TM model has been shown to better agree with the simulator FE model than the LPM above 6 kHz regarding the IL simulation since the TI derived from the LPM (model 2) failed to precisely capture the earplug IL in this frequency range. The traditional TI model (model 3) seems adequate when adopted to calculate the earplug IL at frequencies below 8.5 kHz however it becomes less reliable in higher frequency bands. The influence of the studied TI models on the IL simulation was proved to be only pronounced over 6 kHz. The TM model of the IEC 60318-4 simulator proposed in this work with acoustic parameters directly related to the simulator geometric dimensions constitutes a step forward for designing artificial ear simulators that meet the authors' needs for future investigations.

4.8 Acknowledgement

The authors wish to acknowledge the financial support provided by the Natural Sciences and Engineering Research Council of Canada.

CHAPTER 5

INFLUENCE OF THE INTER-INDIVIDUAL VARIABILITY IN THE EARDRUM IMPEDANCE ON THE EARPLUG INSERTION LOSS

As mentioned in Sec. 0.3.2, a sufficiently accurate eardrum impedance needs to be reproduced by the ear simulator for measuring the sound attenuation of earplugs (Schroeter & Poesselt, 1986). It still remains to be elucidated whether standardized ear simulators specified in IEC 60318-4 (2010) which are designed to reproduce an average acoustic impedance of the human ear prove adequate for earplug attenuation measurements regarding the large inter-individual variability in the eardrum impedance (Hudde, 1983; Rosowski *et al.*, 1990; Hudde & Engel, 1998; Jønsson *et al.*, 2018). In addition, current ear simulators do not only represent the eardrum impedance but also include an earcanal portion mimicked by a simple cylindrical-shaped air cavity in front of the eardrum position which cannot be removed (Brüel *et al.*, 1976; Jønsson *et al.*, 2004).

The transfer matrix (TM) model of the IEC 60318-4 ear simulator and reduced impedance (RI) method proposed in Chapter 4 have shown several advantages that can help deal with the problems mentioned above. First, the TM model combined with the RI method allows for eliminating the acoustic impedance associated with the cylindrical cavity in front of the eardrum position and retrieving directly the equivalent tympanic impedance (TI) of the ear simulator. Compared to the conventional TI model derived from the lumped parameter model of the simulator (Jønsson *et al.*, 2003, 2004), the retrieved equivalent TI is more rigorous from a mathematical point of view. Second, this also makes it possible to account for a more realistic earcanal ahead of the eardrum position in terms of geometry and material properties for the numerical modeling of earplug attenuation. Third, the proposed TM model with acoustic parameters directly related to the ear simulator geometric dimensions also allows for easily carrying out parametric studies on the potential variability in the eardrum impedance.

More specifically, this chapter is a complement of Chapter 4 and aims at investigating the influence of the inter-individual variability in the eardrum impedance on the earplug insertion loss (IL). This is achieved through a two-step methodology. First, the variability in the human eardrum impedance is replicated by further exploring the TM model of the ear simulator (combined with the RI method) using a statistical approach. Second, a 3D finite element (FE) model is used to simulate the IL of an earplug inserted into a realistic-shaped earcanal surrounded by a skin layer. The corresponding method and results partly contribute to my colleague Benacchio's paper (2021) entitled "Design of an acoustic eardrum simulator dedicated to sound attenuation measurements of earplugs: Effect of tympanic impedance inter-individual variability" to be submitted for publication in *Applied Acoustics*.

5.1 Calculation of representative impedance

The aim of this section is to calculate the equivalent TI values representative of the published inter-individual variability in the human eardrum impedance based on the TM model of the ear simulator and RI method. Following the convention used in Chapter 4, the term "impedance" in this work refers to "acoustic impedance" defined as the sound pressure over the acoustic volume velocity. Figure 5.1 presents the acoustic impedance modulus measured in the earcanals of 32 human subjects manually extracted from (Jønsson *et al.*, 2018). For the sake of comparison, the experimental impedance data have been propagated by these authors back or forth along the curved center axis of each earcanal to a common reference plane based on the Webster's horn equation so that the half-wavelength resonances of earcanals all align at about 9.4 kHz. The shape of each earcanal was determined from the magnetic resonance imaging datasets of the same participants (Darkner *et al.*, 2018). In the figure, the dashed blue curve together with the blue zone corresponds to the average experimental data plus or minus one standard deviation. Results are displayed within the same range as in (Jønsson *et al.*, 2018) between 10^6 and 4×10^8 Pa·s/m^3, and in the working frequency range of the ear simulator from 100 Hz to 10 kHz (IEC, 2010). As expected, the width of the blue zone indicates an important variability in the acoustic impedance at the common reference plane especially at 5 – 6 kHz and above, which also reflects a large variability in the impedance at the eardrum.

In order to capture the measured impedance variability of the human ear, the TM model in Chapter 4 is further exploited through a Monte Carlo simulation to calculate the input impedance

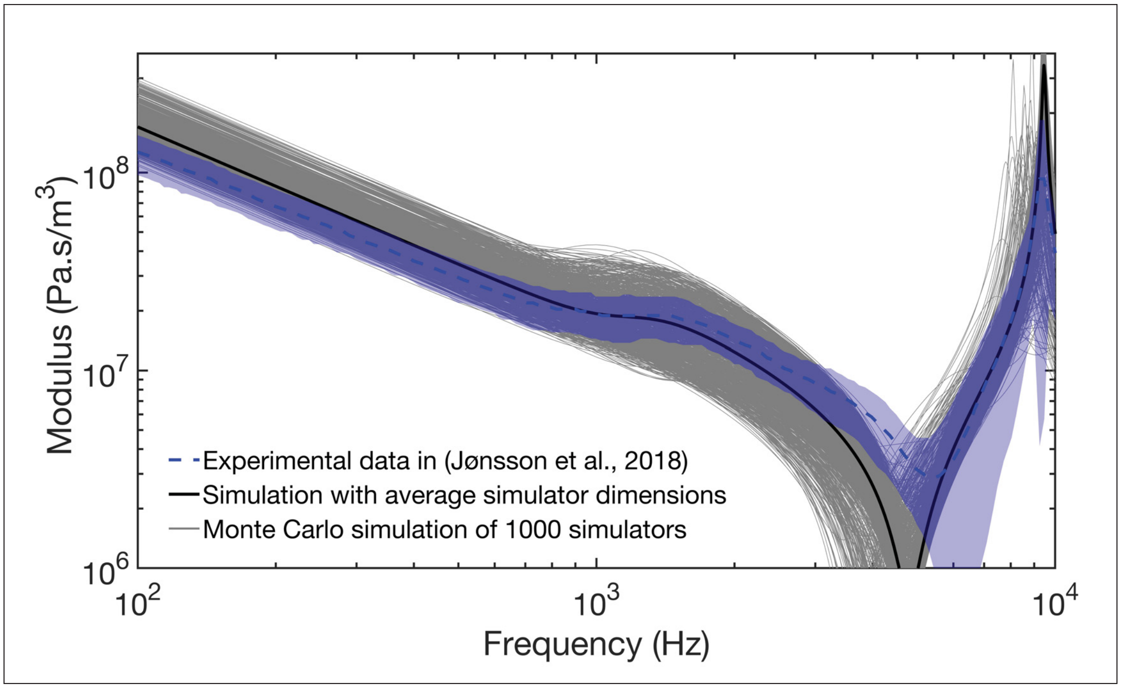

Figure 5.1 Acoustic impedance at the reference plane measured on human subjects and simulated with the ear simulator TM model: average value (dashed blue curve) plus or minus one standard deviation (blue zone) of the experimental data in (Jønsson *et al.*, 2018); simulation result using the average simulator geometric dimensions (black curve); Monte Carlo simulation results of 1000 ear simulators by varying the simulator geometric dimensions (grey curves)

of 1000 ear simulators (see grey curves in Fig. 5.1). More precisely, the input impedance of the ear simulator is calculated 1000 times with the TM model by varying the simulator geometric dimensions. Each time, a random combination of the simulator dimensions is generated assuming a uniform distribution of ±20% around the average value of each dimension concerned (see Table 4.1 in Chapter 4). Note that for the FE modeling of the earcanal (see Sec. 5.2), the area of the tympanic membrane is chosen to be equal to the average cross-section area of the simulator main cavity, thus the radius of the latter is not varied for the Monte Carlo simulation and remains constant at its average value. In addition, the input impedance of the ear simulator calculated with the combination of its average geometric dimensions is also presented in Fig. 5.1 using the black curve. The simulation results are all propagated to the same reference plane as that used for the experimental data with the RI method.

The Monte Carlo simulation results enable to capture the overall tendency of the human eardrum impedance, and cover a considerable part of its actual variability over the frequency range studied with the selected number of simulations and interval of dimension variation. This is further illustrated when analyzing the results in Fig. 5.2. The ear simulator impedance calculated using its average dimensions (black curve) is found close to the average experimental data obtained in human ears (dashed blue curve) at most frequencies except between 3 kHz and 5.5 kHz. Moreover, around the quarter wavelength anti-resonance at 5 – 6 kHz, more differences between the simulation and measurement results (grey curves vs. blue zone) are observed. This could be explained by the fact that the experimental data were propagated to the reference plane based on the Webster's horn equation to account for the variable cross-section area along the center axis of the human earcanal (Jønsson *et al.*, 2018), whereas the propagation of the simulation results is achieved using the RI method for a simple cylindrical earcanal of the acoustic test fixture (see Sec. 4.4.2). A second possible reason is that the modeled ear simulator was originally designed based on the average acoustic impedance measured in another group of human ears which may slightly differ from that shown in Fig. 5.1. At frequencies above 6 kHz controlled by the half wavelength resonance at 9.4 kHz, the simulation and measurement results are in relatively good agreement.

The corresponding equivalent TI values of 1000 ear simulators are then derived from the Monte Carlo results shown in Fig. 5.1 using the RI method. Figure 5.2 presents the modulus of these values in dB using the grey curves. In particular, the equivalent TI obtained from the input impedance of the simulator based on its average geometric dimensions is presented using the black curve for comparison. Consistently with the phenomenon already observed in Chapter 4, the differences in the acoustic impedance at the reference plane induce even more significant ones in the equivalent TI. Additionally, maximum and minimum values of the experimental impedance data at the human eardrum are manually picked at different frequencies from (Rosowski *et al.*, 1990) and (Hudde & Engel, 1998), and displayed respectively with the black diamonds and asterisks in Fig. 5.2. These values again reveal an important variability in the human eardrum impedance. In general, the TI simulation results are shown to be able to

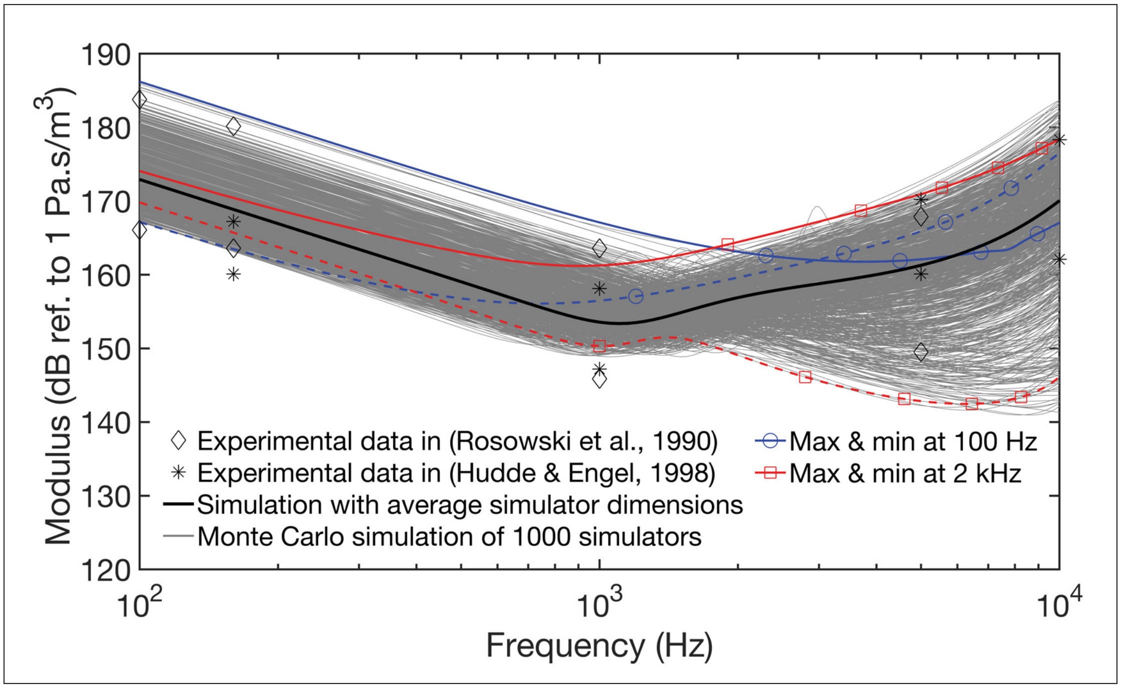

Figure 5.2 Equivalent TI results derived from the Monte Carlo simulation of 1000 ear simulators using the RI method (grey curves). Black curve corresponds to the equivalent TI obtained from the simulator input impedance based on its average geometric dimensions. Color curves correspond to the representative maximum (solid curves) and minimum (dashed curves) TI values at 100 Hz (blue curves with circles) and 2 kHz (red curves with squares). Black diamonds and asterisks represent the extreme eardrum impedance experimental data reported in (Rosowski *et al.*, 1990) and (Hudde & Engel, 1998)

reproduce the inter-individual variability of the eardrum impedance in the literature, especially that reported in (Rosowski *et al.*, 1990). Compared to the latter, the impedance variability in (Hudde & Engel, 1998) appears to be less important, probably due to the different groups of human ears used for the measurements. The TI results can then be used in a FE model to investigate the potential influence of the eardrum impedance variability on the IL of a typical earplug (see Sec. 5.2). However, carrying out earplug IL simulations using all the 1000 equivalent TI values in a FE model can be time consuming. Additionally, no simulation curve in Fig. 5.2 can always correspond to the maximum or minimum TI value over the entire frequency range studied. For correctly covering the eardrum impedance variability in a wide frequency range while efficiently evaluating its influence on the earplug IL with a small number of numerical simulations, two representative sets of equivalent TI are selected from the ones shown in Fig. 5.2 and displayed using the color curves. More specifically, the results in the first set (blue curves with circles) correspond respectively to the maximum (solid curve) and minimum (dashed curve) values at 100 Hz among the equivalent TI values of 1000 ear simulators, while those in the second set (red curves with squares) correspond to the maximum and minimum TI values at 2 kHz. These two sets of impedance together cover nearly the total variability of equivalent TI presented in Fig. 5.2.

5.2 Finite element modeling of the open and occluded earcanals of realistic geometry

The 3D FE model of the earplug inserted into an earcanal of realistic geometry (see Fig. 5.3) is developed in the software COMSOL Multiphysics (v.5.6 COMSOL®, Sweden). A skin layer of about 1.5 mm thickness surrounding the earcanal is also accounted for. The geometry of the earcanal together with the skin layer was reconstructed from the magnetic resonance images of a real human ear by Benacchio *et al.* (2018). The circular surface at the end of the earcanal (see S_4 in Fig. 5.3) corresponds to the eardrum position. The orientation of this surface is identical to that of a real tympanic membrane. Its area equals about 44 mm^2 which is approximately the same as the average cross-section area of the ear simulator main cavity (see Table 4.1 in Chapter 4). The area of the earcanal entrance surface (see S_2 in Fig. 5.3) is about 69 mm^2. The studied earplug is a silicone custom-molded earplug assumed to perfectly fit the shape of the earcanal. It is entirely inserted into the earcanal with an insertion depth of about 10 mm from the earcanal entrance. Only a single earplug type with one insertion depth is studied as the objective is to investigate the independent influence of the eardrum impedance variability on the earplug IL, and the impact of the earplug type or insertion depth is beyond the scope of this work. But the latter can be easily covered in future studies using the proposed FE model.

The earcanal cavity is modeled as an acoustic domain filled with air. The skin layer and earplug are modeled as linear isotropic elastic solids. The mechanical properties of the skin are adopted from (Viallet *et al.*, 2014): Young's modulus (0.42 MPa), density (1050 kg/m^3), Poisson's ratio (0.43) and isotropic loss factor (0.2). The same mechanical properties of the silicone earplug

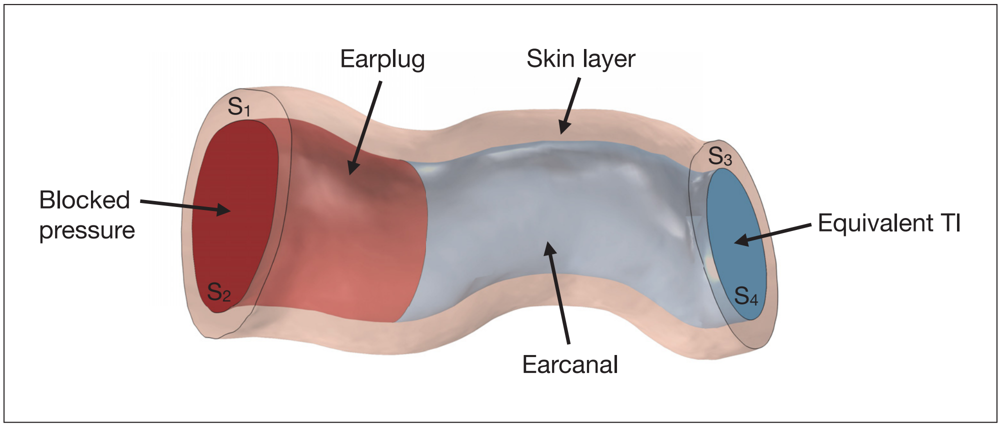

Figure 5.3 FE model adopted to simulate the IL of a silicone earplug inserted into an earcanal of realistic geometry

used in Chapter 4 are adopted: Young's modulus (1.7 MPa), density (1500 kg/m^3), Poisson's ratio (0.48) and isotropic loss factor (0.18). The external lateral boundaries and terminal surface (see S_3 in Fig. 5.3) of the skin layer are considered to be mechanically fixed (Viallet, Sgard, Laville & Nélisse, 2015), and a blocked pressure of 2 Pa induced by a normal incident plane wave is introduced to its front surface (see S_1 in Fig. 5.3). For the occluded earcanal, the same blocked pressure is applied to the earplug outer surface located at the earcanal entrance (i.e., S_2). Particularly for the open earcanal, in order to account for the interaction with the external fluid, a normal acoustic particle acceleration is imposed at the earcanal entrance which depends simultaneously on the blocked pressure and the radiation impedance of a baffled circular piston (Schroeter & Poesselt, 1986). The eardrum impedance is assumed to be independent of the outer ear (including its geometry and material properties), and the four representative equivalent TI results displayed in Fig. 5.2 are successively applied as locally reacting terminal impedance boundary conditions to the eardrum position (i.e., S_4) in order to evaluate their effect on the earplug IL. The latter is calculated by:

$$IL = 20\log_{10}\left(\frac{p_{\text{open}}}{p_{\text{ref}}}\right) - 20\log_{10}\left(\frac{p_{\text{occluded}}}{p_{\text{ref}}}\right), \tag{5.1}$$

with p_{open} and p_{occluded} respectively the root mean square sound pressures averaged over the surface S_4 in the open and occluded earcanals, and $p_{\text{ref}} = 2 \times 10^{-5}$ Pa.

5.3 Influence of the eardrum impedance variability on the earplug insertion loss

The earplug IL simulation results are presented in Fig. 5.4 with the blue curves (circles) and red curves (squares) corresponding respectively to the results obtained using the two sets of equivalent TI shown in Fig. 5.2. The earplug IL calculated using the equivalent TI based on the average simulator geometric dimensions is displayed using the dotted black curve.

These results reveal that the inter-individual variability in the eardrum impedance can induce non-negligible differences in the earplug IL in nearly the whole frequency range studied from 100 Hz to 10 kHz. The highest difference between the IL results obtained with the first set of equivalent TI (blue curves with circles) is about 8 dB and observed around 100 Hz. For the IL results calculated using the second set of equivalent TI (red curves with squares), the most important difference is about 15 dB and found around 3.1 kHz. Note that the differences in the IL may also depend on the geometry of the earcanal and insertion depth of the earplug. At frequencies below 1 kHz, a common phenomenon is seen that a higher equivalent TI generally leads to a lower IL of the earplug. This can be explained by the fact that in this frequency range, the sound pressure at the eardrum in the occluded earcanal clearly increases with the equivalent TI, whereas the effect of the latter is of relatively minor importance in the open earcanal. However, at frequencies above 1 kHz, it is difficult to predict the IL tendency from the equivalent TI probably due to a more complicated interaction between the earplug and eardrum impedance. The earplug IL obtained with the equivalent TI based on the average simulator dimensions (dotted black curve) lies well within the range of the other four curves below about 1.5 kHz. But consistently with the results shown in Fig. 5.2, it is found to be far from the IL related to the minimum TI value at 2 kHz (dashed red curve with squares) and close to the other three curves in most higher frequency bands. Again, it should be kept in mind that the aim of this work is not to reproduce the total variability in the earplug IL that may be caused by the eardrum impedance variability, but to efficiently evaluate the overall influence of the latter on the earplug IL. The observation above suggests that standardized occluded ear simulators which represent an average acoustic impedance of the human ear do not seem to allow for adequately assessing the sound attenuation of earplugs. For instance, as demonstrated in this work, four ear

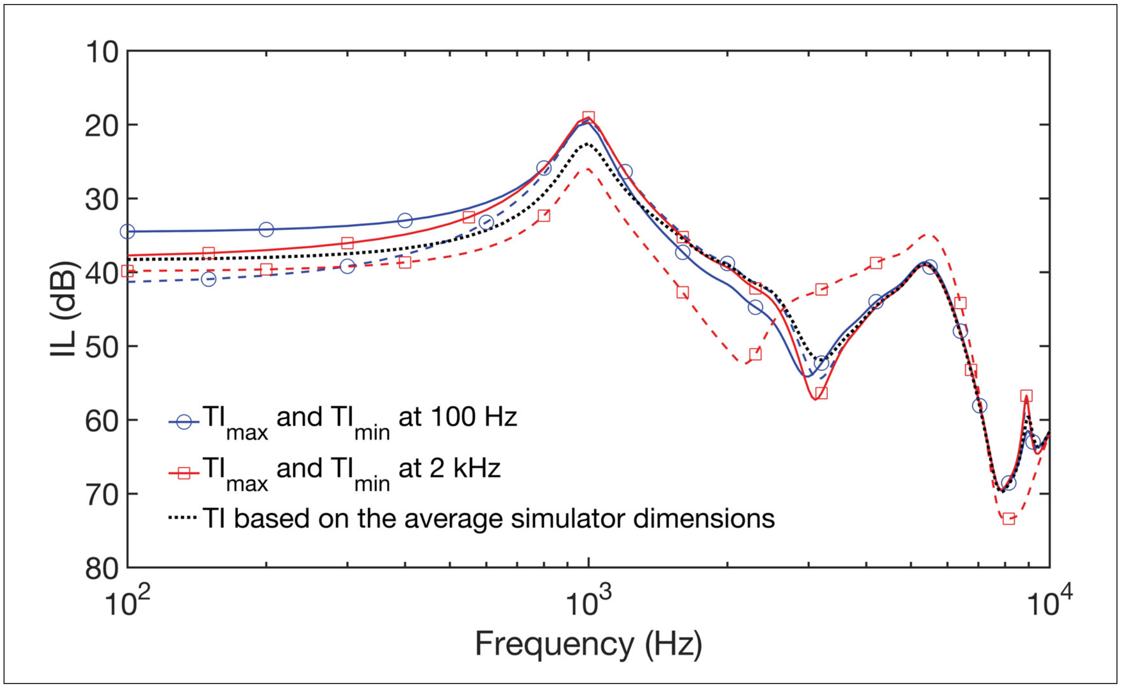

Figure 5.4 Earplug IL results calculated using the representative maximum (solid curves) and minimum (dashed curves) TI values at 100 Hz (blue curves with circles) and 2 kHz (red curves with squares). Dotted black curve corresponds to the earplug IL obtained with the equivalent TI based on the average simulator geometric dimensions

simulators of different designs may be needed to roughly cover the IL variability of a typical earplug induced by the variability in the eardrum impedance.

CONCLUSION AND RECOMMENDATIONS

This chapter summarizes the main results obtained within the framework of this project. The research problems and objectives are first briefly recalled (see Sec. 6.1). The main contributions, limitations as well as the perspectives associated with each step of the methodology detailed in the preceding chapters are then presented and discussed (see Secs. 6.2 and 6.3). Finally, the potential scientific and technological impacts of this work are provided in a general conclusion (see Sec. 6.4).

6.1 Synthesis of research problems and objectives

As an initial step towards a more realistic characterization of hearing protector sound attenuation on acoustic test fixtures (ATFs) in the future, this work sought to address two primary issues related to the vibroacoustic design features of current ATFs through experimental and numerical approaches: (i) the attenuation prediction of double hearing protectors (DHPs) which involves structure-borne (SB) sound transmission through the ATF; (ii) the impact of the IEC 60318-4 ear simulator impedance in the ATF earcanal on the hearing protector attenuation.

More specifically, the DHP overall attenuation is difficult to predict due to the occurrence of the DHP effect. This refers to the phenomenon where the attenuation achieved by the DHP falls short of the algebraic sum of each single protector's attenuation due to the flanking bone conduction (BC) paths on human subjects. This effect can also be observed on ATFs and characterized by the decrease of the earplug noise reduction (NR) after adding the earmuff. However, current ATFs are not designed to account for the BC paths, and the related sound paths yet remain unclear. The first objective consisted in studying the DHP effect on an ATF (characterized by the earplug NR decrease when combined with an earmuff) through experimental measurements and numerical modeling in order to better understand the associated airborne (AB) and SB sound transmission mechanisms, and provide a way to predict the DHP attenuation.

The eardrum impedance has a relatively important impact on assessing the attenuation of earplugs. But it is still unknown whether standardized ear simulators which reproduce an average impedance of the human ear can adequately capture the earplug attenuation regarding the inter-individual variability in the human eardrum impedance. The second objective focused on (i) numerically simulating the insertion loss (IL) of an earplug in an ATF earcanal based on a novel modeling approach of the ear simulator, and (ii) investigating the influence of the eardrum impedance variability on the earplug IL through further exploration of the ear simulator impedance model. Particularly, the proposed model of the ear simulator should allow for accurately describing its acoustic impedance in a wide frequency range compared to the classical lumped parameter model (LPM).

6.2 Sound attenuation of double hearing protectors: contributions, limitations and perspectives

6.2.1 Chapter 2: Experimental study of earplug noise reduction of a double hearing protector on an acoustic test fixture (article n^{o} 1)

In this work, the DHP effect on a commercial ATF was measured in the frequency range from 125 Hz to 8 kHz through a series of specially designed experiments. The DHP effect was characterized by the decrease of the earplug NR when combined with the earmuff. First, the potential influence of several SB sound paths through the ATF to its earcanal (outer ear path), and originating from the earmuff headband and ATF tripod was identified by means of modifying the coupling conditions of the experimental setup. Second, the sound pressure level (SPL) under the earmuff was controlled with a tiny loudspeaker beneath the earcup in order to investigate the relative contributions of the “direct” AB path through the earplug outer surface and possible flanking SB paths involved in the system. Particularly, mechanical tests were conducted using an impact hammer and accelerometers to highlight the SB sound transmission through the earmuff comfort cushion with the aid of a lead cushion.

Contributions

This work is among the first to focus on the experimental analysis of the DHP effect on ATFs. Before carrying out the experiments, an analytical model was developed to support the investigation of the DHP effect which accounts for the SB transmission through the ATF. Despite a few simplifying assumptions as explained in Sec. 2.3.2, the model allows for a quick interpretation of the DHP effect on the ATF and contributes to a preliminary understanding of the related mechanisms. The measurements by modifying the system coupling conditions demonstrated the negligible influence of some SB paths involved, i.e., the vibration of the earmuff headband, sound transmission through the ATF or vibration transmission through the tripod. In addition, the measurements by controlling the SPL under the earmuff proved the insignificant contribution of the acoustical coupling between the earplug and earmuff to the DHP effect. This effect was confirmed to be associated with the SB transmission through the system induced by external acoustic stimulation which dominates over the AB transmission due to a low SPL at the earcanal entrance compared to the single earplug configuration. More specifically, measurement results suggested that the primary SB path responsible for the DHP effect corresponds to the sound transmitted from the earcup, through the earmuff cushion/ATF assembly and finally into the earcanal via the sound radiation of the earplug and/or earcanal lateral walls. Such a SB path involves both (i) the mechanical coupling between the earplug and earmuff through the ATF, and (ii) the vibration of earcanal walls which is similar to the fundamental mechanisms of the occlusion effect. This work also enabled to recognize essential components for adequately describing the vibroacoustic behavior of the system in numerical analysis, such as the earmuff cushion and its mechanical interaction with the ATF.

Limitations and perspectives

Even though mechanical tests were carried out to measure the transfer function between the acceleration on the aluminum plate (screwed onto the ATF) and force imposed on the earmuff headband to highlight the primary SB path responsible for the DHP effect mentioned above, such a sound path was identified in an indirect way by excluding the importance of other potential SB paths in the system. Future work could seek to demonstrate this SB path in a more straightforward manner, such as assessing the transfer function between the sound pressure in the earcanal and force imposed directly on the earcup.

In addition, SB sound transmission is supposed to depend on the constitution of the system (e.g., mechanical properties of the components involved and couplings between them). The DHP effect observed and main sound path identified in this work seem limited to the particular type of ATF used, and may be different from those on human subjects. Following the study presented in Chapter 2, a preliminary work has attempted to further characterize the influence of SB transmission by comparing the DHP effects measured on a commercial ATF and a human subject while wearing the same DHP (see Appx. IV). Particular efforts were made to adjust the earplug and earmuff positions on the ATF in order to obtain a single earplug NR and SPL under the earmuff (in the DHP configuration) similar to those captured on the subject. This made it possible to (i) assume a similar contribution of the AB path on both the ATF and human head, and (ii) thus attribute the observed differences in the DHP effect to the changes in the SB transmission. But the method may need to be revisited since adjusting the earplug and earmuff positions does not only modify the contribution of AB transmission but can also alter the fit between the earplug and earcanal walls, or between the earmuff and pinna simulator of the ATF (i.e., SB transmission). Prospectively, novel approaches could be used to further quantify the contribution of SB transmission, e.g., using active noise reduction earmuffs to eliminate the AB path's contribution. Future work is also required to better explain the differences between the DHP effects on the ATF and subject. Moreover, understanding the DHP effect from a purely experimental point of view can be difficult. Numerical modeling would allow for gaining more insight into the phenomenon as it has been done in Chapter 3.

6.2.2 Chapter 3: A finite element model to predict the double hearing protector effect on an in-house acoustic test fixture (article n^{o} 2)

This work is a continuation of the experimental investigation presented in Chapter 2 which mainly focused on the numerical analysis of the DHP effect on ATFs. In this work, a finite element (FE) model of a DHP/ATF system was proposed. Specially, a silicone cushion was used to replace the comfort cushion of the earmuff for better capturing its vibroacoustic behavior in the model. Moreover, an in-house ATF with a geometry simpler than a commercial one was adopted to more easily account for the SB sound transmission through the ATF. This also facilitated the fabrication of the corresponding setup for experimental validation. First, the FE model was validated in the frequency range from 100 Hz to 5 kHz through NR measurements of the single earmuff, single earplug and earplug in the DHP. Second, the FE model was exploited to simulate several configurations of the in-house ATF and calculate the power balances in the system in order to (i) quantify the contribution of each sound transmission path, and study the impacts of (ii) the artificial skin and (iii) the acoustic excitation on the ATF exterior boundaries.

Contributions

According to the literature, the FE model proposed in this work constitutes the only validated numerical model that can predict the DHP effect on the ATF in a relatively wide frequency range and extend current knowledge of the related sound transmission mechanisms. The simulation results confirmed the finding of Chapter 2 that the DHP effect on the ATF is indeed induced by the SB transmission through the system which dominates over the “direct” AB transmission. This effect tends to be negligible at the acoustical and mechanical resonances of the earmuff since the AB path dominates at these frequencies. More specifically, on the fully “rigid” ATF, the DHP effect was found to be significant between 450 Hz and 3.6 kHz due to the SB sound power transmitted into the earcanal cavity from its terminal surface. On a more realistic ATF with artificial skin parts, the vibration of earcanal lateral walls was proved to be responsible for the DHP effect between 300 Hz and 4 kHz. An indirect SB path contributing to the sound pressure in the earcanal cavity was identified which corresponds to the sound radiation of the earplug excited by the earcanal walls. This configuration also highlighted the importance of taking into account the skin for a more realistic prediction of DHP attenuation. In addition, the DHP effect on the fully “rigid” ATF was found to be affected by the acoustic excitation on its exterior boundaries, especially below 1 kHz and above 3 kHz. But such excitation did not show a significant influence when the skin was accounted for. The SB power injected into the ATF was demonstrated to originate mainly from the earmuff silicone cushion and/or ATF exterior boundaries depending on the materials, boundary conditions and frequency range studied.

Limitations and perspectives

In this work, several simplifications were made to the DHP/ATF system for easily capturing the physical mechanisms involved. These simplifications could influence the SB transmission through the ATF, and thus the DHP effect observed. They seem reasonable at an early stage of research but need to be improved in future work. First, the artificial skin parts were only taken into account for numerical tests and not included in the measurement setup. The simulation configuration with the skin was not experimentally validated. Second, the acoustic impedance produced by the ear simulator in the earcanal was not accounted for. This is not supposed to directly modify the SB transmission through the ATF but as mentioned in Sec. 3.5.3, the resistive part of the impedance may reduce the sound radiation of the earcanal terminal surface in certain configurations of the in-house ATF. Third, standardized ATFs are more or less constrained in practice, and cannot be assumed to be mechanically free (i.e., coupled to external air without mechanical constraints) as the in-house ATF. Future research is necessary to increase the degree of realism of the ATF by incorporating artificial skin parts (through silicone molding) as well as the ear simulator. Spring elements could be added to control the mechanical constraints on the ATF exterior boundaries. Additionally, the original comfort cushion of the earmuff needs to be considered instead of the silicone one to better represent the SB transmission through the former and its mechanical interaction with the ATF. This requires developing a detailed multi-domain cushion model to account for the respective vibroacoustic behaviors of its components (Boyer, 2015).

6.3 Modeling of the ear simulator for the prediction of hearing protector sound attenuation: contributions, limitations and perspectives

6.3.1 Chapter 4: A transfer matrix model of the IEC 60318-4 ear simulator: Application to the simulation of earplug insertion loss (article n° 3)

This work proposed a transfer matrix (TM) model of a commercial IEC 60318-4 ear simulator based on the geometric dimensions determined from computed tomography (CT) scan images. The thermo-viscous dissipation in the ear simulator was calculated using the low reduced frequency (LRF) approximation. First, the TM model was validated respectively (i) using a FE model of the scanned simulator at frequencies from 100 Hz to 20 kHz and (ii) through impedance measurements with a sound intensity probe from 100 Hz to 10 kHz. Second, an equivalent tympanic impedance (TI) was derived from the TM model with the help of the reduced impedance (RI) method. This equivalent TI was then applied as a terminal impedance boundary condition in the FE model of an occluded ATF earcanal to simulate the IL of a silicone earplug. The simulation result was compared to (i) the earplug IL calculated with the TI retrieved from the LPM of the ear simulator and (ii) experimental data on a commercial ATF.

Contributions

In this work, key geometric features of a standardized IEC 60318-4 ear simulator were identified and provided. An analytical model (i.e., TM model) was developed in a direct manner based on the assessed geometric dimensions to describe the input acoustic impedance of the simulator, and validated respectively through numerical and experimental approaches. Particularly, the uncertainty propagation of the simulator dimensions was taken into account using a Monte Carlo method. Compared to the classical LPM commonly used in published work, such an analytical model has the following advantages. First, it can more precisely represent the ear simulator impedance in its working frequency range up to 10 kHz, especially at frequencies above 3 kHz. Second, the LRF approximation has been shown to better capture the thermo-viscous effects in the narrow slits of the simulator. Additionally, the TM model proposed whose acoustic outputs are directly related to the geometric inputs makes it possible to easily perform parametric studies on different design features of the simulator. On the other hand, the TM model combined with the RI method allows to eliminate the acoustic impedance associated with the simulator main cavity, and to retrieve directly the equivalent TI at the eardrum position. From a mathematical point of view, the equivalent TI retrieved in this way is more rigorous compared to the conventional lumped TI model given in (Jønsson *et al.*, 2003, 2004). This also allows for the implementation of a more realistic earcanal ahead of the eardrum position in terms of geometry and material properties for the numerical simulation of earplug IL as it has been done in Chapter 5. Furthermore, the present work confirmed that it is valid up to 10 kHz to simulate the earplug IL in an ATF earcanal by considering the ear simulator as a cylindrical cavity terminated by an equivalent TI.

Limitations and perspectives

Considering the uncertainty propagation of ear simulator geometric dimensions based on the TM model, this work seems to be limited in several ways. First, the sizes of certain components in the simulator are not far from the resolution of the CT scanner, such as the thicknesses of the narrow slits. The geometric errors related to these components are larger than those for the others. Second, each dimension of interest was only measured three times. Future work needs to consider using a CT scanner of higher resolution and increasing the number of measurements on CT scan images for adequately covering the geometric uncertainties. Moreover, as mentioned in Sec. 4.6.1, the experimental validation of the TM model suffered from the diffraction of the sound intensity probe placed in front of the ear simulator. Future work could try to assess the simulator acoustic impedance with other measurement methods, such as using the reciprocity principle which enables the acoustic impedance of the simulator to be determined from electrical impedance measurements on two calibrated microphones (Brüel *et al.*, 1976; Bravo *et al.*, 2012).

6.3.2 Chapter 5: Influence of the inter-individual variability in the eardrum impedance on the earplug insertion loss

This work constitutes a complement of Chapter 4 which focused on further exploiting the TM model of the ear simulator in order to investigate the influence of the eardrum impedance variability on the earplug IL at frequencies from 100 Hz to 10 kHz. First, 1000 equivalent TI values representative of the published variability in the human eardrum impedance were determined through a Monte Carlo simulation by varying the simulator geometric dimensions in the TM model (combined with the RI method). Second, two representative sets of equivalent TI were selected among these values and applied as impedance boundary conditions in a FE model to simulate the corresponding ILs of a silicone earplug in a realistic-shaped earcanal surrounded by a skin layer.

Contributions

In general, the Monte Carlo simulation based on the TM model of the ear simulator was shown to capture the overall tendency of the measured human ear impedance in the literature, and cover a considerable part of its actual variability. The earplug IL simulation results revealed that the inter-individual variability in the eardrum impedance can induce non-negligible differences in the earplug attenuation in the frequency range of interest up to 10 kHz. To be specific, standardized ear simulators designed to reproduce an average acoustic impedance of the human ear did not prove adequate for earplug attenuation measurements. At frequencies below 1 kHz, a higher equivalent TI was found to cause a lower earplug IL. But at higher frequencies, no general IL tendency was detected from the equivalent TI probably due to a more complicated interaction between the earplug and eardrum impedance.

Limitations and perspectives

This work has some limitations. First, as mentioned in Sec. 5.1, the reference impedance data extracted from the literature are limited to specific panels of human subjects. The Monte Carlo simulation results generated to capture these data may tend to underestimate or overestimate the actual variability of the human ear impedance. More experimental impedance data are needed in order to represent a large majority of the population. Second, instead of the RI method for a simple cylindrical ATF earcanal, it would be ideal to retrieve the eardrum impedance variability directly from the impedance data measured in human earcanals based on the chain matrices of the earcanals which enable their real curvilinear shapes to be accounted for (Hudde, 1983; Larson *et al.*, 1993; Rodrigues *et al.*, 2015a). This however requires experimental measurements on a sufficiently large group of subjects and detailed geometric knowledge of their earcanals. Third, the earplug IL may also depend on the type of earplug or its insertion depth. Further numerical work should concentrate on investigating the influence of the eardrum impedance variability on the IL by varying the earplug type and insertion depth.

6.4 General conclusion

In the present thesis, two primary research topics concerning the vibroacoustic design features of ATFs have been addressed. On the one hand, the DHP effect on the ATF has been studied through experimental and numerical approaches in order to better understand the associated sound transmission mechanisms and improve the prediction of DHP attenuation. The results obtained will provide researchers in the related field with clues to achieve further protection in extreme noise exposure scenarios, such as by shielding the head (e.g., Berger *et al.*, 2003a) or controlling the vibration transmission through the earmuff comfort cushion. The developed FE model can constitute a useful computational tool for better evaluating the performance of DHPs by increasing the degree of realism of the ATF. Prospectively, this could be achieved using "anatomically-correct" human head FE models, such as that proposed by Xu and her colleagues (Xu *et al.*, 2019; Xu, Sgard, Carillo, Wagnac & De Guise, 2020), and the corresponding artificial head under development (Sgard *et al.*, 2018). They will allow for exhibiting more realistic SB sound transmission with essential anatomical features included (e.g., skull, skin and cartilage). In addition, this head model is of particular interest as it comes from a living human subject, which will enable to evaluate the realism of SB transmission mechanisms by direct comparisons with the DHP attenuation measurements on the same subject.

On the other hand, a novel analytical model of the IEC 60318-4 ear simulator has been proposed and used for investigating the potential influence of the eardrum impedance inter-individual variability on the earplug attenuation. From a technological point of view, the proposed model can serve as a base for designing artificial eardrum simulators with their input impedance representing directly the human eardrum impedance (i.e., without cylindrical cavities ahead of the eardrum position). These eardrum simulators will have the potential to (i) incorporate more realistic earcanals in terms of geometry and material properties, and (ii) take into account the diversity of the eardrum impedance with multiple designs.

Overall, the experimental methodology and numerical models presented in this work have been promising for investigating the ATF vibroacoustic features of interest, and in the long term, for ultimately improving the current design of ATFs for a more realistic characterization of hearing protector sound attenuation.

APPENDIX I

ACOUSTIC INDICATORS IN THE DOUBLE HEARING PROTECTOR ANALYTICAL MODEL

Based on the decoupled assumption, the NR of the DHP considering only the AB sound transmission through the hearing protectors (see Sec. 2.3) can be calculated as:

$$NR_{\mathrm{DHP}}^{\mathrm{AB}} = 10\log_{10}(p_{\mathrm{out}}^{\mathrm{DHP,\,AB}^2}) - 10\log_{10}(p_{\mathrm{in}}^{\mathrm{DHP,\,AB}^2}), \tag{A I-1}$$

where $p_{\mathrm{out}}^{\mathrm{DHP,AB}}$ and $p_{\mathrm{in}}^{\mathrm{DHP,AB}}$ denote the sound pressure outside in the vicinity of the earmuff ($\mathrm{MIC_{out}}$ in Fig. 2.1(b)) excited by the external sound field and that in the earcanal ($\mathrm{MIC_{in}}$) resulting from the AB transmission. The NR of the DHP when the SB paths alone (SB1 to SB4) are accounted for is expressed as:

$$NR_{\mathrm{DHP}}^{\mathrm{SB}} = 10\log_{10}(p_{\mathrm{out}}^{\mathrm{DHP,\,AB}^2}) - 10\log_{10}(p_{\mathrm{in}}^{\mathrm{DHP,\,SB}^2}), \tag{A I-2}$$

where $p_{\mathrm{in}}^{\mathrm{DHP,SB}}$ corresponds to the sound pressure in the earcanal resulting from the SB paths. The overall NR of the DHP when all the possible sound paths (AB and SB1 to SB4) are considered can be written as:

$$NR_{\mathrm{DHP}} = 10\log_{10}(p_{\mathrm{out}}^{\mathrm{DHP,\,AB}^2}) - 10\log_{10}(p_{\mathrm{in}}^{\mathrm{DHP,\,AB}^2} + p_{\mathrm{in}}^{\mathrm{DHP,\,SB}^2}). \tag{A I-3}$$

Similarly, the NR of the earplug in the DHP due to the AB path alone and that caused by both the AB and SB paths are respectively:

$$NR_{\mathrm{EP}}^{\mathrm{DHP,AB}} = 10\log_{10}(p_{\mathrm{mid}}^{\mathrm{DHP,\,AB}^2}) - 10\log_{10}(p_{\mathrm{in}}^{\mathrm{DHP,\,AB}^2}), \tag{A I-4}$$

$$NR_{\mathrm{EP}}^{\mathrm{DHP}} = 10\log_{10}(p_{\mathrm{mid}}^{\mathrm{DHP,\,AB}^2}) - 10\log_{10}(p_{\mathrm{in}}^{\mathrm{DHP,\,AB}^2} + p_{\mathrm{in}}^{\mathrm{DHP,\,SB}^2}). \tag{A I-5}$$

$p_{\mathrm{mid}}^{\mathrm{DHP,AB}}$ denotes the sound pressure under the earmuff ($\mathrm{MIC_{mid}}$) resulting from the AB transmission. In addition, the NR of the earmuff in the DHP (mainly the AB transmission is considered to be involved) is defined as:

$$NR_{\mathrm{EM}}^{\mathrm{DHP,AB}} = 10\log_{10}(p_{\mathrm{out}}^{\mathrm{DHP,\,AB}^2}) - 10\log_{10}(p_{\mathrm{mid}}^{\mathrm{DHP,\,AB}^2}). \tag{A I-6}$$

If the sound pressure generated by the loudspeaker under the earmuff p_{spk} which is incoherent with $p_{\mathrm{mid}}^{\mathrm{DHP,AB}}$ is accounted for and assuming that it does not contribute to the SB transmission (see Sec. 2.3.2), one has:

$$p_{\mathrm{in}}^{\mathrm{DHP,\,AB}^2} = \frac{p_{\mathrm{mid}}^{\mathrm{DHP,\,AB}^2} + p_{\mathrm{spk}}^2}{10^{NR_{\mathrm{EP}}^{\mathrm{DHP,\,AB}}/10}}. \tag{A I-7}$$

APPENDIX II

BACKGROUND NOISE COMPARED TO THE SOUND PRESSURE LEVELS IN THE EARCANAL OF CONFIGURATIONS 3.1 AND 4.1

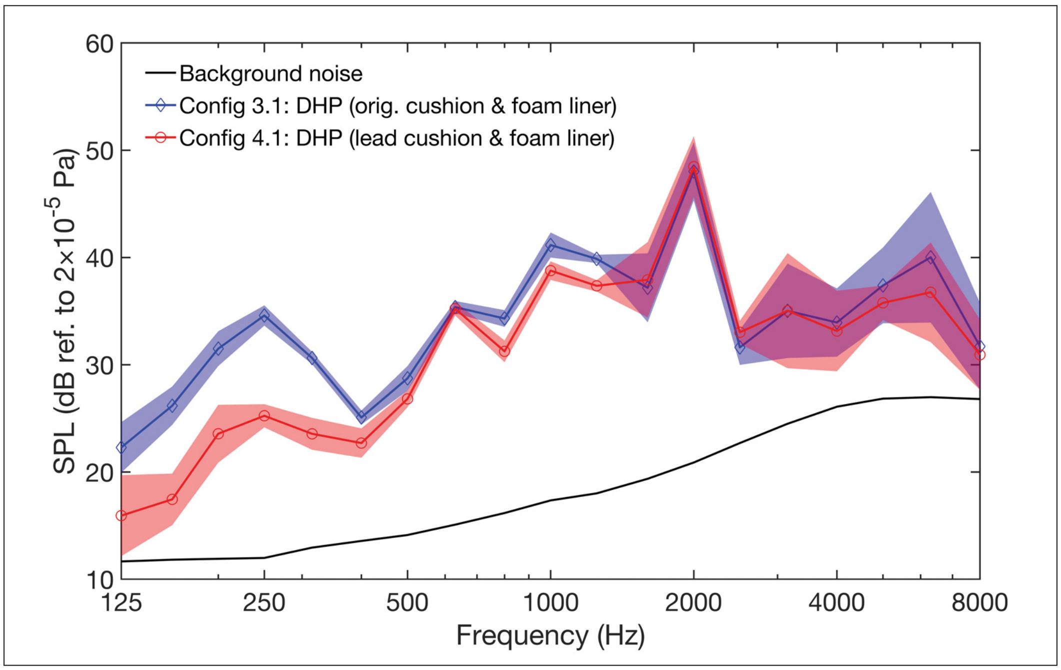

Figure-A II-1 Background noise (black) compared to the SPL measured in the earcanal excited by the external source alone: configuration 3.1 (blue diamonds), original cushion with foam liner; configuration 4.1 (red circles), lead cushion with foam liner. Results are displayed as "mean ± standard deviation"

APPENDIX III

EARPLUG NOISE REDUCTION MEASUREMENT RESULTS OF CONFIGURATIONS 2.2, 2.3 AND 2.4

Table-A III-1 Mean earplug NR and standard deviation (SD) values in dB of configurations 2.2, 2.3 and 2.4

Frequency (Hz)	Config 2.2		Config 2.3		Config 2.4	
	Mean	SD	Mean	SD	Mean	SD
125	50.3	0.1	50.9	0.4	50.7	0.1
160	50.8	0.3	49.8	0.3	50.3	0.6
200	51.0	0.2	50.1	0.7	51.4	1.8
250	50.5	0.2	49.9	0.3	51.5	1.9
315	48.9	0.4	47.7	0.2	49.1	1.5
400	42.1	0.3	41.2	0.8	41.6	1.1
500	34.1	0.2	33.6	0.4	36.0	0.7
630	24.7	0.1	25.6	0.6	27.8	0.8
800	19.7	0.3	19.3	0.3	21.4	0.2
1000	6.1	0.1	5.2	0.3	11.9	1.3
1250	2.9	0.1	2.9	0.2	8.4	4.4
1600	11.3	1.0	12.7	0.3	11.7	2.0
2000	9.0	0.7	9.5	0.0	9.5	2.2
2500	23.9	1.4	20.6	1.1	25.7	1.8
3150	23.9	2.0	24.2	2.7	28.1	1.8
4000	38.5	0.7	43.4	0.5	46.2	0.8
5000	36.5	0.6	36.2	0.8	41.0	0.5
6300	34.4	1.0	34.4	0.8	39.1	2.6
8000	39.2	0.5	38.2	0.1	40.7	0.9

APPENDIX IV

COMPARISON BETWEEN THE DOUBLE HEARING PROTECTOR EFFECTS ON AN ACOUSTIC TEST FIXTURE AND A HUMAN SUBJECT

Following the experimental analysis presented in Chapter 2, this section provides a preliminary work which attempts to further evaluate the influence of SB sound transmission by comparing the DHP effect (i.e., difference between the NRs of the earplug alone and in the DHP) measured on a commercial ATF to that assessed on a human subject under similar conditions.

1. Setup

The experimental setup is presented in Fig.-A IV-1. An earpiece equipped with a high-insulation Comply^{TM} Isolation T-400 eartip (Hearing Components, Inc., St. Paul, USA) is adopted (see Figs.-A IV-1(a) and IV-1(b)). Such an eartip is used (and referred to) as a foam earplug. The earpiece was designed by Bonnet and his colleagues (Bonnet, Nélisse & Voix, 2018; Bonnet, 2019) which allows an earplug insertion depth of approximately 8 mm. This device makes it possible to assess the earplug NR by simultaneously measuring the SPLs at the entrance of the occluded earcanal and at the earplug inner tip with two integrated miniature microphones. Similarly to the work presented in Chapter 2, a G.R.A.S. 45CB ATF and an EAR-MODEL-1000 earmuff are adopted as well (see Fig.-A IV-1(c)). A particular human subject who has a normal hearing also participates in the tests using the same hearing protectors (not presented in the figure). The system is excited acoustically by a pink noise with an overall level of about 107 dB(A) in a reverberant room (diffuse field).

2. Procedures

First, tests are carried out on the human subject. The subject is seated on a chair with each of his ear occluded by an earpiece with a foam earplug. The NR of the single earplug is measured with the earpiece. The earmuff is then worn over the subject's head. The SPL under the earmuff, and earplug NR in the DHP are measured. Each configuration is repeated three times by removing

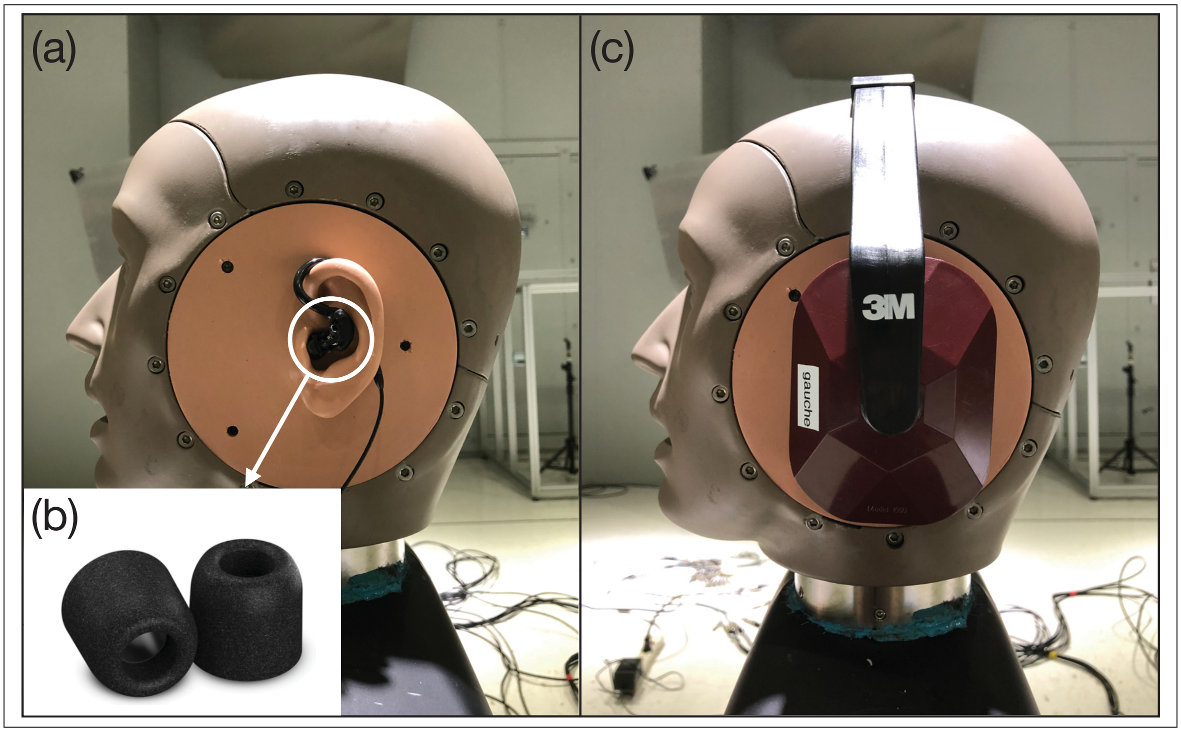

Figure-A IV-1 Experimental setup: (a) G.R.A.S. 45CB ATF wearing a dual-microphone earpiece with (b) a foam eartip; (c) ATF wearing the earpiece combined with a commercial earmuff

and repositioning the hearing protectors to account for the associated variability. The noise level and exposure time selected comply with the legislation in Canada (CSA, 2014), and the protocol was approved by the Research Ethics Committee at École de Technologie Supérieure.

Second, the same measurements are repeated on the ATF. As the NR of the single earplug measured on the ATF is much higher than that on the human subject, a number of tests are conducted by varying the insertion depth of the earpiece in order to obtain a single earplug NR close to that assessed on the subject. Afterwards, the earpiece together with the earplug stays still, and the earmuff is placed on the ATF. The relative positioning between the earmuff and pinna simulator of the ATF is adjusted so that the SPL under the earmuff also resembles that for the subject. The earplug NR in the DHP is then measured.

The adjustment of the earplug and earmuff positions allows for assuming a similar contribution of the AB path on both the ATF and human subject. The changes in the SB transmission (through $NR_{\mathrm{DHP}}^{\mathrm{SB}}$, see Eqs. (2.2) and (2.3) in Chapter 2) can therefore be studied by comparing the DHP effects (i.e., ΔNR_{DHP}) obtained in the two steps above.

3. Results

The measurement results are shown in third octave bands from 125 Hz to 8 kHz in Fig.-A IV-2. The results for the subject are displayed with mean values and standard deviations for the three repetitions of each configuration. The NRs of the earplug alone and in the DHP configuration are illustrated in Fig.-A IV-2(a) using the blue zone with diamonds and red zone with circles. The SPL under the earmuff is presented in Fig.-A IV-2(b) with the red zone with circles. In the case of the ATF, only the results of one test are presented for which the single earplug NR (see purple curve in Fig.-A IV-2(a)) and SPL under the earmuff (see dashed green curve in Fig.-A IV-2(b)) are relatively close to those captured on the subject. The corresponding earplug NR in the DHP configuration is displayed with the dashed green curve in Fig.-A IV-2(a).

Figure-A IV-2 shows that it is difficult to closely reproduce the single earplug NR and SPL under the earmuff obtained on the subject over the entire frequency range by simply adjusting the positions of the earplug and earmuff on the ATF. But as expected, at frequencies between about 125 Hz and 2 kHz where these two indicators are similar on the ATF and subject, the comparison between the earplug NRs in the DHP configuration in Fig.-A IV-2(a) (red zone with circles vs. dashed green curve) somewhat indicates different contributions of the SB transmission through the ATF and human head. Additionally, from 3 kHz to 5 kHz where the SPLs under the earmuff are similar for the ATF and subject, the DHP effect on the ATF is found to be higher than that on the subject (i.e., compared to the subject, the difference between the single earplug NR and earplug NR in the DHP configuration is higher for the ATF). This seems to suggest that the contribution of the SB transmission through the ATF is more important in this frequency range, which remains to be further investigated.

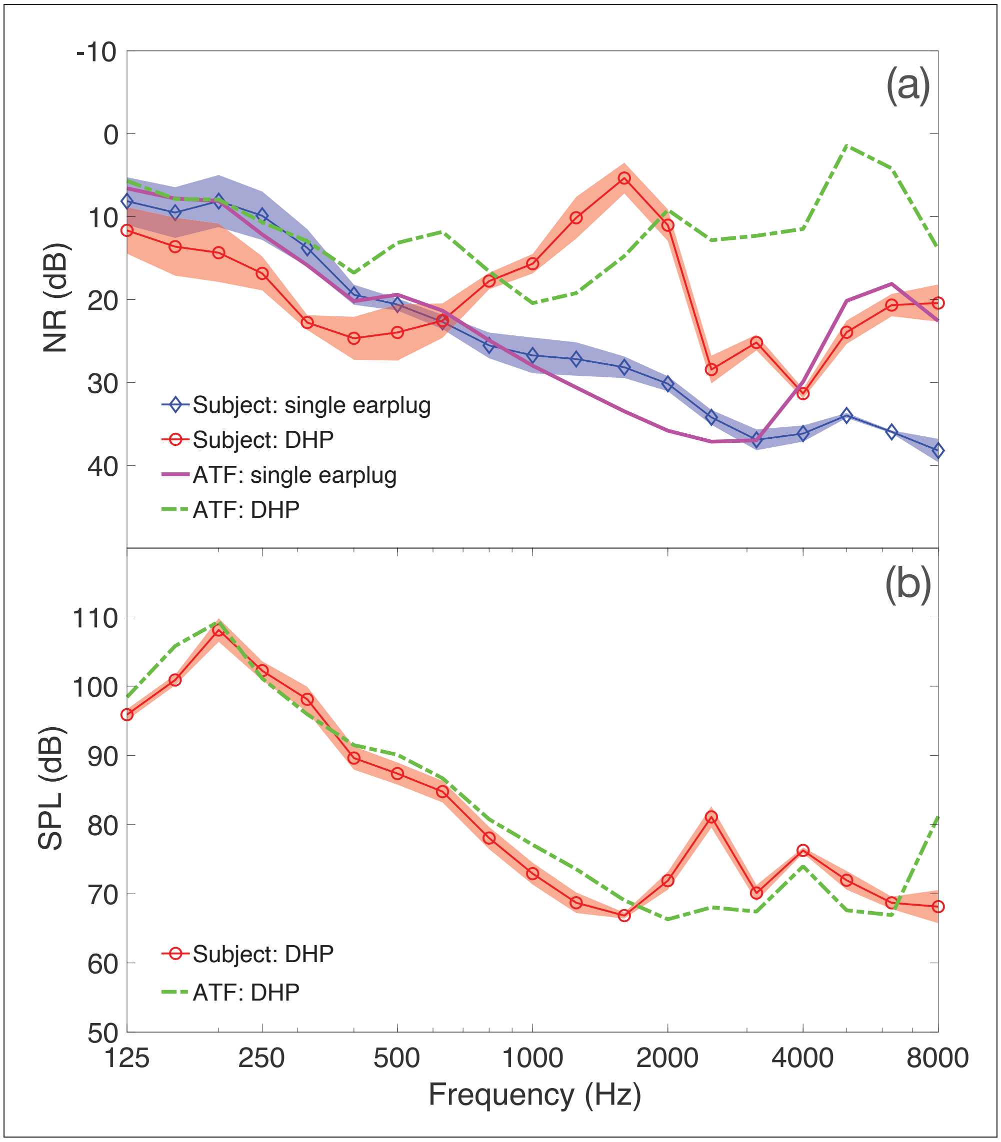

Figure-A IV-2 (a) Earplug NR in the DHP configuration and (b) SPL under the earmuff measured on the human subject (red circles) and ATF (dashed green). NRs of the single earplug measured on the human subject (blue diamonds) and ATF (purple) are presented for comparison. Results for the subject are displayed as “mean ± standard deviation”

APPENDIX V

SIMULATIONS USING ATF#3 AND ATF#4

1. Simulation configurations

ATF#3 and ATF#4 are similar to ATF#1 and ATF#2 respectively but all the exterior boundaries of the ATF outside the earmuff are considered to be decoupled from the external air domain (see Fig.-A V-1). Note that for the simulations with the single earplug, the decoupled boundaries as shown in the figure remain the same.

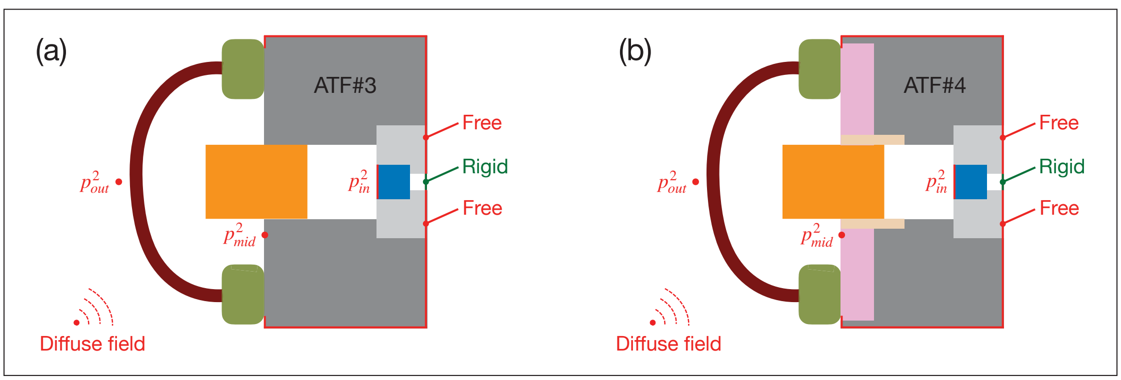

Figure-A V-1 Schematic representation of the DHP worn on (a) fully "rigid" ATF#3 and (b) ATF#4 with artificial skin portions (cross-section view). Exterior boundaries of ATF#3 and ATF#4 outside the earmuff are decoupled from the external air domain

2. Earplug noise reductions

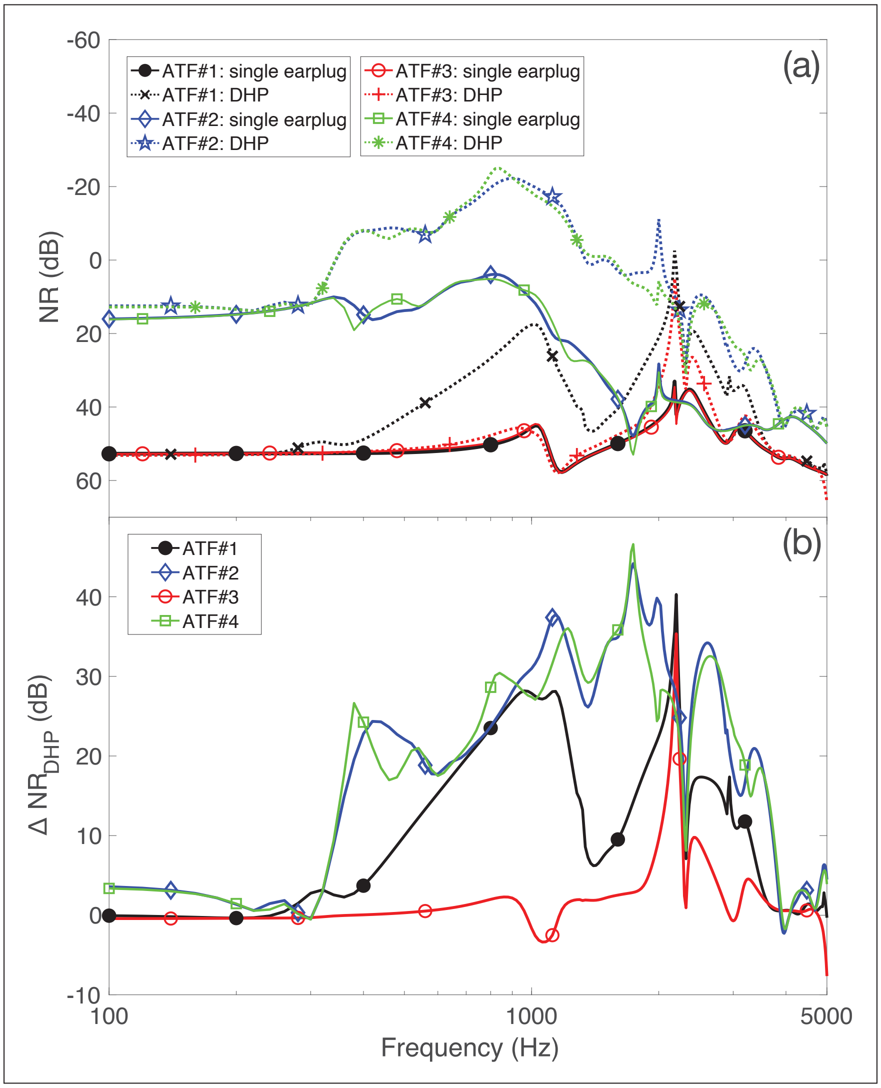

Figure-A V-2 Simulation results of (a) earplug NRs: results of the single earplug on ATF#1 – ATF#4 corresponding to black dots, blue diamonds, red circles and green squares, and results of the earplug in the DHP on ATF#1 – ATF#4 corresponding to dotted black crosses, dotted blue pentagrams, dotted red plus signs and dotted green asterisks; (b) ΔNR_{DHP}: results on ATF#1 – ATF#4 corresponding to black dots, blue diamonds, red circles and green squares

3. Power balances

3.1 ATF#3

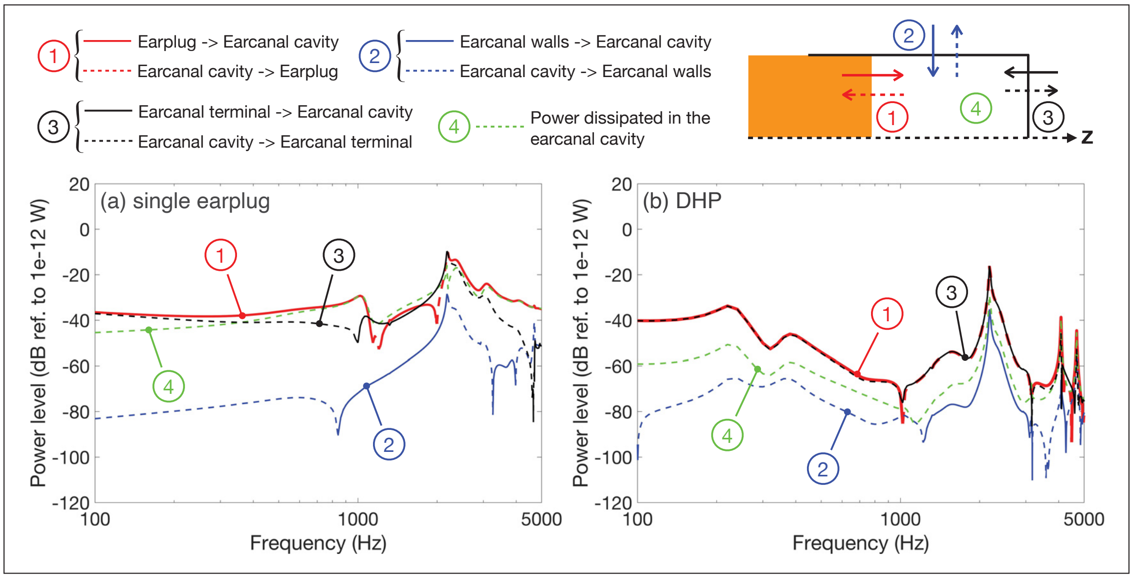

Figure-A V-3 Power balances in the earcanal cavity of ATF#3 for (a) single earplug configuration and (b) DHP configuration: power spectra levels exchanged at the earplug/earcanal cavity interface (red); exchanged at the earcanal lateral walls (blue); exchanged at the earcanal terminal surface (black); dissipated in the earcanal cavity (green). Numbers 1 – 4 correspond to the associated geometric zones where the powers are calculated. Solid line: power flowing into the earcanal cavity; dashed line: power flowing out of (or dissipated in) the earcanal cavity

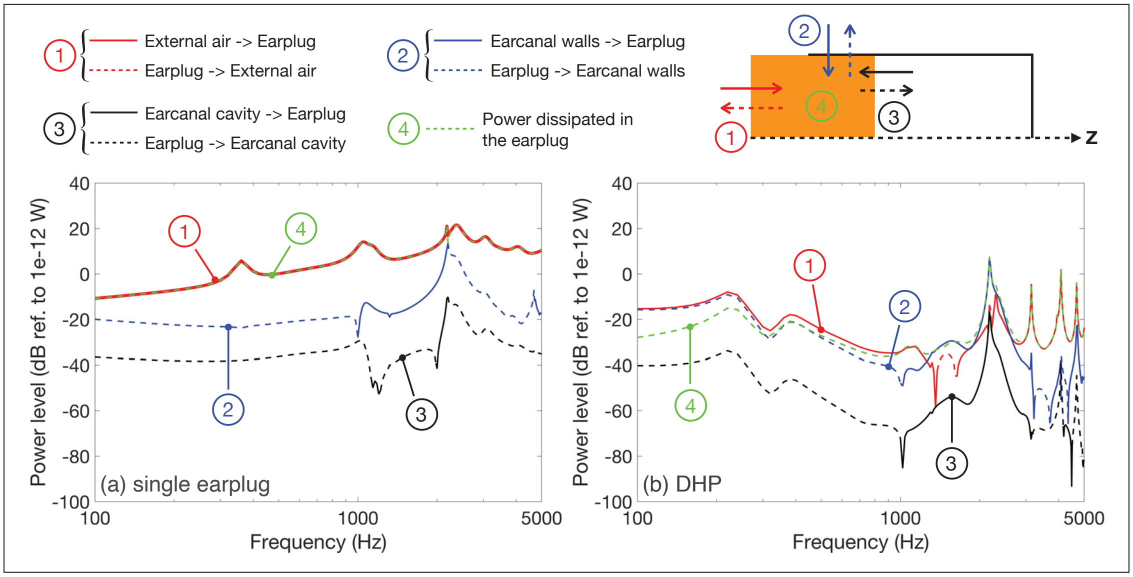

Figure-A V-4 Power balances in the earplug in ATF#3 for (a) single earplug configuration and (b) DHP configuration: power spectra levels exchanged at the earplug outer surface (red); exchanged at the earplug/earcanal walls interface (blue); exchanged at the earplug/earcanal cavity interface (black); dissipated in the earplug (green). Numbers 1 – 4 correspond to the associated geometric zones where the powers are calculated. Solid line: power flowing into the earplug; dashed line: power flowing out of (or dissipated in) the earplug

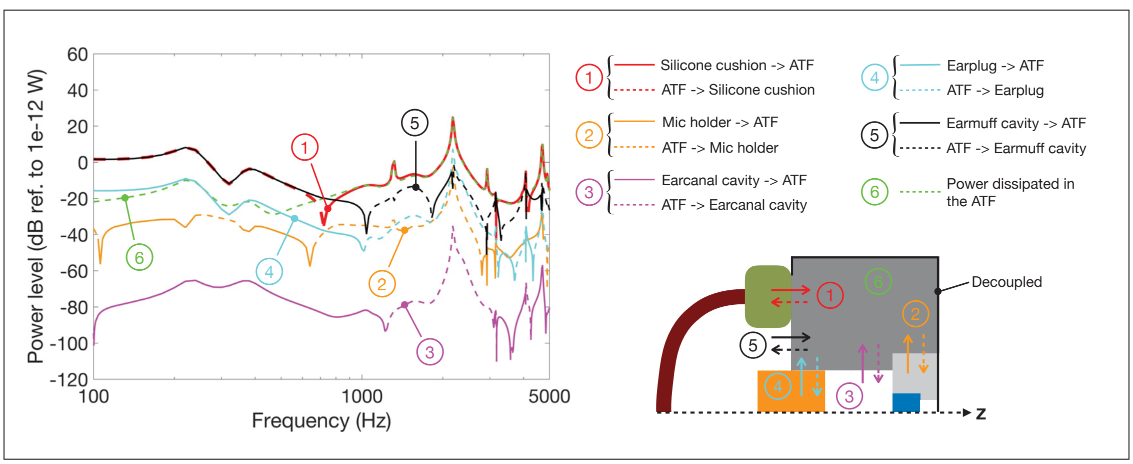

Figure-A V-5 Power balance in ATF#3 for the DHP configuration: power spectra levels exchanged at the silicone cushion/ATF interface (red); exchanged at the microphone holder/ATF interface (orange); exchanged at the earcanal lateral walls (purple); exchanged at the earplug/earcanal walls interface (cyan); exchanged at the ATF boundaries under the earmuff (black); dissipated in the ATF (green). Numbers 1 – 6 correspond to the associated geometric zones where the powers are calculated. Solid line: power flowing into the ATF; dashed line: power flowing out of (or dissipated in) the ATF

3.2 ATF#4

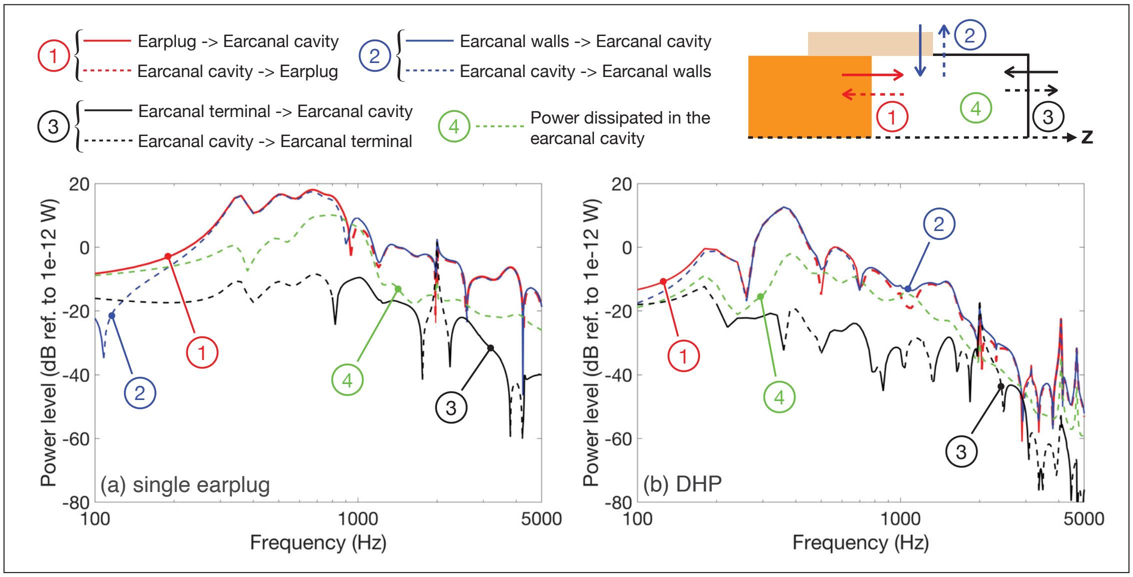

Figure-A V-6 Power balances in the earcanal cavity of ATF#4 for (a) single earplug configuration and (b) DHP configuration: power spectra levels exchanged at the earplug/earcanal cavity interface (red); exchanged at the earcanal lateral walls (blue); exchanged at the earcanal terminal surface (black); dissipated in the earcanal cavity (green). Numbers 1 – 4 correspond to the associated geometric zones where the powers are calculated. Solid line: power flowing into the earcanal cavity; dashed line: power flowing out of (or dissipated in) the earcanal cavity

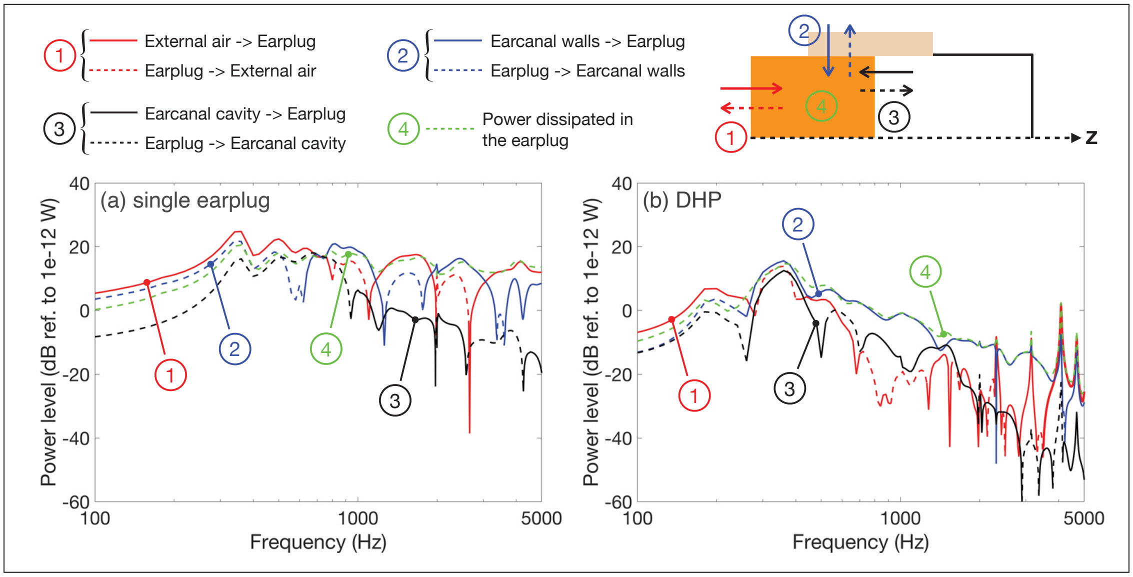

Figure-A V-7 Power balances in the earplug in ATF#4 for (a) single earplug configuration and (b) DHP configuration: power spectra levels exchanged at the earplug outer surface (red); exchanged at the earplug/earcanal walls interface (blue); exchanged at the earplug/earcanal cavity interface (black); dissipated in the earplug (green). Numbers 1 – 4 correspond to the associated geometric zones where the powers are calculated. Solid line: power flowing into the earplug; dashed line: power flowing out of (or dissipated in) the earplug

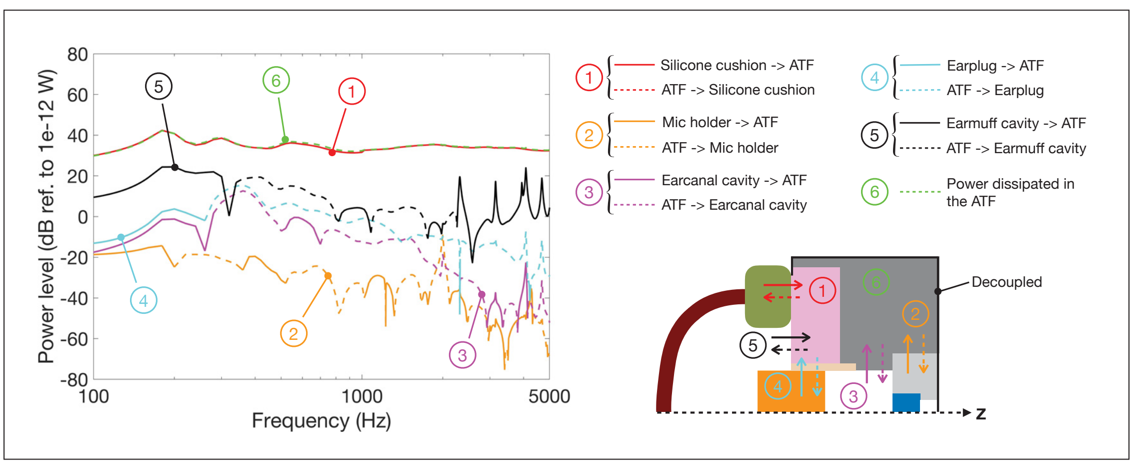

Figure-A V-8 Power balance in ATF#4 for the DHP configuration: power spectra levels exchanged at the silicone cushion/ATF interface (red); exchanged at the microphone holder/ATF interface (orange); exchanged at the earcanal lateral walls (purple); exchanged at the earplug/earcanal walls interface (cyan); exchanged at the ATF boundaries under the earmuff (black); dissipated in the ATF (green). Numbers 1 – 6 correspond to the associated geometric zones where the powers are calculated. Solid line: power flowing into the ATF; dashed line: power flowing out of (or dissipated in) the ATF

APPENDIX VI

YOUNG'S MODULUS AND LOSS FACTOR OF THE SILICONE CUSHION

The fractional derivative Zener model is defined in Eq. (A VI-1). In this model, $M(f)$ denotes the complex-valued stiffness, M_0 denotes the static stiffness, M_∞ is the high frequency limit of the stiffness, α is an exponent ($0 < \alpha < 1$) and t_r refers to a relaxation time. The model parameters obtained by curve fitting the QMA data are given in Table-A VI-1. The frequency dependent Young's modulus and loss factor of the silicone cushion are calculated respectively by $E(f) = \Re(M(f))$ and $\eta(f) = \Im(M(f))/\Re(M(f))$, and are presented in Fig.-A VI-1.

$$M(f) = \frac{M_0 + M_\infty (\mathrm{j}2\pi f t_\mathrm{r})^\alpha}{1 + (\mathrm{j}2\pi f t_\mathrm{r})^\alpha}. \tag{A VI-1}$$

Table-A VI-1 Mechanical properties of the silicone cushion (fractional derivative Zener model)

α (1)	**M_0 (Pa)**	**M_∞ (Pa)**	**t_r (s)**
0.29068	101469	958471	9.89e^{-7}

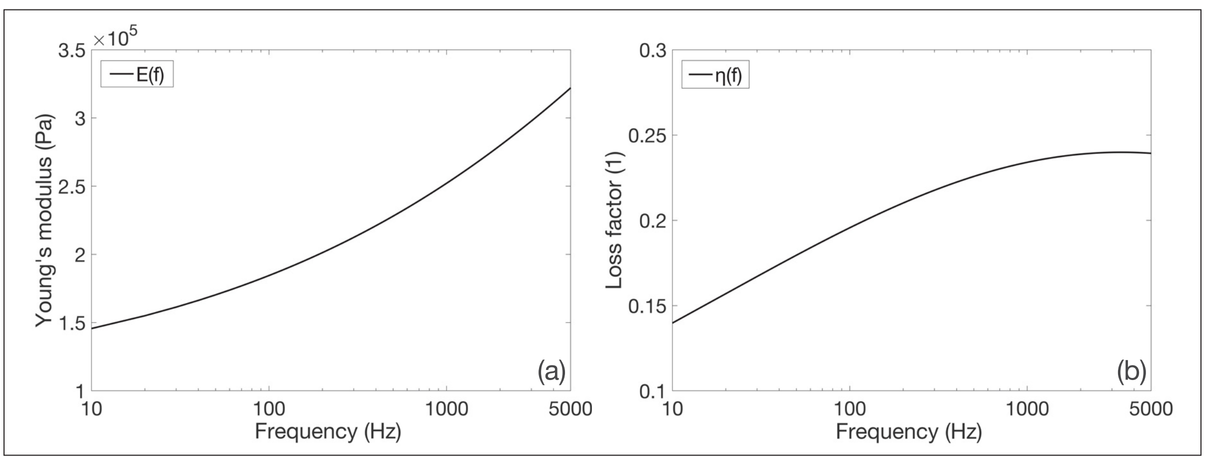

Figure-A VI-1 (a) Young's modulus and (b) loss factor of the silicone cushion

APPENDIX VII

INPUT IMPEDANCE OF THE HELMHOLTZ RESONATORS

1. Input impedance of the first Helmholtz resonator

$$Z_{\mathrm{HR},2} = Z_{\mathrm{slit},2} + Z_{\mathrm{cav},2}, \tag{A VII-1}$$

where $Z_{\mathrm{slit},2}$ and $Z_{\mathrm{cav},2}$ denote the impedance of the rectangular slit and the first side cavity. The former can be derived from:

$$Z_{\mathrm{slit},2} = \mathrm{j}Z_{l,2} \tan(k_{l,2}(a_2 + 2\Delta l_2)), \tag{A VII-2}$$

where $k_{l,2}$ and $Z_{l,2}$ are the complex wavenumber and characteristic impedance in the LRF model of the rectangular slit which depend on the mean values of the corresponding thermal and viscous fields $K_{h,2}$, $K_{v,2}$ and the modified mean thermal field $K'_{h,2}$ (Kampinga, 2010).

$$k_{l,2}^2 = k_0^2 \frac{K'_{h,2}}{K_{v,2}}, \quad Z_{l,2}^2 = \frac{(\rho_0 c_0)^2}{S_{\mathrm{slit},2}^2 K'_{h,2} K_{v,2}}, \tag{A VII-3}$$

$$K'_{h,2} = \gamma - (\gamma - 1) K_{h,2}, \tag{A VII-4}$$

$$K_{h(v),2} = 1 - \frac{\tan(k_{h(v)} h_2/2)}{k_{h(v)} h_2/2}. \tag{A VII-5}$$

k_h and k_v in the equation above denote the thermo-viscous wavenumbers which are associated with the thermal and viscous characteristic lengths $l_h = \lambda/(\rho_0 c_0 C_p)$ and $l'_v = \mu/(\rho_0 c_0)$ (see Table 4.2 for parameters of the thermo-viscous fluid).

$$k_h = \frac{1-\mathrm{j}}{\sqrt{2}}\sqrt{k_0/l_h}, \quad k_v = \frac{1-\mathrm{j}}{\sqrt{2}}\sqrt{k_0/l'_v}. \tag{A VII-6}$$

When calculating the total impedance of the IEC 60318-4 simulator, end corrections should be added to the actual lengths of the narrow slits to account for the radiation impedance at the corresponding locations. Thus, the end correction for a baffled rectangular piston according to (Mechel, 2008) is adopted:

$$\frac{\Delta l_2}{h_2} = \frac{1}{3\pi}\left[\beta_2 + \frac{1-\varepsilon_2^{3/2}}{\beta_2^2}\right] + \frac{1}{\pi}\left[\frac{1}{\beta_2}\ln\left(\beta_2 + \sqrt{\varepsilon_2}\right) + \ln\left(\frac{1}{\beta_2}\left(1+\sqrt{\varepsilon_2}\right)\right)\right], \qquad \text{(A VII-7)}$$

where $\varepsilon_2 = 1 + \beta_2^2$ and $\beta_2 = h_2/b_2$ is the ratio of the thickness of the narrow slit over the width.

$$Z_{\text{cav},2} = \frac{\mathrm{j}\rho_0 c_0\left[B_{\text{s},2}J_0(k_0 r_2) - Y_0(k_0 r_2)\right]}{S_{\text{cav},2}\left[B_{\text{s},2}J_1(k_0 r_2) - Y_1(k_0 r_2)\right]}, \qquad \text{(A VII-8)}$$

in which $S_{\text{cav},2}$ is the cross-section area of the first side cavity (Rodrigues *et al.*, 2008). J_0, J_1 and Y_0, Y_1 are Bessel functions of the first and second kind.

$$B_{\text{s},2} = \frac{Y_1(k_0 R_2)}{J_1(k_0 R_2)}. \qquad \text{(A VII-9)}$$

2. Input impedance of the second Helmholtz resonator

$$Z_{\text{HR},4} = Z_{\text{slit},4} + Z_{\text{cav},4}, \qquad \text{(A VII-10)}$$

where $Z_{\text{slit},4}$ and $Z_{\text{cav},4}$ denote the impedance of the annular slit and the second side cavity. $Z_{\text{slit},4}$ can be determined (Rodrigues *et al.*, 2008) by:

$$Z_{\text{slit},4} = \frac{\mathrm{j}Z_{l,4}\left[A_\text{s}J_0(k_{l,4}R_0^{\text{in}}) - Y_0(k_{l,4}R_0^{\text{in}})\right]}{A_\text{s}J_1(k_{l,4}R_0^{\text{in}}) - Y_1(k_{l,4}R_0^{\text{in}})}, \qquad \text{(A VII-11)}$$

$$A_\text{s} = \frac{Y_0(k_{l,4}r_4^{\text{out}})}{J_0(k_{l,4}r_4^{\text{out}})}, \qquad \text{(A VII-12)}$$

with $R_0^{\text{in}} = R_0 - \Delta l_{4,\text{in}}$ and $r_4^{\text{out}} = r_4 + \Delta l_{4,\text{out}}$. $\Delta l_{4,\text{in}}$ and $\Delta l_{4,\text{out}}$ denote respectively the end corrections added to the inner and outer radii of the annular slit which depend on its inner and outer perimeters as the equivalent widths (see Eq. (A VII-7)).

$$k_{l,4}^2 = k_0^2\frac{K'_{h,4}}{K_{v,4}}, \quad Z_{l,4}^2 = \frac{(\rho_0 c_0)^2}{S_{\text{slit},4}^2 K'_{h,4}K_{v,4}}. \qquad \text{(A VII-13)}$$

$k_{l,4}$ and $Z_{l,4}$ are the LRF wavenumber and impedance in the annular slit related to the corresponding thermal and viscous fields $K_{h,4}$, $K_{v,4}$ and $K'_{h,4}$ (Kampinga, 2010).

$$K'_{h,4} = \gamma - (\gamma - 1)K_{h,4}, \tag{A VII-14}$$

$$K_{h(v),4} = 1 - \frac{\tan(k_{h(v)}h_4/2)}{k_{h(v)}h_4/2}, \tag{A VII-15}$$

$$Z_{\mathrm{cav},4} = \frac{\mathrm{j}\rho_0 c_0 \left[B_{\mathrm{s},4}J_0(k_0 r_4) - Y_0(k_0 r_4)\right]}{S_{\mathrm{cav},4}\left[B_{\mathrm{s},4}J_1(k_0 r_4) - Y_1(k_0 r_4)\right]}. \tag{A VII-16}$$

$S_{\mathrm{cav},4}$ in Eq. (A VII-16) is the cross-section area of the second side cavity.

$$B_{\mathrm{s},4} = \frac{Y_1(k_0 R_4)}{J_1(k_0 R_4)}. \tag{A VII-17}$$

BIBLIOGRAPHY

Abel, S. M. & Armstrong, N. M. (1992). The combined sound attenuation of earplugs and earmuffs. *Applied Acoustics*, 36(1), 19–30.

Abel, S. M. & Odell, P. (2006). Sound attenuation from earmuffs and earplugs in combination: maximum benefits vs. missed information. *Aviation, Space and Environmental Medicine*, 77(9), 899–904.

ANSI. (2014). *American National Standard for an Occluded Ear Simulator*. ANSI/ASA S3.25-2009 (R2014). Washington D.C., USA: American National Standards Institute.

ANSI. (2016). *Methods for Measuring the Real-Ear Attenuation of Hearing Protectors*. ANSI/ASA S12.6-2016. Washington D.C., USA: American National Standards Institute.

ANSI. (2018). *American National Standard Specification for a Manikin for Simulated in-situ Airborne Acoustic Measurements*. ANSI/ASA S3.36-2012 (R2018). Washington D.C., USA: American National Standards Institute.

ANSI. (2020). *Methods for the Measurement of Insertion Loss of Hearing Protection Devices in Continuous or Impulsive Noise Using Microphone-in-Real-Ear or Acoustic Test Fixture Procedures*. ANSI/ASA S12.42-2020. Washington D.C., USA: American National Standards Institute.

Atalla, N. & Sgard, F. (2015). *Finite Element and Boundary Methods in Structural Acoustics and Vibration*. Boca Raton, USA: CRC Press.

Bech, B. (2007). *Variables affecting the real ear to coupler difference*. (Master's thesis, Technical University of Denmark, DTU, DK-2800 Kgs. Lyngby, Denmark).

Behar, A. (1991). Sound attenuation from combinations of earplugs and earmuffs. *Applied Acoustics*, 32(2), 149–158.

Behar, A. & Kunov, H. (1999). Insertion loss from using double protection. *Applied Acoustics*, 57(4), 375–385.

Benacchio, S., Doutres, O., Le Troter, A., Varoquaux, A., Wagnac, E., Callot, V. & Sgard, F. (2018). Estimation of the ear canal displacement field due to in-ear device insertion using a registration method on a human-like artificial ear. *Hearing Research*, 365, 16–27.

Benacchio, S., Luan, Y., Sgard, F. & Doutres, O. (2021). *Design of an acoustic eardrum simulator dedicated to sound attenuation measurements of earplugs: Effect of tympanic impedance inter-individual variability*. Unpublished manuscript, École de Technologie Supérieure, Montreal, Canada.

Berger, E. H. (1983). Laboratory attenuation of earmuffs and earplugs both singly and in combination. *American Industrial Hygiene Association Journal*, 44(5), 321–329.

Berger, E. H. (1986). Methods of measuring the attenuation of hearing protection devices. *The Journal of the Acoustical Society of America*, 79(6), 1655–1687.

Berger, E. H. & Kerivan, J. E. (1983). Influence of physiological noise and the occlusion effect on the measurement of real-ear attenuation at threshold. *The Journal of the Acoustical Society of America*, 74(1), 81–94.

Berger, E. H. & Voix, J. (2019). Hearing protection devices. In *The Noise Manual* (ed. 6). American Industrial Hygiene Association (AIHA).

Berger, E. H., Kieper, R. W. & Gauger, D. (2003a). Hearing protection: surpassing the limits to attenuation imposed by the bone-conduction pathways. *The Journal of the Acoustical Society of America*, 114(4), 1955–1967.

Berger, E. H., Royster, L. H., Royster, J. D., Driscoll, D. P. & Layne, M. (2003b). *The Noise Manual* (ed. 5). American Industrial Hygiene Association (AIHA).

Berger, E. H. (2005). Preferred methods for measuring hearing protector attenuation. *Proceedings of the 34th International Congress on Noise Control Engineering (InterNoise 2005)*, pp. 4432–4441.

Bériot, H. & Gabard, G. (2019). Anisotropic adaptivity of the p-FEM for time-harmonic acoustic wave propagation. *Journal of Computational Physics*, 378, 234–256.

Blackstock, D. T. (2000). *Fundamentals of Physical Acoustics*. New York, USA: John Wiley & Sons.

Bockstael, A., de Greve, B., Van Renterghem, T., Botteldooren, D., D'Haenens, W., Keppler, H., Maes, L., Philips, B., Swinnen, F. & Vinck, B. (2008). Verifying the attenuation of earplugs in situ: Method validation using artificial head and numerical simulations. *The Journal of the Acoustical Society of America*, 124(2), 973–981.

Bonnet, F. (2019). *Méthode de mesure individuelle de l'exposition sonore effective intra-auriculaire en milieu de travail [Personal dosimetry method to measure the effective in-ear noise exposure in the workplace].* (Ph.D. thesis, École de Technologie Supérieure, Montreal, Canada).

Bonnet, F., Nélisse, H. & Voix, J. (2018). Effects of ear canal occlusion on hearing sensitivity: A loudness experiment. *The Journal of the Acoustical Society of America*, 143(6), 3574–3582.

Boyer, S., Doutres, O., Sgard, F., Laville, F. & Boutin, J. (2014). Objective assessment of the sound paths through earmuff components. *Applied Acoustics*, 83, 76–85.

Boyer, S., Doutres, O., Sgard, F., Laville, F. & Boutin, J. (2015). Low frequency finite element models of the acoustical behavior of earmuffs. *The Journal of the Acoustical Society of America*, 137(5), 2602–2613.

Boyer, S. (2015). *Étude de la transmission sonore à travers un protecteur de type "coquilles": modélisation numérique et validation expérimentale [Study of the sound transmission through earmuffs: numerical modeling and experimental validation].* (Ph.D. thesis, École de Technologie Supérieure, Montreal, Canada).

Bravo, A., Barham, R., Ruiz, M., López, J. M., De Arcas, G. & Recuero, M. (2008). A new 3D finite element model of the IEC 60318-1 artificial ear. *Metrologia*, 45(4), 448–458.

Bravo, A., Barham, R., Ruiz, M., López, J. M., De Arcas, G. & Alonso, J. (2012). A new 3D finite element model of the IEC 60318-1 artificial ear: II. Experimental and numerical validation. *Metrologia*, 49(6), 785–802.

Brüel, P. V., Frederiksen, E., Mathiasen, H., Rasmussen, G. & Sigh, E. (1976). *Impedance of real and artificial ears - Part I: Investigations of a new insert earphone coupler* (Report n°bn0221). Brüel & Kjær. Retrieved from: https://www.bksv.com/media/doc/bn0221.pdf.

Bruneau, A. M., Bruneau, M., Herzog, P. & Kergomard, J. (1987). Boundary layer attenuation of higher order modes in waveguides. *Journal of Sound and Vibration*, 119(1), 15–27.

Bruneau, M., Herzog, P., Kergomard, J. & Polack, J. D. (1989). General formulation of the dispersion equation in bounded visco-thermal fluid, and application to some simple geometries. *Wave Motion*, 11(5), 441–451.

Byrne, D. & Murphy, W. J. (2016). *Double hearing protection: 5 dB or not to be*. Communication presented in Annual Conference of National Hearing Conservation Association (NHCA), San Diego, USA. doi: 10.13140/RG.2.1.4713.2569.

Carillo, K., Sgard, F. & Doutres, O. (2018). Numerical study of the broadband vibro-acoustic response of an earmuff. *Applied Acoustics*, 134, 25–33.

Chaigne, A. (2001). *Ondes acoustiques [Acoustic waves]*. Paris, France: Édition de l'École polytechnique.

Clavier, O. H., Norris, J. A., Wilbur, J. C., Cragin, K. J., Dietz, A. J., Wismer, M. G. & O'Brien, W. D. (2010a). Experimental validation of a computational model of bone-conducted sound transmission. *Hearing Research*, 1(263), 243–244.

Clavier, O. H., Wismer, M. G., Wilbur, J. C., Dietz, A. J. & O'Brien, W. D. (2010b). Development and validation of a computational model of bone-conducted sound transmission for improved hearing protection design. *Journal of the Acoustical Society of America*, 127(3), 1986–1986.

COMSOL. (2017). COMSOL Multiphysics® tutorial (Version 5.3a) [Software]. Generic 711 coupler - An occluded ear-canal simulator. Retrieved from: https://www.comsol.com/model/generic-711-coupler-8212-an-occluded-ear-canal-simulator-12227.

CSA. (2014). *Hearing protection devices: performance, selection, care and use*. CSA Z94.2-14. Mississauga, Canada: Canadian Standards Association.

Damongeot, A., Lataye, R. & Kusy, A. (1989). An empirical formula for predicting the attenuation given by double hearing protection (earplugs and earmuffs). *Applied Acoustics*, 28(3), 169–175.

Dancer, A., Lataye, R. & Damongeot, A. (1988). *Intérêt de la double protection acoustique [Interest of double acoustic protection]* (Report n°RT 503/88). St. Louis, France: French-German Research Institute of Saint-Louis.

Darkner, S., Sommer, S., Schuhmacher, A., Ingerslev, H., Baandrup, A. O., Thomsen, C. & Jønsson, S. (2018). *An Average of the Human Ear Canal: Recovering Acoustic Properties with Shape Analysis*. Cornell Univ. Libr. Retrieved from: https://arxiv.org/pdf/1811.03848.pdf.

Du, Y., Homma, K. & Saunders, W. R. (2008). Noise attenuation performance of deep-insert custom earplugs under single and double hearing protection. *Noise Control Engineering Journal*, 56(3), 183–202.

EPA. (1979). *Noise Labeling Requirements for Hearing Protectors*. Federal Register 44 (190). Washington D.C., USA: Environmental Protection Agency.

Farmer-Fedor, B. L. & Rabbitt, R. D. (2002). Acoustic intensity, impedance and reflection coefficient in the human ear canal. *The Journal of the Acoustical Society of America*, 112(2), 600–620.

Gallagher, H. L., Bjorn, V. S. & McKinley, R. L. (2010). Attenuation performance of double hearing protection devices. *Proceedings of the 160th Meeting of the Acoustical Society of America*, 11, 040005.

Gorman, A. G. (1982). New design concepts in personal hearing protectors. In Alberti, P. W. (Ed.), *Personal Hearing Protection in Industry* (pp. 427–445). New York, USA: Raven Press.

Hammershøi, D. & Møller, H. (1996). Sound transmission to and within the human ear canal. *The Journal of the Acoustical Society of America*, 100(1), 408–427.

Hiipakka, M. (2008). *Measurement apparatus and modelling techniques of ear canal acoustics*. (Master's thesis, Helsinki University of Technology, Helsinki, Finland).

Hudde, H. (1983). Measurement of the eardrum impedance of human ears. *The Journal of the Acoustical Society of America*, 73(1), 242–247.

Hudde, H. & Engel, A. (1998). Measuring and modeling basic properties of the human middle ear and ear canal. Part III: Eardrum impedances, transfer functions and model calculations. *Acta Acustica united with Acustica*, 84(6), 1091–1108.

IEC. (2009). *Simulators of human head and ear - Part 1: Ear simulator for the measurement of supra-aural and circumaural earphones*. IEC 60318-1. Geneva, Switzerland: International Electrotechnical Commission.

IEC. (2010). *Simulators of human head and ear - Part 4: Occluded-ear simulator for the measurement of earphones coupled to the ear by means of ear inserts*. IEC 60318-4. Geneva, Switzerland: International Electrotechnical Commission.

ISO. (2007). *Acoustics - Hearing protectors - Part 3: Measurement of insertion loss of ear-muff type protectors using an acoustic test fixture*. ISO 4869-3. Geneva, Switzerland: International Organization for Standardization.

ISO. (2011). *Mechanical vibration and shock - Characterization of the dynamic mechanical properties of visco-elastic materials - Part 5: Poisson ratio based on comparison between measurements and finite element analysis*. ISO 18437-5. Geneva, Switzerland: International Organization for Standardization.

ITU. (2021). *Telephone transmission quality, telephone installations, local line networks - Objective measuring apparatus: Artificial ears*. ITU-T P.57. Geneva, Switzerland: Telecommunication Standardization Sector, International Telecommunication Union.

James, C. (2006). *Finite element modeling and exploration of double hearing protection systems*. (Master's thesis, Virginia Polytechnic Institute and State University, Blacksburg, USA).

Jønsson, S., Liu, B., Nielsen, L. & Schuhmacher, A. (2003, March). *Simulation of couplers*. Communication presented in 114th Audio Engineering Society Convention, Workshop 7, Amsterdam, Netherlands.

Jønsson, S., Liu, B., Schuhmacher, A. & Nielsen, L. (2004). Simulation of the IEC 60711 occluded ear simulator. *Proceedings of the 116th Audio Engineering Society Convention, Paper 6162*.

Jønsson, S., Schuhmacher, A. & Ingerslev, H. (2018). *Wideband impedance measurement in the human ear canal; In vivo study on 32 subjects*. Cornell Univ. Libr. Retrieved from: https://arxiv.org/pdf/1811.03389.pdf.

Kampinga, W. R. (2010). *Viscothermal acoustics using finite-elements - Analysis tools for engineers*. (Ph.D. thesis, University of Twente, Enschede, Netherlands).

Keefe, D. H., Ling, R. & Bulen, J. C. (1992). Method to measure acoustic impedance and reflection coefficient. *The Journal of the Acoustical Society of America*, 91(1), 470–485.

Khanna, S. M., Tonndorf, J. & Queller, J. E. (1976). Mechanical parameters of hearing by bone conduction. *The Journal of the Acoustical Society of America*, 60(1), 139–154.

Kunov, H. & Giguère, C. (1989). An acoustic head simulator for hearing protector evaluation. I: Design and construction. *The Journal of the Acoustical Society of America*, 85(3), 1191–1196.

Larson, V. D., Nelson, J. A., Cooper, W. A. & Egolf, D. P. (1993). Measurements of acoustic impedance at the input to the occluded ear canal. *Journal of Rehabilitation Research and Development*, 30, 129–136.

Lavergne, T., Rodrigues, D., Neimanns, V., Olsen, E. S. & Barham, R. (2013). Universal ear simulator: Specifications and artificial ear canal design. *Proceedings of the 42nd International Congress on Noise Control Engineering (InterNoise 2013)*, 247(4), 3892–3899.

Luan, Y., Sgard, F., Benacchio, S., Nélisse, H. & Doutres, O. (2019). A transfer matrix model of the IEC 60318-4 ear simulator: Application to the simulation of earplug insertion loss. *Acta Acustica united with Acustica*, 105(6), 1258–1268.

Luan, Y., Doutres, O., Nélisse, H. & Sgard, F. (2021). Experimental study of earplug noise reduction of a double hearing protector on an acoustic test fixture. *Applied Acoustics*, 176, 107856.

Mechel, F. P. (Ed.). (2008). *Formulas of Acoustics* (ed. 2). Berlin, Germany: Springer.

Mercy, S. E. & James, S. H. (2011). Exposure to very high noise levels and the effect of double hearing protection. *Proceedings of the 10th International Congress on Noise as a Public Health Problem (ICBEN)*.

Mercy, S. E., Tubb, C. & James, S. H. (2005). Experimentation to address appropriate test techniques for measuring the attenuation provided by double ANR hearing protectors. *Meeting Proceedings RTO-MP-HFM-123, Paper 18*.

Nélisse, H., Sgard, F., Gaudreau, M.-A. & Padois, T. (2017). Attenuation of dual hearing protection: measurements and finite-element modeling. *The Journal of the Acoustical Society of America*, 141(5), 3633–3633.

Nelson, D. I., Nelson, R. Y., Concha-Barrientos, M. & Fingerhut, M. (2005). The global burden of occupational noise-induced hearing loss. *American Journal of Industrial Medicine*, 48(6), 446–458.

Nixon, C. W. & von Gierke, H. E. (1959). Experiments on the bone-conduction threshold in a free sound field. *The Journal of the Acoustical Society of America*, 31(8), 1121–1125.

Nixon, C. W., McKinley, R. L. & Steuver, J. W. (1992). Performance of active noise reduction headsets. In Dancer, A. L., Henderson, D., Salvi, R. J. & Hamernik, R. P. (Eds.), *Noise Induced Hearing Loss* (pp. 389-400). St. Louis, USA: Mosby-Yearbook Inc.

Norris, J. A., Chambers, R., Kattamis, N., Davis, B. & Bieszczad, J. (2012). *Effects of custom earplug design parameters on achieved attenuation*. Poster presented in Annual Conference of National Hearing Conservation Association (NHCA), New Orleans, USA.

Pääkkönen, R. (1992). Effects of cup, cushion, band force, foam lining and various design parameters on the attenuation of earmuffs. *Noise Control Engineering Journal*, 38(2), 59–65.

Parmentier, G., Dancer, A., Buck, K., Kronenberger, G. & Beck, C. (2000). Artificial head (ATF) for evaluation of hearing protectors. *Acta Acustica united with Acustica*, 86(5), 847–852.

Ravicz, M. E. & Melcher, J. R. (2001). Isolating the auditory system from acoustic noise during functional magnetic resonance imaging: examination of noise conduction through the ear canal, head and body. *The Journal of the Acoustical Society of America*, 109(1), 216–231.

Reinfeldt, S., Stenfelt, S., Good, T. & Håkansson, B. (2007). Examination of bone-conducted transmission from sound field excitation measured by thresholds, ear-canal sound pressure and skull vibrations. *The Journal of the Acoustical Society of America*, 121(3), 1576–1587.

Rodrigues, D., Guianvarc'h, C., Durocher, J.-N., Bruneau, M. & Bruneau, A.-M. (2008). A method to measure and interpret input impedance of small acoustic components. *Journal of Sound and Vibration*, 315(4-5), 890–910.

Rodrigues, D., Lavergne, T., Olsen, E. S., Fedtke, T., Barham, R. & Durocher, J.-N. (2015a). Methodology of designing an occluded ear simulator. *Acta Acustica united with Acustica*, 101(5), 1007–1015.

Rodrigues, D., Lavergne, T., Olsen, E. S., Barham, R., Fedtke, T. & Durocher, J.-N. (2015b). Design of a new occluded ear simulator. *Proceedings of the 44th International Congress on Noise Control Engineering (InterNoise 2015)*.

Rosowski, J. J., Davis, P. J., Donahue, K. M., Merchant, S. N. & Coltrera, M. D. (1990). Cadaver middle ears as models for living ears: comparisons of middle ear input immittance. *Annals of Otology, Rhinology & Laryngology*, 99(5), 403–412.

Sanborn, P.-E. (1998). Predicting hearing aid response in real ears. *The Journal of the Acoustical Society of America*, 103(6), 3407–3417.

Sasajima, M., Yamaguchi, T., Watanabe, M. & Koike, Y. (2015). FEM Analysis of Occluded Ear Simulator with Narrow Slit Pathway. *International Journal of Mechanical, Aerospace, Industrial, Mechatronic and Manufacturing Engineering*, 9(9), 1430–1433.

Sasajima, M., Yamaguchi, T., Hu, Y. & Koike, Y. (2016). Finite Element Method Analysis of Occluded-Ear Simulator and Natural Human Ear Canal. *International Journal of Mechanical and Mechatronics Engineering*, 9(12), 2213–2217.

Schroeter, J. (1986). The use of acoustical test fixtures for the measurement of hearing protector attenuation. Part I: Review of previous work and the design of an improved test fixture. *The Journal of the Acoustical Society of America*, 79(4), 1065–1081.

Schroeter, J. & Els, H. (1982). On basic research towards an improved artificial head for the measurement of hearing protectors. *Acta Acustica united with Acustica*, 50(4), 250–260.

Schroeter, J. & Poesselt, C. (1986). The use of acoustical test fixtures for the measurement of hearing protector attenuation. Part II: Modeling the external ear, simulating bone conduction, and comparing test fixture and real-ear data. *The Journal of the Acoustical Society of America*, 80(2), 505–527.

Sgard, F., Atalla, N. & Nicolas, J. (2000). A numerical model for the low frequency diffuse field sound transmission loss of double-wall sound barriers with elastic porous linings. *The Journal of the Acoustical Society of America*, 108(6), 2865–2872.

Sgard, F., Benacchio, S., Luan, Y., Xu, H., Carillo, K., Doutres, O., Nélisse, H., Wagnac, E. & De Guise, J. (2018). Vibroacoustic modeling of an in vivo human head wearing a hearing protection device using the finite element method. *Proceedings of the 11th European Congress and Exposition on Noise Control Engineering (Euronoise 2018).*

Sgard, F., Nélisse, H., Gaudreau, M.-A., Boutin, J., Voix, J. & Laville, F. (2010). *Étude de la transmission sonore à travers les protecteurs auditifs et application d'une méthode pour évaluer leur efficacité en milieu de travail - Partie 2: Étude préliminaire d'une modélisation par éléments finis [Study of the sound transmission through hearing protection devices and application of a method for evaluating their real efficiency in the workplace - Part 2: preliminary study of finite element modeling]* (Report n°R-680). Montreal, Canada: IRSST.

Stenfelt, S. & Goode, R. L. (2005). Bone-conducted sound: physiological and clinical aspects. *Otology & Neurotology*, 26(6), 1245–1261.

Stenfelt, S., Wild, T., Hato, N. & Goode, R. L. (2003). Factors contributing to bone conduction: The outer ear. *The Journal of the Acoustical Society of America*, 113(2), 902–913.

Tubb, C., Mercy, S. E. & James, S. H. (2005). Investigating double hearing protection using human subjects. *Meeting Proceedings RTO-MP-HFM-123, Paper 19.*

Viallet, G., Sgard, F., Laville, F. & Boutin, J. (2013). Axisymmetric versus three-dimensional finite element models for predicting the attenuation of earplugs in rigid walled ear canals. *The Journal of the Acoustical Society of America*, 134(6), 4470–4480.

Viallet, G., Sgard, F., Laville, F. & Boutin, J. (2014). A finite element model to predict the sound attenuation of earplugs in an acoustical test fixture. *The Journal of the Acoustical Society of America*, 136(3), 1269–1280.

Viallet, G. (2014). *Étude de la transmission sonore par voie externe d'un bouchon d'oreille couplé au conduit auditif: modélisation numérique et validation expérimentale [Study of the sound transmission by outer ear path through an earplug coupled to an earcanal: numerical simulation and experimental validation].* (Ph.D. thesis, École de Technologie Supérieure, Montreal, Canada).

Viallet, G., Sgard, F., Laville, F. & Nélisse, H. (2015). Investigation of the variability in earplugs sound attenuation measurements using a finite element model. *Applied Acoustics*, 89, 333–344.

von Gierke, H. E. (1956). Personal protection. *Noise Control*, 2(1), 37–44.

WHO. (2021). Deafness and hearing loss. Retrieved from: https://www.who.int/news-room/fact-sheets/detail/deafness-and-hearing-loss.

Williams, R. (2012). *Assessment of the Applicability of ANSI S12.42-2010 as a General Measure of Protection from Impulsive Noise by Measurement of Impulsive and Continuous Noise Insertion Loss of the HGU-56/P and the CEP* (Report n°2012-14). Sensory Research Division, U.S. Army Aeromedical Research Laboratory.

Xu, H., Sgard, F., Wagnac, E. & De Guise, J. (2019). Development of an entire human head finite element model based on in-vivo medical images for investigation of sound transmission. *Proceedings of the 26th International Congress on Sound and Vibration (ICSV26).*

Xu, H., Sgard, F., Carillo, K., Wagnac, E. & De Guise, J. (2020). A three-dimensional finite-element model of a human head for predicting the objective occlusion effect induced by earplugs. *The Journal of the Acoustical Society of America*, 148(4), 2780–2780.

Zwislocki, J. (1957). In search of the bone-conduction threshold in a free sound field. *The Journal of the Acoustical Society of America*, 29(7), 795–804.